Advancing hydro-geomechanical subsurface characterisation using the groundwater response to tidal forces

Zur Erlangung des akademischen Grades eines

DOKTORS DER INGENIEURWISSENSCHAFTEN
(Dr.- Ing.)

von der

KIT-Fakultät für Bauingenieur-, Geo- und Umweltwissenschaften

des

Karlsruher Instituts für Technologie (KIT)

genehmigte

DISSERTATION

von

José M. Bastías Espejo

Tag der mündlichen Prüfung:
04. Juli 2023

Referent: *PD Dr. Dipl.-Ing. Gabriel C. Rau*

Korreferent: *Prof. Dr.-Ing. Rainer Helmig*

Karlsruhe, 2023

Ohana means family.
Family means nobody gets left behind, or forgotten.
— Lilo & Stitch

Para mi familia y amigos, por enseñarme a volar.

Abstract

Groundwater is a critical but over-exploited resource, and its sustainable management requires detailed knowledge of subsurface hydro-geomechanical properties. Passive characterisation methods estimate hydraulic and geomechanical subsurface properties from the well water level responses to harmonic Earth and atmospheric tides. Despite their potential, passive methods are currently underutilised, likely due to a lack of research into their practical feasibility and robustness in real-world applications. Firstly, the groundwater response to Earth and atmospheric tides has never been adequately numerically modelled by solving the coupled hydraulic and geomechanical equations. Secondly, the reliability of the most sophisticated available analytical solution for realistic subsurface conditions has not been thoroughly tested. Lastly, analytical solutions with appropriate boundary conditions that accurately reflect the physics of real-world scenarios are still missing. To address these shortcomings, this thesis carries out three different studies. The overall scope of this thesis encompasses advanced analytical and numerical modelling, as well as the analysis of field datasets.

The first study involved the development, verification, and documentation of RHEA (Real HEterogeneity App), an open-source, fully coupled, finite-element application capable of modeling the effect of tides on the subsurface. RHEA incorporates element-resolution hydro-geomechanical properties for performing coupled simulations. The accuracy of RHEA was verified through analytical solutions in one and two dimensions, and a benchmark semi-analytical problem was proposed to assess systems with heterogeneous properties and sharp gradients. Furthermore, the capabilities of RHEA were demonstrated with a comprehensive example that included realistic properties. The findings indicate that RHEA is a validated open-source application capable of handling complex geology and conducting scalable, fully coupled, hydro-geomechanical simulations. Consequently, a valuable tool is provided by this work for the evaluation of real-world hydro-geomechanical systems presenting challenges, such as heterogeneous geology and sharp property gradients.

In the second study, the theory was reviewed and the most sophisticated analytical solution that relates well water levels to Earth tides was analysed. Subsequently, a new numerical model that couples hydraulics and geomechanics to Earth tide strains was developed and verified. Subsurface conditions over depth were then evaluated for a range of realistic properties. Finally, the well water level response to Earth tide strains within a 2D poroelastic layered aquifer system confined by a 100 m thick aquitard was simulated. The findings indicate that the initial guess significantly influences the sensitivity of the non-linear inversion of analytical solutions to match two observations (amplitudes and phases) to multiple unknown parameters. The validity of the analytical solution requires undrained, confined conditions, and unconsolidated systems exhibit its applicability, while consolidated systems necessitate additional consideration of the Biot modulus. Overall, interpreting the groundwater response necessitates critical prior knowledge of the subsurface system. The results contribute to an improved understanding of the effect of Earth tides on groundwater systems and its interpretation for subsurface properties.

In the third study, a new and rigorous analytical solution for modelling flow between a subsurface-well system induced by harmonic atmospheric loading is presented. This solution is incorporated into a comprehensive workflow that also includes the estimation of subsurface properties using a well-established Earth tide method. The workflow was applied to groundwater monitoring datasets obtained from two boreholes screened in a sand aquifer in the Mary-Wildman Rivers region (Northern Territory, Australia). The results demonstrate agreement between the estimated hydraulic conductivity and specific storage, indicating the presence of small vertical leakage in the vicinity of both boreholes. Additionally, the estimated geomechanical properties fall within the range reported in the literature for similar lithological settings.

This thesis introduces a novel numerical simulator that integrates tidal loading and incorporates the damping effect of observation wells. The simulator was employed to compare the performance of analytical solutions for modelling flow to wells caused by tides in hydro-geomechanical systems. Additionally, a new analytical solution for modelling flow to wells due to atmospheric tides is presented and validated using field data. Overall, this work contributes to the advancement of knowledge regarding the use of passive methods for estimating subsurface properties.

Kurzfassung

Grundwasser ist eine kritische, aber übernutzte Ressource, deren nachhaltige Bewirtschaftung detaillierte Kenntnisse über die hydro-geomechanischen Eigenschaften des Untergrunds erfordert. Passive Methoden zur Charakterisierung bestimmen die hydraulischen und geomechanischen Eigenschaften des Untergrunds anhand der Reaktionen des Brunnenwasserspiegels auf harmonische Erd- und atmosphärische Gezeiten. Trotz ihres Potenzials werden passive Methoden derzeit nicht weitläufig verwendet, was wahrscheinlich darauf zurückzuführen ist, dass ihre praktische Durchführbarkeit und Robustheit in realen Anwendungen noch nicht ausreichend erforscht wurde. Erstens wurde die Reaktion des Grundwassers auf Erd- und atmosphärische Gezeiten noch nie angemessen numerisch modelliert, indem die gekoppelten hydraulischen und geomechanischen Gleichungen gelöst wurden. Zweitens wurde die Zuverlässigkeit der anspruchsvollsten verfügbaren analytischen Lösung für realistische Untergrundbedingungen nicht gründlich getestet. Und schließlich fehlen immer noch analytische Lösungen mit geeigneten Randbedingungen, die die Physik realer Szenarien genau widerspiegeln. Um diese Defizite zu beheben, werden in dieser Arbeit drei verschiedene Studien durchgeführt. Der Gesamtumfang dieser Arbeit umfasst fortgeschrittene analytische und numerische Modellierung sowie die Analyse von Felddaten.

Die erste Studie umfasste die Entwicklung, Überprüfung und Dokumentation von RHEA (Real HEterogeneity App), einer vollständig gekoppelten Open-Source-Anwendung, die die Auswirkungen von Gezeiten auf den Untergrund auf der Basis von Finiten-Elementen modellieren kann. RHEA enthält hydrogeomechanische Eigenschaften in Elementauflösung zur Durchführung gekoppelter Simulationen. Die Genauigkeit von RHEA wurde durch analytische Lösungen in einer und zwei Dimensionen verifiziert, und es wurde ein halbanalytisches Benchmark-Problem vorgeschlagen, um heterogene Systeme mit starken Eigenschaftsunterschieden zu bewerten. Darüber hinaus wurden die Fähigkeiten von RHEA anhand eines umfassenden Beispiels mit realistischen Eigenschaften demonstriert. Die Ergebnisse zeigen, dass RHEA eine validierte Anwendung ist, die komplexe Geologie bewältigen und skalierbare, vollständig gekoppelte hydro-geomechanische Simulationen durchführen kann. Folglich wird durch diese Arbeit ein wertvolles Werkzeug für die Modellierung realer hydrogeomechanischer Systeme bereitgestellt, die Herausforderungen wie heterogene Geologie mit starken Eigenschaftsunterschieden aufweisen.

In der zweiten Studie wurde die mathematische Theorie überprüft und die anspruchsvollste analytische Lösung analysiert, die den Zusammenhang zwischen Brunnenwasserständen und Gezeiten der Erde herstellt. Anschließend wurde ein neues numerisches Modell entwickelt und verifiziert, das Hydraulik und Geomechanik mit Gezeitendeformationen der Erde koppelt. Die Untergrundbedingungen über die Tiefe hinweg wurden dann für eine Reihe realistischer Eigenschaften bewertet. Schließlich wurde die Wasserstandsantwort in einem 2D poroelastischen Schichtaquifer, begrenzt durch eine 100 m dicke, wasserundurchlässige Schicht, auf Gezeit-

endeformationen der Erde simuliert. Die Ergebnisse zeigen, dass die Wahl der Anfangsbedingungen wesentlichen Einfluss auf die Empfindlichkeit der nichtlinearen Inversion der analytischen Lösungen hat, um mehrere unbekannten Parametern aus zwei Beobachtungen (Amplituden und Phasen) zu bestimmen. Die analytische Lösung ist gültig unter undrainierten und abgeschlossenen Bedingungen. Allerdings ist sie nur in Lockergestein anwendbar, während in Festgestein zusätzlich das Biot-Modul berücksichtigt werden muss. Insgesamt wird die Interpretation der Grundwasserreaktion durch Vorabkenntnis des Untergrundsystems verbessert. Die Ergebnisse dieser Studie tragen zu einem besseren Verständnis der Auswirkungen von Gezeiten auf Grundwassersysteme und deren Interpretation für Untergrundeigenschaften bei.

In der dritten Studie wird eine neue und präzise analytische Lösung für die Beschreibung der Strömung zwischen einem Brunnen-Untergrund-System präsentiert, die durch harmonische atmosphärische Druckänderungen an der Oberfläche verursacht wird. Diese Lösung wurde in einen umfassenden Arbeitsablauf integriert, der auch die Schätzung der Eigenschaften des Untergrunds mit Hilfe einer etablierten Erdgezeitenmethode umfasst. Die Analyse wurde auf Zeitreihen von Grundwasserspiegeländerungen angewandt, welche aus zwei Brunnen in einem Sandgrundwasserleiter in der Region Mary-Wildman Rivers (Northern Territory, Australien) stammen. Die Ergebnisse zeigen, dass die geschätzte hydraulische Leitfähigkeit und der Speicherkoeffizient übereinstimmen und ein Vergleich beider Methoden deutet auf das Vorhandensein kleiner vertikaler Leckagen in der Nähe der beiden Bohrlöcher hin. Darüber hinaus liegen die geschätzten geomechanischen Eigenschaften in dem Bereich, der in der Literatur für ähnliche lithologische Verhältnisse angegeben wird.

In dieser Arbeit wird ein neuartiger numerischer Simulator vorgestellt, der die Gezeitenbelastung integriert und den Dämpfungseffekt von Beobachtungsbrunnen einbezieht. Der Simulator wurde eingesetzt, um die Leistung analytischer Lösungen für die Modellierung der durch Gezeiten verursachten Strömung zu Brunnen in hydrogeomechanischen Systemen zu vergleichen. Darüber hinaus wird eine neue analytische Lösung für die Modellierung der Strömung in Brunnen aufgrund von atmosphärischen Gezeiten vorgestellt und anhand von Felddaten validiert. Insgesamt trägt diese Arbeit zur Erweiterung des Wissens über den Einsatz passiver Methoden zur Abschätzung der Eigenschaften des Untergrunds bei.

Contents

List of Figures

List of Tables

Chapter 1

Introduction

1.1 Background

Groundwater is the water found underground, in the rock cracks and spaces in between soil particles. The study of groundwater is interdisciplinary by nature. To assess subsurface systems that interact with groundwater, different areas of sciences often converge; chemistry, physics, geology, hydrology, ecology, biology, and engineering. The ground base study of groundwater has been, therefore, built by scientists of diverse fields; geologists, civil engineers, mechanical engineers, agricultural engineers, ecologists, hydrologists, soil scientists, reservoir engineers, geophysicists, and many others. Thus, the study of groundwater is not trivial, requires multidisciplinary knowledge and continuous collaboration of different areas of science. Understanding groundwater is critical for a wide variety of geological processes, among them, the genesis of mineral deposits, landforms, soil and rock types, oil and gas deposits, and earthquakes. Subsurface characterization is key to assessing how groundwater is transported, stored and interacts in geological systems.

Almost all freshwater in the world is groundwater (Freeze & Cherry, 1979a). Groundwater is not only the main source of drinking water in the world, but also the largest water source for agricultural and crop irrigation (Siebert et al., 2010). Moreover, groundwater plays a critical role in industries that highly impact today's economy such as the gas and oil, mining, energy, construction and municipal water distribution (Hiscock & Bense, 2021). Proper resources management is key to prevent water scarcity which threats not only economic growth but also the quality of life of the world population. When done correctly, groundwater is a valuable asset that can be exploited in a sustainable manner (Gupta, 2011).

Groundwater is available in most parts of the world, and its exploitation has been mostly driven by technologies such as electric pumps (Famiglietti, 2014; de Graaf et al., 2015). The use or extraction method of groundwater largely depends on the location of the aquifers relative to the demand. Globally, 65% of groundwater utilization is used for irrigation, 25% to supply drinking water, and 10% to the industry (Hiscock & Bense, 2021). Heavy use of groundwater can lead to its irreversible depletion, which occurs when the rate of groundwater abstraction exceeds the rate of natural groundwater recharge, over extensive areas, and for long periods of time (Konikow & Kendy, 2005). Assessing whether an aquifer has favorable storage and transmission properties to supply the demand has become one of the fundamental tasks of scientists that study the subsurface (Bear & Cheng, 2010).

1.2 Subsurface characterization

Aquifers have different types of properties that determine the rate and capacity of an underground system to recharge, store, and transmit groundwater (Freeze & Cherry, 1979a). The nature of an aquifer is, by definition, dynamic: the behavior of an aquifer changes in time and space as it is affected by natural processes such as precipitation and infiltration, as well as human activities such as pumping, land use changes, and pollution. The response of aquifers to an external perturbation will be determined by the resulting combination of external factors and the intrinsic properties of the aquifer. Therefore, accurately assessing the behavior of aquifers is crucial for sustainable groundwater management. However, the behavior of aquifers is complex and advanced simulation tools are required to accurately predict the response of aquifers to different perturbations such as pumping rates, climate patterns, land use, or contamination levels (Bear & Cheng, 2010).

Groundwater resources and their interaction with subsurface systems are often evaluated using numerical modeling, which has become a standard tool. Such models have been developed in various languages, with flexible and efficient codes, and some even come equipped with user-friendly graphical interfaces (GUIs) (Kumar, 2019; Condon et al., 2021; LaBolle et al., 2003). Numerical models can simulate various phenomena, including aquifer stresses, transport of heat, chemical reactions, pollutant transport in groundwater, recharge rates, and evaporation (Kumar, 2019; Condon et al., 2021; LaBolle et al., 2003). However, the accuracy of a groundwater model depends on the appropriateness of the underlying conceptual model of the subsurface system and the quality of the parameters included in the model (Rojas et al., 2008; Wu & Zeng, 2013; Ye et al., 2010). Aquifer hydraulic conductivity is a critical parameter for modeling groundwater, and its measurement requires expert knowledge, as it can vary widely at small scales. Direct measurements of hydraulic conductivity are often limited in number or at an inappropriate scale for the processes of interest. To address this uncertainty, probabilistic approaches such as stochastic tools, multiple-point statistics, and even artificial intelligence have been developed (He et al., 2010; Huysmans & Dassargues, 2009; Rogers & Dowla, 1994; Chitsazan et al., 2015). High-quality data are essential for assessing groundwater resources, and this requires active interaction among numerical modellers, data scientists, and field practitioners with expert knowledge.

Aquifers exhibit natural variability in their properties, which is driven by geological processes that have shaped the subsurface over time (Freeze & Cherry, 1979a). Heterogeneity can occur at various scales and directions, making it a crucial factor to consider when designing groundwater models. Determining the appropriate degree of heterogeneity to incorporate into models and selecting the most appropriate methods for characterising heterogeneity are key challenges in groundwater modeling (Maliva, 2016; Bridge & Hyndman, 2004). This decision-making process is supported by the quality of data and proper characterisation of the aquifer.

Aquifer characterisation involves describing the spatial distribution of a hydrogeological system, with particular emphasis on hydraulic conductivity, which can vary widely among several orders of magnitude and plays a crucial role in determining groundwater flow and velocity. Other properties, such as mechanical deformation and heat transport, are also relevant when different physical processes are coupled. Various techniques and tools have been developed to quantify the properties of aquifers, including active characterisation methods such as pumping, slug, pressure, and packer tests, as well as laboratory analyses of cores (Maliva, 2016; Bridge & Hyndman, 2004). While these techniques are laborious and involve logistical expenses, the benefits of proper aquifer characterisation are significant for accurate groundwater modelling.

Field practitioners are responsible for evaluating the feasibility of subsurface characterisation studies based on hydrogeological constraints and available resources. The choice of characterisation technique depends on subsurface conditions, such as lithification, consolidation, or the presence of a casing, and the budget available for drilling and testing (Maliva, 2016).

Subsurface characterisation techniques vary in the type of information provided, spatial scale, and precision of parameters measured. Large-scale methods, such as remote sensing, provide a broad spatial view of hydraulic distribution at a relatively low cost, but with limited interpretation of near-surface conditions. Medium-scale methods, such as multi-well pumping and tracer tests, cover deeper scales and can determine critical information such as flow paths, transport parameters, and leakage. However, drilling and well-based testing can be expensive and constrained by the available budget. Small and fine-scale techniques can deliver high-precision measurements of parameters; however, groundwater models require numerous measurements in different locations, making sparse measurements impractical. Therefore, effective aquifer characterization programs must consider the information provided by various techniques, the limitations and spatial scales of each method, and how the data will be processed and used to achieve project objectives (Maliva, 2016).

1.3 Passive Subsurface Characterisation

Passive characterisation methods use measurements of the well water level response to natural forces to calculate subsurface hydraulic and geomechanical properties (McMillan et al., 2019a). Earth and atmospheric tides are natural and ubiquitous phenomena that elastically deform subsurface systems producing small changes in the confined hydraulic head (i.e. confined pore pressure) (Rau et al., 2019). The effect of tides over the subsurface has long been reported (Meinzer, 1939) and is observed by wells that routinely measure hydraulic pressure around the world. Tides offer an ideal opportunity for passively estimating subsurface properties, as their widespread application can reduce the effort and cost of the characterisation investigations (McMillan et al., 2019a).

The deformation exerted by Earth and barometric pressure within aquifers has been used to estimate subsurface properties, an approach that has been termed as *Passive Subsurface Characterisation* (PSC) (Rau & Blum, 2021). Earth tides are generated by gravity changes caused by the movement of celestial bodies relative to Earth. Atmospheric tides are caused by gravitational and thermally induced changes in barometric pressure (Agnew, 2005). While their origin and mechanisms differ, both phenomena cause relatively small deformations of the subsurface and affect the mechanical force balance between the solid matrix and the fluid contained within, resulting in changes to the confined pore pressure (Verruijt & Van Baars, 2007; Lambe & Whitman, 1991; Freeze & Cherry, 1979a). Such changes propagate into groundwater monitoring wells (Rau et al., 2019) and can be analysed to estimate subsurface properties (Hsieh et al., 1988; Rau et al., 2020a).

Tides are cyclic signals that consist of several embedded harmonic constituents (Agnew, 2005). The first step to estimate subsurface properties with PSC is to extract the amplitude and phases of the harmonic constituents from field measurements that are often noisy discrete time series (Turnadge et al., 2019; Schweizer et al., 2021). Most relevant tidal signals oscillate between 0.8 to 2.0 cycles per day, and their frequencies are closely spaced, making it difficult to extract (Agnew, 2005). Signal analysis and treatment have been investigated intensively, and many methods are implemented in major software platforms (Unpingco, 2016). For discrete

data points, the harmonic least-squares method for amplitude and phase estimation (HALS) is an optimisation approach that aims to minimise the sum of the squared residuals between a model combining harmonics with known frequencies and some discretely measured data points (Stoica et al., 2008). HALS has been proven to be robust and outperforms other signal extraction methods for Earth and atmospheric tides, such as Discrete Fourier Transform (DFT) (Schweizer et al., 2021).

Most relevant Earth and atmospheric tides have been documented in the literature (Agnew, 2005). Since tides are made up of many constituents, it is convenient to use common nomenclature to refer to them. For instance, the dominant frequencies present in groundwater pressure measurements are the M_2 (1.93 cpd) and the S_1 (1.0 cpd). Darwin symbols are used as nomenclature for tides, where the Sun and Moon tides are represented as S and M, respectively. The subscript indicates the frequency in cycles per day (cpd). The M_2 and S_1 generally show a higher amplitude in comparison with other tidal harmonics and are, therefore, more likely to be contained in field datasets (Agnew, 2005). Their harmonic constituents are often targeted when tidal signals are decomposed (Rau et al., 2019).

Well-established tidal catalogues can be used to compute with precision the gravity changes caused by Earth tides. Various software packages use such catalogues to compute time series of strain variations at a given location on the Earth's surface, for a given temporal duration (Tamura & Agnew, 2008; Pawlowicz et al., 2002; Van Camp & Vauterin, 2005). These catalogues, compute the tidal potential (i.e., gravity variations) based on the force balance between a given point on the Earth's crust and celestial bodies. This computation takes into account the distance between celestial bodies, their mass and angular distance, as well as more advanced considerations such as ellipticity of the orbits, inclination angles, and other orbital parameters in modern catalogues (Agnew, 2005). This is a complex algebraic problem, which can be simplified with certain assumptions. The most relevant simplification is to consider the Earth as Spherical, Non-Rotating, Elastic, Isotropic, and Oceanless (SNREIO). This simplifies tidal calculations for two reasons: (1) the real Earth has oceans that respond, in complicated ways, to the tidal potential and (2) real strain, vertical displacement, the potential, and gravity are all scaled versions of each other, which allows us to correlate all these quantities through known elastic correlations (Agnew, 2005).

Gravity changes produce by Earth tides cause strains that deform the volume of a porous medium (Figure 5.1a). If the system is confined and undrained (i.e. no groundwater is exchange in any boundary), changes in volume of the porous medium cause instantaneous changes in the confined pore pressure of the aquifer and such change can be recorder by observation wells. This processes occurs in three steps: (1) the porous medium is in hydro-static equilibrium with the observation well (Figure 1.2a). (2) a volumetric Earth tidal deformation is applied which causes an instantaneous response of the confined pore pressure of the aquifer as fluid moves out of storage (Figure 1.2b). (3) the hydraulic gradient between the aquifer and the water level in the well produce water exchange between them until equilibrium is reached (Figure 1.2c).

Atmospheric tides are generated by a combination of both gravitational tidal forces and thermal induced forces. Barometric pressure, temperature changes and wind speed have thermal origin and dominate the tidal effect in the near surface of the Earth (Figure 5.1b). Atmospheric tides can be measured with pressure loggers as barometric pressure. Atmospheric tides exert vertical load over the subsurface, if the porous medium is confined and saturated, the confined pore pressure will change as the load is bared by both the filling fluid and the porous skeleton. This process occurs in three steps: (1) the porous medium is in hydro static equilibrium with

the observation well (Figure 1.3a). (2) barometric pressure loads the porous medium which generate instantaneous response of the confined pore pressure caused by the compressibility balance between fluid and porous skeleton (Figure 1.3b). (3) if the well is open to the atmosphere, the hydro static balance is reached by equalising the pressure of the aquifer with the change in barometric pressure (Figure 1.3c).

Figure 1.1: A well that is screened in the subsurface shows water level changes caused by the effect of Earth tides and barometric pressure. Changes in confined pore pressure that propagate into wells are caused by (a) volumetric deformation due to Earth tide strains, (b) subsurface loading due to barometric pressure changes on the surface. These are two separate mechanisms that require distinction (McMillan et al., 2019b).

Although the underlying physic in which Earth and atmospheric tide are based differ, their process is very similar: tides deform the subsurface which changes the confine pore pressure which is then recorder by an observation well. The discrepancy between the magnitude of well water level variation and the magnitude of subsurface pore pressure variation can be expressed as an amplitude ratio (Figure 1.2d and Figure 1.3d). Separately, time delay required for groundwater exchange between the subsurface and a well to occur can be expressed as a phase shift or phase lag (Figure 1.2d and Figure 1.3d) (Hsieh et al., 1987). The occurrence of positive phase shifts (i.e., when well water levels respond before subsurface water pressures to Earth tide induced strain variations) have been related to vertical connectivity with adjoining hydrostratigraphic units (Roeloffs et al., 1989). Amplitude ratios and phase shifts, which can be readily extracted from measurements, can be inverted using established analytical solutions in order to estimate subsurface hydro-geomechanical properties (Hsieh et al., 1987).

1.3.1 Analytical solutions

Analytical solutions that model flow towards a well due to the effect tides in aquifers can be inverted to estimate subsurface parameters with field data. Cooper Jr et al. (1965) studied the response of confined aquifers to seismic waves and its effect over groundwater monitoring wells.

Figure 1.2: Representation of the pore pressure change and well water level in a semi-confined aquifer due to Earth tide strains. Earth tides induce subsurface stress which results in strains that generate changes in the pore water pressure. This leads to pressure gradients between the subsurface and observation wells that cause water movement in or out of the well. The ratio between the Earth tide strain and the well water level response can be expressed as amplitude ratio whereas the time difference between both signals as phase shift. (a) Aquifer and well pressure are in hydro-static equilibrium. (b) Earth tidal strain changes confined pore pressure. (c) Pressure gradients move fluid to the observation well. (d) Confined pore pressure changes due to Earth tidal forcing and well water level changes over time (Bastias et al., 2022).
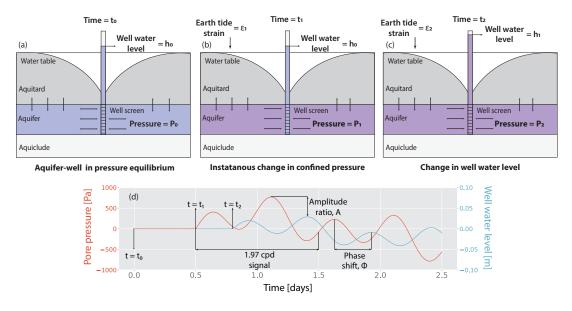
In his work, Cooper Jr et al. (1965) derived an analytical solution for the non-steady drawdown in the aquifer due to a harmonic motion of the water level in a well. Although the analysis was developed for seismic disturbances, it can be applied to flow to wells due to earth tides and atmospheric tides. Bredehoeft (1967) proposed a method to interpret the effect of Earth tides response in observation wells, the method allowed to estimate specific storage of the aquifer if the Poisson's ratio of the porous medium is known. The method of Bredehoeft (1967) was rather intuitive and did not follow the consolidation theory of Biot (Biot, 1941). In the following years, many authors discussed the interpretation of Earth tides on the subsurface; Bodvarsson (1970) derived an equation to model flow in aquifers with Earth tidal perturbation; Robinson & Bell (1971) derived a method to estimate subsurface properties in confined aquifers with poroelastic relations and applied to field data, however the authors did not included the fluid movement towards the observation well which can diminish the amplitude and phase; Arditty et al. (1978) derived a flow equation where the pore pressure varies is an harmonic function of the Earth tides, the solution was applied to field data to estimate aquifer properties, the study does not include the effect of an observation well. Van der Kamp & Gale (1983) derived a general formulation for the effect of Earth tides in the subsurface based on the consolidation theory of Biot.

Hsieh et al. (1987) proposed an analytical solution to determinate hydraulic conductivity of the aquifer and specific storage by combining the work of Cooper Jr et al. (1965) and Bredehoeft (1967). This was the first analytical solution that combines the effect Earth tides in subsurface and the amplitude and phase diminishing caused by an observation well. Hsieh et al. (1988) revisited and discussed the proposed method of Bredehoeft (1967) and demonstrated its robustness with by comparing it with the consolidation theory. Similarly, Rojstaczer (1988) derived an analytical solution to model flow to wells due to atmospheric tides, the solution also

Figure 1.3: Representation of the pore pressure and well water level change in a semi-confined aquifer due to barometric loading. This induces subsurface stress which results in vertical deformation that generate changes in the pore water pressure. This further leads to pressure gradients between the subsurface and observation wells that cause water movement in or out of the well. The ratio between the exerted from atmospheric tides and the well water level response can be expressed as amplitude ratio, whereas the time difference between both signals as phase shift. (a) Aquifer and well pressure are in hydro-static equilibrium. (b) Atmospheric tidal state of stress changes confined pore pressure. (c) Pressure gradients move fluid to the observation well. (d) Confined pore pressure changes due to atmospheric tides forcing and well water level changes over time.

includes the effect of the unsutared zone on the generated confined pore pressure. However, to include this effect vadose properties are needed that are very likely unknown. Rojstaczer (1988) utilised the description of flow to wells by Hantush & Jacob (1955), but this form of the fluid continuity equation does not considerate the barometric loading effect (i.e. instantaneous change in pore pressure) by the vertical stress caused by atmospheric tides. In the solution of Rojstaczer (1988), the barometric effect of atmospheric tides is coupled only by vertical leakage from the semi confining layer and the barometric efficiency caused by confined conditions was not considerate. Based on the work of Rojstaczer & Agnew (1989), Rojstaczer & Riley (1990) presented an analytical solution to model atmospheric tides which includes the barometric effects (i.e. barometric efficiency) over the confined pore pressure, but the model does not include vertical leakage caused by the semi confined layer. Further, in the formulation of Rojstaczer & Riley (1990), the mean stress only considerate the vertical component and the lateral directions are ignored. For typical values of Poisson's ratio this assumption, is in fact, not valid and can lead to significant errors (Biot, 1941).

Both analytical solutions, Hsieh et al. (1988) for Earth tides and Rojstaczer (1988) for atmospheric tides assume (1) only horizontal flow in the aquifer; (2) the confining layer has no storativity and (3) the well is a line source that matches the depth of the confined aquifer. Since then, several studies have applied these analytical solutions to estimate subsurface properties, many times, violating the mentioned assumptions.

1.3.2 Numerical approaches

Numerical approaches have been used to model the effect of tides in the subsurface. Many simulation studies have been performed in coastal aquifers where the harmonic effect of waves confined with pressure changes due to ocean tides can have catastrophic consequences causing soil liquefaction in off-shore structures such as oil platforms and pipelines (Abarca et al., 2013; Zhang et al., 2021a; Wang et al., 2015; Li & Jeng, 2023; Zhang et al., 2022). Studies in aquifers that are close to the coast have also been perform to evaluate the effect of sea level change over monitoring wells (Jardani et al., 2012; Pendiuk et al., 2020; Alcaraz et al., 2021). There are only few studies involving numerical simulations that focus on the effect of Earth and atmospheric tides, perhaps because the loading effect of ocean tides can produce significantly higher pressure gradients than Earth and atmospheric tides.

So far, modelling the subsurface response to ocean tides has considered poroelastic conditions and harmonic loading by the weight of the water, therefore, solved as a consolidation problem. This approach can be applied to model atmospheric tides, as the boundary conditions are similar (i.e. harmonic load at the top boundary). In contrast, the pressurisation of an aquifer caused by Earth tides is produced by changes in the pore space volume of the porous material due to strains (i.e., eigenstrains) caused by the gravitational influence from the movement of celestial bodies. Moreover, the change of the confined pore pressure is generally measured using an observation well which causes fluid movement which has to be considerate in the model.

Studies that model the effect of Earth tides over the subsurface have only considerate fluid hydraulics neglecting the poro elastic response of the aquifer. For example, Wang et al. (2019) simulated the effect of capillarity of the unsaturated zone in one dimension. They found out that the assumption of fixed water table can lead to erroneous estimation of subsurface properties with analytical solutions. Zhu & Wang (2020) simulated a multi-layered system to study the effect of leakage through an aquitard and concluded that simplifications in the analytical model lead to overly conservative estimates of vertical flux between layers. Wang & Manga (2021) provide a summary of these works.

To successfully model the effect of Earth and atmospheric tides over the water level changes that they cause in an observation well in an elastic saturated aquifer, coupled physics between fluid hydraulics and mechanical deformation need to be considerate. This rises several challenges, for example; how to properly couple the aquifer physics with the one that describe the well physics, time steps needed to obtain accurate solution, size of the model and boundary conditions. Hence, realistic modelling of PSC requires precise description of the underground and underlying physics of the process.

The elastic deformation of a porous medium was first described by Terzaghi Terzaghi (1923), he performed consolidation experiments in a soil column and described the physics coupling between hydraulic and mechanical deformation in one direction. This work was later on generalised by Biot, who considerate the deformation of a porous medium in three dimension giving rise to the Biot consolidation theory Biot (1941). The consolidation theory has been implemented in several numerical codes White et al. (2018). They have wide number of applications, for instance, reservoir modelling for gas and oil, CO_2 storage, rock fracking, soil compaction and consolidation, subsurface subsidence and earthquakes (Haagenson et al., 2020; Alnæs et al., 2015; Keilegavlen et al., 2017, 2021).

Modeling of Earth and atmospheric tides requires the coupling of flow and poroelasticity equations and can be performed in two ways, i.e. via sequential coupling or simultaneous coupling. In sequential coupling, the fundamental equations are represented in a loose form

where differential equations are solved independently and in linear order, that way information is transfer between partial differential equations until convergence is found Kim et al. (2011); Mikelić & Wheeler (2013). This type of coupling is very efficient in terms of computational resources, but its performance decreases with the amount of partial differential equations to be solved (Kim et al., 2011; Beck et al., 2020). Notable examples are geomechanics models based on TOUGH (Transport Of Unsaturated Groundwater and Heat) (Pruess et al., 1999; Xu et al., 2006; Lei et al., 2015; Lee et al., 2019). These consist of different libraries to solve for coupled thermo-hydro-mechanical (THM) applications relying on the numerical capabilities provided by TOUGH. The libraries differ in their fundamental equations, numerical solution methods and discretization schemes (Rutqvist, 2017). Another massively parallel subsurface flow package is PFLORTRAN, an open-source, multi-scale and multi-physics code for subsurface and surface processes (Hammond et al., 2014). PFLORTRAN solves non-isothermal multi-phase flow, reactive transport and geomechanics in a porous medium. It has previously been applied to simulate hydro-geomechanical systems (Lichtner & Karra, 2014).

In simultaneous coupling, the system of partial differential equations are solved at the same time by inverting one single Jacobian matrix. This process often requires big computational efforts, but with the development of more powerful hardware and parallel code, tools based on simultaneous coupling are becoming more frequent. A notable code that is based on simultaneous coupling is OpenGeoSys (OGS), a well-known open source library to solve multi-phase and fully coupled thermo-hydro-mechanical (THM) physics (Kolditz et al., 2012). The code is well documented and features several examples in different subsurface areas. Further, different developers are constantly contributing new features to the source code (Graupner et al., 2011; Kosakowski & Watanabe, 2014; Li et al., 2014). Similarly, DuMux is a free and open source, fully coupled numerical simulator for multi-phase flow and transport in a porous medium, (Flemisch et al., 2011). It is based on the Distributed Unified Numeric Environments (DUNE), a C++ based ecosystem that solves finite element models based on PETSc.

A notable simulation framework that features simultaneous coupling and parallelization is Multiphysics Object Oriented Simulation Environment (MOOSE) (Permann et al., 2020). MOOSE also allows easy coupling of new physics by an plug and play architecture. Within MOOSE, the complex mathematics that involve the code numeric are hard coded, and located in the base of the code. On top of that, the user can easily add new differential equations to be solved by MOOSE with a friendly programming interface. Hence the average user does not need to deal with complex numerical technicalities. An example of MOOSE's capabilities in simulating coupled processes in a porous media was illustrated by Cacace & Jacquey (2017), who developed a MOOS E-based application named GOLEM. It was optimised to model three-dimensional THM processes in fractured rock (Freymark et al., 2019). Another cutting-edge implementation is PorousFlow, an embedded MOOSE library to simulate multi-phase flow and Thermal-Hydraulic-Mechanical-Chemical (THMC) processes in a porous medium (Wilkins et al., 2020).

The friendly interface of MOOSE offers a suitable platform to simulate Earth and atmospheric tides, since hydro-geomechanical physics can be solved in a coupled manner and integrated to the framework in only few lines of code. Further, realistic scenarios such as the observation well physics can also be included. This type of simulation can then grow in complexity to include even more realistic scenarios such as heterogeneous systems, non-elastic material correlations (eigenstrains), different types of boundary conditions or coupling of different space and time scales.

1.4 Objectives

The characterization of subsurface properties using passive methods has the potential to estimate hydro-geomechanical properties at considerably lower costs than traditional sampling methods, such as hydraulic testing. The goal is to improve the accuracy and reliability of passive subsurface characterization methods and provide a more cost-effective alternative to traditional sampling methods. This thesis involves a combination of theoretical analysis, numerical simulations, and field experiments to achieve its objectives. The outcomes of this research will have significant implications for the field of hydro-geomechanics and will contribute to the development of sustainable and efficient groundwater management strategies. In particular, this thesis aims to:

1. Investigating the physics of PSC by analyzing the underlying principles and mechanisms that govern its behavior. This can be achieved by using the Biot consolidation theory to derive the basic equations that describe PSC. By doing so, the limitations and assumptions of the analytical solutions can be identified, which can provide insight into the accuracy and reliability of the method. Overall, investigating the physics of PSC is essential for understanding its potential and limitations, as well as for improving its application in various geotechnical and environmental engineering projects.

2. Developing a flexible numerical framework to model the effect of tides in the subsurface to provide a powerful tool for simulating complex scenarios and subsurface setups. By using numerical models, it is possible to investigate the behavior of the subsurface under different conditions and to test the validity of PSC analytical solutions in situations where their underlying assumptions may not be valid. Moreover, numerical simulations can provide a more comprehensive understanding of the subsurface response to tidal forcing, which can help to improve the accuracy and reliability of subsurface characterization methods.

3. Derive a new analytical solution to model the flow to wells caused by the barometric loading of atmospheric tides based in the mean stress flow equation. This new analytical solution can estimate geomechanical properties and can be used to test the validity of existing analytical solutions. Test the derived model with field data to evaluate the its accuracy and reliability, and provide insight into its potential applications.

1.5 Structure of this thesis

This thesis is a compilation of three studies presented in Chapters 2, 3, and 4. The chapters are structured in a logical order, with each subsequent study building upon the previous one in terms of complexity. All three studies were submitted to peer-reviewed ISI-listed journals, with two of them already published (i.e., Chapters 2 and 3), and one currently under review (Chapter 4). Chapter 5 provides a synthesis of the studies and establishes the connection between them. Overall, this thesis represents a significant contribution to the improvement of hydrogeological characterization strategies.

Chapter 2, entitled *"RHEA v1.0: Enabling Fully Coupled Simulations with Hydro-Geomechanical Heterogeneity"* presents a paper published in the journal Geoscientific Model Development. The chapter describes the Real Heterogeneity App (RHEA), which is a fully coupled numerical solver for hydro-geomechanical applications. The study explains how the Biot consolidation equations are integrated into the MOOSE parallel numerical framework and verifies the code against three well-known poroelastic problems. Furthermore, the study

demonstrates how RHEA can import large data sets to simulate realistic subsurface conditions, using a consolidation problem as an example. Overall, RHEA is an excellent case study that highlights the potential of massive numerical frameworks for integrating new physics and simplifying mathematical technicalities in the geosciences field.

Chapter 3 entitled "*Groundwater responses to Earth tides*": This presents the paper published in the journal *Journal of Geophysical Research: Solid Earth*. The paper has also been published in *Eos Science News*. The study focuses on Earth tidal analysis and presents a comprehensive review of the underlying physics that drives changes in pore pressure due to Earth tides. The study also discusses the solution space of the analytical solutions used to estimate subsurface parameters with Earth tidal analysis. Furthermore, a novel numerical model developed in RHEA that can solve for the effects of Earth tides in the subsurface is presented. The paper concludes with a comparison of the RHEA numerical model with standard analytical tools used for parameter estimation with Earth tidal analysis. Overall, this study demonstrates the advantages of using numerical simulation to evaluate and validate analytical solutions and, hence, limitations of analytical models can be studied.

Chapter 4 entitled "*Technical note: Novel analytical solution for groundwater response to atmospheric tides*": This presents the manuscript accepted for review in *Hydrology and Earth System Sciences* in which a newly developed analytical solution for modeling groundwater flow to wells caused by atmospheric tides is described. The analytical solution is derived in basis of the poroelasticity theory and validated using field data collected from a study site located in northern Australia. The results obtained from the new analytical solution are compared to current PSC methods and previous knowledge of the study site. The new approach enhances the current established hydro-geomechanical subsurface characterization methods and improves understanding of the subsurface.

Chapter 5 summarizes the overall results and findings of this thesis by combining and discussing the new findings and outcomes from the three studies. The conclusions of this thesis are then contextualized with the current state-of-the-art research. Finally, ideas for further work are presented, which may help to continue the development of, and build further confidence in, the application of PSC.

Chapter 2

RHEA v1.0: Enabling fully coupled simulations with hydro-geomechanical heterogeneity

Abstract

Realistic modelling of tightly coupled hydro-geomechanical processes is relevant for the assessment of many hydrological and geotechnical applications. Such processes occur in geologic formations and are influenced by natural heterogeneity. Current numerical libraries offer capabilities and physics couplings that have proven to be valuable in many geotechnical fields like gas storage, rock fracturing and Earth resources extraction. However, implementation and verification of full heterogeneity of subsurface properties using high resolution field data in coupled simulations has not been done before. We develop, verify and document RHEA (Real HEterogeneity App), an open-source, fully coupled, finite-element application capable of including element-resolution hydro-geomechanical properties in coupled simulations. To extend current modelling capabilities of the Multiphysics Object-Oriented Simulation Environment (MOOSE), we added new code that handles spatial distributed data of all hydro-geomechanical properties. We further propose a simple, yet powerful workflow to facilitate the incorporation of such data to MOOSE. We then verify RHEA with analytical solutions in one and two dimensions, and propose a benchmark semi-analytical problem to verify heterogeneous systems with sharp gradients. Finally, we demonstrate RHEA's capabilities with a comprehensive example including realistic properties. With this we demonstrate that RHEA is a verified open-source application able to include complex geology to perform scalable, fully coupled, hydro-geomechanical simulations. Our work is a valuable tool to assess challenging real world hydro-geomechanical systems that may include different levels of complexity like heterogeneous geology and sharp

gradients produced by contrasting subsurface properties.

2.1 Introduction

The complexity of processes occurring in a fluid saturated deformable porous medium and their importance to a wide range of subsurface applications presents a major challenge for numerical modelling especially when including realistic heterogeneity. Example applications in geo-engineering that inherently require coupling of hydro-geomechanical processes are the interaction between pressure, flow and fracturing of rocks (Atkinson, 2015; Weng, 2015; Berre et al., 2019), land surface subsidence caused by the extraction of Earth resources (Peng, 2020; Ye et al., 2016), underground gas storage (Yang et al., 2016; Tarkowski, 2019) and mass movement (Zaruba & Mencl, 2014; Haque et al., 2016; Gariano & Guzzetti, 2016). Even though the fundamental mathematical description of coupled hydro-geomechanical processes has reached general consensus (Cheng, 2016; Wang, 2017), realistic modelling of such processes requires a precise description of the underground.

Heterogeneity is ubiquitous across scales and strongly affects the mechanical properties as well as the movement of fluids through the subsurface. For instance, the hydraulic conductivity of fractures within a porous rock is often orders of magnitude greater than that of unfractured rock, so that fine spatial discretization around fractures is needed in certain numerical models, resulting in expensive computational demands (Morris et al., 2006; Eaton, 2006). As a result, the development of coupled hydro-geomechanical models generally requires simplifying or averaging heterogeneity, i.e. homogenising (Blum et al., 2005, 2009). Recent research has identified the need to improve modelling of coupled hydro-geomechanical systems (Lecampion et al., 2018; Grigoli et al., 2017; Birkholzer et al., 2019), and particularly also the importance of introducing high-resolution details to improve the accuracy of numerical simulations (McMillan et al., 2019b). However, integrating spatially distributed material properties to numerical tools is not trivial because the shape of geological formations can consist of complex geometries produced by natural processes acting over a long period.

Terzaghi (1923) first described the elastic interactions between a porous medium and a fluid occupying its pore space, and the unidirectional system's dynamic responses to external forces. Biot (1941) later generalised this theory to three dimensions giving rise to the well-known theory of consolidation or poroelasticity, also termed *Biot* theory. Since the 1970's, a large number of numerical libraries have been developed, optimised and applied to a diverse range of poroelastic applications (Bear & Verruijt, 1987; Verruijt, 1995; Cundall & Hart, 1993; Boone & Ingraffea, 1990). Notable is the work of Verruijt (2013), who designed a number of numerical solvers for typical one and two dimensional poroelastic problems.

Well-known subsurface simulation libraries are concisely reviewed in the following. Since the number of subsurface simulation codes is vast, we only included platforms that are relevant to modelling spatially distributed heterogeneity. For an exhaustive list of codes the reader is referred to White et al. (2018). Current subsurface hydro-geomechanical simulation codes can be classified based on the numerical solution scheme and modelling approach of the coupled physics. For example, sequential coupling solves for the hydraulic and geomechanical variables independently and in sequence. Notable examples are geomechanics models based on TOUGH (Transport Of Unsaturated Groundwater and Heat) (Pruess et al., 1999; Xu et al., 2006; Lei et al., 2015; Lee et al., 2019). These consist of different libraries to solve for coupled thermo-hydro-mechanical (THM) applications relying on the numerical capabilities provided by TOUGH.

The libraries differ in their fundamental equations, numerical solution methods and discretization schemes (Rutqvist, 2017). Although sequential codes allow flexible and efficient code management in conjunction with reasonable computational costs, they tend to perform poorly in tightly coupled processes, since transient interaction between variables may not be computed accurately (Kim et al., 2011; Beck et al., 2020). However, sequential coupling combined with iterative schemes can significantly improve the numerical accuracy. In such implementations, feedback between variables occurs by transferring hydraulic variables to the geomechanics implementation, followed by returning the calculated stress and strain back into the flow problem for the next iteration (Beck et al., 2020). The numerical stability of such iterative methods is discussed by Kim et al. (2011) and Mikelić & Wheeler (2013). Another massively parallel subsurface flow package is PFLORTRAN, an open-source, multi-scale and multi-physics code for subsurface and surface processes (Hammond et al., 2014). PFLORTRAN solves non-isothermal multi-phase flow, reactive transport and geomechanics in a porous medium. It has previously been applied to simulate hydro-geomechanical systems (Lichtner & Karra, 2014).

Another concept is to solve the hydro-geomechanical equations as a fully-coupled system (i.e. all equations are solved simultaneously). This is often performed using an implicit time-stepping scheme, which has unconditional numerical stability and high accuracy, but is computationally expensive. This approach has proven to be useful in geo-engineering applications (Nghiem et al., 2004; Hein et al., 2016; Pandey et al., 2018). Various fully coupled hydro-geomechanical libraries have been developed and released. Proprietary software such as COMSOL (Holzbecher, 2013) has been used intensively in geomechanical applications, in particular for modelling of coastal aquifers (Zhao et al., 2017). COMSOL can import material data from text files into simulations. However, an automatic interpolation between neighboring materials is performed automatically and may lead to undesired results. More recently, Pham et al. (2019) included geomechanical and poroelastic capabilities into the proprietary groundwater modelling environment FEFLOW (Finite Element Flow). MRST is an open-source code developed within the proprietary software MATLAB for fast prototyping of new tools in reservoir modelling (Lie, 2019). While MRST is not a simulator itself, it supports multi-phase flow with THM physics. MRST has been usedforn hydro-geomechanical problems, such as fracture rocks (Zhao & Jha, 2019) as well as several other subsurface applications (Garipov et al., 2018; Ahmed et al., 2017; Edwards et al., 2017). Notably also, two open source Python codes have been developed. The first is the FEniCS project (Haagenson et al., 2020; Alnæs et al., 2015), while the second is called Porepy and was specifically developed to simulate THM processes in rock fractures (Keilegavlen et al., 2017, 2021). Despite the fact that python-based coding offers the advantage of high-level programming within a relatively friendly user interface, these codes are designed to facilitate rapid development of features that cannot be properly represented by standard simulation tools rather than general multiphysics problems. Other fast-prototyping novel codes include (Dang & Do, 2021; Tran & Jha, 2020; Reichenberger, 2003; Martin et al., 2005; Frih et al., 2012).

An additional option is OpenGeoSys (OGS), a well-known open source library to solve multi-phase and fully coupled THM physics (Kolditz et al., 2012). The code is well documented and features several examples in different subsurface areas. Further, different developers are constantly contributing new features to the source code (Graupner et al., 2011; Kosakowski & Watanabe, 2014; Li et al., 2014). Similarly, DuMux is a free and open source, fully coupled numerical simulator for multi-phase flow and transport in a porous medium, (Flemisch et al., 2011). It is based on the Distributed Unified Numeric Environments (DUNE), a C++ based ecosystem that solves finite element models based on PETSc. DuMux is well known for its

strong focus on multi-phase flow and transport in a porous medium. Its recent release adds extra features which facilitates physics coupling, such as Navier-stokes models (Koch et al., 2021). From our experience, however, users without some computational background and experience in programming in C++ or python as well as using a debugger may require a significant amount of time to take full advantage of the features that OGS and DuMux offer. Furthermore, to our best knowledge we are unaware of a peer-reviewed verification of these codes that includes fully distributed hydraulic and geomechanical heterogeneity.

The multi-physics coupling framework MOOSE (Multiphysics Object Oriented Simulation Environment) (Permann et al., 2020) offers a unique environment where users can couple different physical processes in a modular approach. Within the object-oriented ecosystem of MOOSE, each physical process (or its partial differential equation, PDE) is treated separately as an individual MOOSE object and coupling is performed by the back end routines of MOOSE. The MOOSE numerical scheme is based on the finite element (FE) method. It offers clean and effective numerical PDEs solvers as well as mesh capabilities with a uniform approach for each class of problem. This design enables easy comparison and use of different algorithms (for example, to experiment with different Krylov subspace methods, preconditioners, or truncated Newton methods) which are under constant development. MOOSE enables the user to focus on describing the governing equations while the underlying numerical technicalities are taken care of by the system.

We have found that mastering the basic concepts of the MOOSE workflow requires a steep learning curve. However, it requires minimum C++ coding skills which facilitates the learning experience from users that not necessarily have a computer science background. Once the basics are mastered the benefits are significant, for example an experienced user can easily modify the source code to add desired features such as multi-scale physics, non-linear material properties, complex boundary conditions or even basic post-processing tools with only a few lines of code.

An example of MOOSE's capabilities in simulating coupled processes in a porous medium was illustrated by Cacace & Jacquey (2017), who developed a MOOSE-based application named GOLEM. It was optimised to model three-dimensional THM processes in fractured rock (Freymark et al., 2019). Another cutting-edge implementation is PorousFlow, an embedded MOOSE library to simulate multi-phase flow and Thermal-Hydraulic-Mechanical-Chemical (THMC) processes in a porous medium (Wilkins et al., 2020). Porous Flow has been verified and applied to simulate a number of complex and realistic systems, for example shallow geothermal systems (Birdsell & Saar, 2020), CO_2 sequestration (Green et al., 2018) and groundwater modelling with plastic deformation (Herron et al., 2018). However, it has not yet been extended and verified for the simulation of spatial heterogeneity of mechanical parameters. In other words, despite its ability to handle spatially distributed heterogeneity of permeability and porosity, it does not support spatially distributed heterogeneity of mechanical properties such as bulk and Young's moduli. To the best of the authors' knowledge no existing open source numerical tool is able to integrate full heterogeneity including all hydro-geomechanical parameters representative of complex geologic formations.

The aim of this paper is therefore to develop, verify and illustrate a novel and generic workflow for modelling fully coupled hydro-geomechanical problems allowing the inclusion of hydraulic and geomechanical heterogeneity inherent to realistic geological systems. This was achieved by extending the current capabilities of the MOOSE of two its native physical modules, namely Porous Flow and Tensor Mechanics. We call this workflow RHEA (Real HEterogeneity

App). RHEA is based on MOOSE's modular ecosystem and combines the capabilities of Porous Flow and Tensor Mechanics with material objects that are newly developed in our work and provide the novel ability to allocate spatially distributed properties at element-resolution in the mesh. By integrating new C++ objects, we modified the underlying MOOSE code within PorousFlow and Tensor Mechanics. To streamline pre-processing efforts arising from this improvement, we developed a Python-based, automated workflow which uses standard data format to generate input files that are compatible with the material objects in MOOSE format. Finally, we verified the correctness of RHEA with a newly developed, analytical benchmark problems allowing vertical heterogeneity and illustrated its performance using a sophisticated 2D example with distributed hydraulic and mechanical heterogeneity. In this work, we first describe the workflow required to compile a RHEA app, formulate a modelling problem and run a simulation. We then compare RHEA's simulation results with one and two dimensional analytical solutions, and propose a benchmark semi-analytical solution to validate RHEA's performance when sharp gradients are present. Finally, we apply RHEA to a complicated two dimensional problem with centimetre-scale heterogeneities demonstrating its capabilities. We anticipate that our work will lay the foundation for accurate numerical modelling of hydro-geomechanical problems allowing full spatial heterogeneity.

2.2 Governing equations

Modelling of coupled hydro-geomechanical processes requires solving the equations describing fluid flow in a deformable porous medium. The coupled processes can be described physically in a representative elementary volume (REV) by a balance of fluid, mass and momentum, where local equilibrium of thermodynamics is assumed and macroscopic balance equations are considered to be the governing equations. In this section, the governing equations for hydro-geomechanical processes in a fully saturated porous medium with liquid fluid are presented on the basis of Biot's theory of consolidation. In the pore pressure formulation, the field variables are the liquid phase pressure p_f and the displacement vector $\vec{u}$. The material parameters can be spatially variable, but remain independent of time. Permeability and elastic parameters are described as tensors, whereas the Biot coefficient is a scalar.

Fluid flow within a deformable and fully saturated porous medium is described by the continuity equation

$$\frac{1}{M}\frac{\partial p_f}{\partial t} + \alpha\frac{\partial \varepsilon_{kk}}{\partial t} + \nabla \cdot \vec{q}_d = Q_f \ , \tag{2.1}$$

where α is the Biot coefficient, ε_{kk} the volumetric strain, Q_f a fluid sink or source term and M is the Biot modulus of the porous medium (the reciprocal of the storage coefficient). In Biot's consolidation theory, the Biot modulus is defined as

$$\frac{1}{M} = \frac{\phi}{K_f} + \frac{(\alpha - \phi)}{K_s} \ , \tag{2.2}$$

where ϕ, K_f, K_s represent the porosity, fluid and solid bulk modulus respectively. As Darcy flow is assumed, the fluid discharge $\vec{q}_d$ can be expressed as a momentum balance of the fluid like

$$\vec{q}_d = \phi(\vec{v}_f - \vec{v}_s) = -\frac{\vec{k}}{\rho_f \vec{g}}(\nabla p_f - \rho_f \vec{g}) \ , \tag{2.3}$$

where $\vec{v}_f$ and $\vec{v}_s$ are the fluid and solid matrix velocities respectively; $\vec{k}$ is the permeability tensor; μ_f is the dynamic viscosity of the fluid; ρ_f is the density of the fluid and $\vec{g}$ is the gravitational

acceleration vector.

The mechanical model is defined via momentum balance in terms of the effective Cauchy stress tensor $\vec{\sigma}'(x, t)$ as

$$\nabla(\vec{\sigma}' - \alpha p_f \mathbb{I}) + \rho_b \vec{g} = 0 , \tag{2.4}$$

where $\mathbb{I}$ is the rank-two identity tensor. The mass of fluid per volume of porous medium is expressed as the sum of the phases

$$\rho_b = \phi \rho_f + (1 - \phi)\rho_s , \tag{2.5}$$

where ρ_s is the solid density. The elastic strain can be expressed in terms of displacements with the relation

$$\vec{\varepsilon} = \frac{1}{2}(\nabla \vec{u} + \nabla^T \vec{u}) . \tag{2.6}$$

The effective stress is related to elastic strains by the generalized Hooke's law:

$$\vec{\varepsilon} = \varepsilon_{ij} = \mathbb{C}_{ijlk} \sigma'_{ij} , \tag{2.7}$$

where $\mathbb{C}_{ijkl}$ is the elastic compliance tensor.

Together, Eqs. 2.1 to 2.7 constitute the coupled system that represents hydro-geomechanical systems with linear elastic deformation.

As a derivative of the MOOSE framework, RHEA enables access to a wide array of options to fine tune a simulation. Solver options such as numerical schemes, adaptive time-stepping as well as general PETSc options are available. By default, RHEA uses a first order fully-implicit time integration (backward Euler) for unconditional stability and solves the coupled equations simultaneously (full coupling) (Kavetski et al., 2002; Manzini & Ferraris, 2004; Gaston et al., 2009). RHEA also allows operator splitting to implement loose coupling, i.e., solving the fluid flow while keeping the mechanics fixed, then solving the mechanics while keeping the fluid-flow fixed. While this can be executed on separate meshes with different time-stepping schemes, this feature is not explored in the current article (Martineau et al., 2020).

Explicit time integration (with full or loose coupling) and other schemes such as Runge-Kutta are available in MOOSE and RHEA, but stability limits the time-step size, so these are rarely used in the type of subsurface problems handled by RHEA. By default, MOOSE and RHEA use linear Lagrange finite elements (tetrahedra, hexahedra and prisms for 3D problems, triangles and quads for 2D problems), but higher-order elements may be easily chosen if desired (Hu, 2017).

RHEA does not implement any numerical stabilization for the fluid equation to eliminate overshoots and undershoots, however, fluid volume is conserved at the element level (Cacace & Jacquey, 2017). Although not explored in this study, RHEA's fluid flow may be extended to multi-phase, multi-component flow with high-precision equations of state, as well as finite-strain elasto-plasticity (Wilkins et al., 2020).

2.3   Building RHEA

Real Heterogeneity App (RHEA) is an open-source simulation workflow and tool specifically developed to allow fully coupled numerical simulations in a saturated porous medium with spatially distributed heterogeneity in hydraulic and geomechanical properties. We built RHEA as

a derivative of MOOSE, the massively parallel and open source FE simulation environment for coupled multi-physics processes (Gaston et al., 2009; Permann et al., 2020). MOOSE offers virtually unlimited simulation capabilities covering a wide spectrum of applications. This is based on a workflow where the end user does not need to know the details of the FE implementation. To achieve that, MOOSE utilises the libMesh library, a framework capable of manipulating multi-scale, multi-physics, parallel and mesh-adaptive FE simulations (Kirk et al., 2006). While the numerical methods, solvers and routines are executed by PETSc libraries (Balay et al., 2019), MOOSE is designed to allow the user to interact and control these two libraries without having to do any complex programming. Instead, the user frames the problem simply through an input file with unique syntax.

We found that learning how to perform numerical simulations based on the MOOSE framework is not a trivial task. Our aim is to further develop modelling capabilities while simplifying the complexity of the problem through an easy to follow workflow accompanied by a visual summary. The RHEA workflow can be summarised as follows:

Step 1 - RHEA compilation: The user creates the RHEA application following the structure outlined in Fig. 2.1. In other words, the user creates an executable file which is able to model fully coupled hydro-gemechanical systems in a heterogenous medium. We accomplished this through new MOOSE-based materials functions able to allocate data in each element of the mesh based on a pre-generated input file. Furthermore, we integrated the multi-physics of Section 2.2 to RHEA by adding the Porous Flow (Wilkins et al., 2020) and Tensor Mechanics modules that are part of the MOOSE framework. Once RHEA is downloaded, the user can access the necessary files to build RHEA, and can even access those files to modify the physics. This procedure is generic for any new MOOSE application. The core components of any MOOSE app such as RHEA are (Fig. 2.1):

Block 1 - Kernels: The *kernels* (or partial differential equation terms) describing the physics are implemented in their weak form (Jacob & Ted, 2007). In the MOOSE ecosystem, PDEs are represented by one simple line of code, this is highlighted with a cyan rectangle in Fig. 2.1. This straightforward way of describing complex multi-physics constitutes the most powerful feature of MOOSE.

Block 2 - Material properties: Values, including spatially-distributed values can be prescribed for each of the materials appearing in the *kernels*.

Block 3 - Kernel coupling: The user can couple different physics by including different *kernels* in its model, or by creating new *kernels*.

This dynamic procedure allows flexible creation of the RHEA application or any MOOSE-based application requiring minimal knowledge of C++ programming skills.

Step 2 - Preparation of material properties: The spatially distributed data is formatted to the structure required by the RHEA app compiled in Step 1. We implemented this with a custom Python script that imports and formats the original CSV or VTK dataset into a RHEA-compatible data structure. Within RHEA, the hydro-geomechanical material properties are field properties which means that each value in the data set has to be allocated to a respective mesh element. Therefore, when the mesh is generated, the discretization has to match the number of data points of the data set. That way, each property value is represented within the simulation. Note that if this is not done correctly, RHEA may assign undesired property values. This is because RHEA will automatically linearly interpolate any values provided to the mesh. Thus, if the initial mesh discretization does not match

Step 1 - RHEA compilation

Clone RHEA — MOOSE

```
>>
cd ~/projects
git clone https://github.com/josebastiase/RHEA.git
```

Block 1 - Kernels

```
>>
QPResidual()
{
  return _velocity[_qp] *_grad_u[_qp];
}
```

Block 2 - Material properties

```
>>
QpStatefulProperties()
{
  _material[_qp] = _input_material;
}
```

Block 3 - Physics coupling

```
>>
  Kernel(parameters),
  _coupled_var(
    coupledGradient("coupled_variable"))
```

Build RHEA

```
>>
cd ~/projects/RHEA
make -j4
```

RHEA

Define, retrieve and store coupled variable

Material plumbing

Step 2 - Preparation of material properties

Import properties — Prepare data files

CSV

Assign properties to mesh elements

Porosity · Permeability · Shear modulus · Bulk modulus

```
x:
  x₁  x₂  x₃
y:
  y₁  y₂
Data:
```

Export material property in MOOSE compatible file format

Step 3 - Simulation setup and control

Create a RHEA simulation

System	Input file

Mesh
Mesh dimensions and refinement
 - MOOSE mesh generator system
 - Import mesh from file

```
>>
[Mesh]
  type = GeneratedMesh
  dim = 1
  xmin = 0
  xmax = 10
  nx = 10
[]
```

Functions
Load spatially distributed material properties into RHEA

```
[Functions]
  [ShearModulusFcn]
    type = PiecewiseMulticonstant
    direction = 'right left'
    data_file = ShearModulus.data
  []
[]
```

Variables
Unknowns of PDE system used by the "Kernels" block

```
[Variables]
  [diffused]
    order = FIRST
    family = LAGRANGE
  []
[]
```

AuxVariables
Variable where the imported material properties is stored

```
[AuxVariables]
  [ShearModulus]
    order = CONSTANT
    family = MONOMIAL
  []
[]
```

Kernels
Physics of the governing equations. Defined in the weak form of PDEs

```
[Kernels]
  [./diff]
    type = Diffusion
    variable = diffused
  []
[]
```

AuxKernels
Assign the spatial distributed data to the AuxVariables

```
[AuxKernels]
  [ShearModulus]
    type = FunctionAux
    function = ShearModulusFcn
    Variable = ShearModulus
    execute_on = initial
  []
[]
```

Boundary conditions
System's contraints. Adaptable to system's physics

```
[BCs]
  [bottom]
    type = DirichletBC
    variable = diffused
    boundary = 'top bottom'
    value = 0
  []
[]
```

Materials
System properties
Spatially varying and nonlinear behavior

```
[Materials]
  [VariableIsotropicTensor]
    shear_modulus = ShearModulus
    bulk_modulus = BulkModulus
  []
[]
```

Executioner
Control solver behavior and time stepping

```
[Executioner]
  type = Steady
  solve_type = Newton
[]
```

Outputs
Define the simulation's output file

```
[Outputs]
  exodus = true
[]
```

Run simulation and visualize results

```
>>
./RHEA-opt -i YourRHEAFile.i
```
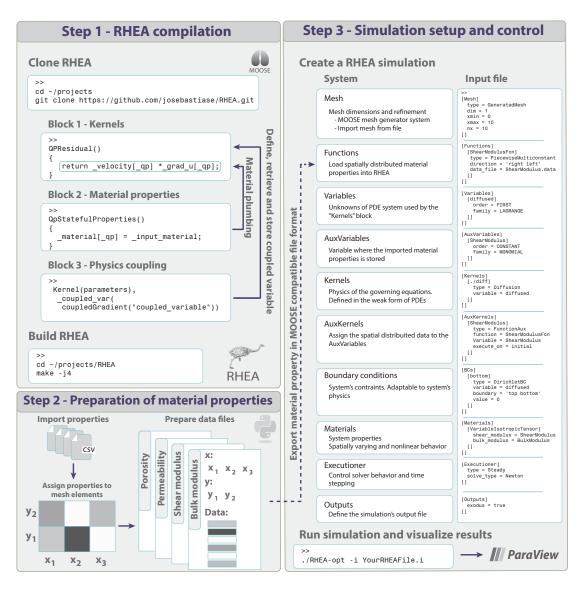→ ParaView

Figure 2.1: Visual illustration of the steps required to create RHEA, generate distributed material properties files and write a simulation script.

the user-supplied samples, interpolated values are assigned which could lead to undesired results.

Step 3 - Simulation setup: To define the numerical model, a RHEA script has to be created in the standard MOOSE syntax. The script consists of an array of systems that describe the mesh, physics, boundary conditions, numerical methods and outputs. A short example along with brief system descriptions is illustrated in Fig. 2.1. The blocks consist of MOOSE functions that are written and design in a generic manner and independently of the nature of the problem, this way the blocks can be recycled and reused. The spatially distributed material properties can be imported into the *Function* system and subsequently be stored in the *AuxVariable* system to be assigned as material property in the *Materials* block.

In summary, numerical simulations of hydro-geomechanical problems with spatially distributed material properties can be performed by calling RHEA's executable file (created in Step 1) using the simulation control script (created in Step 3) which contains the necessary instructions as well as reading in the spatially distributed material properties (created in Step 2).

2.4 Verifying RHEA

To test if RHEA accurately solves the differential equations stated in Sect. 2.2 and if boundary conditions are correctly satisfied, four different tests were developed. The proposed tests use predefined material properties that were imported into RHEA using the workflow presented in Sect. 2.3. The tests were designed to gradually build up complexity and cover the typical spectrum of consolidation problems. In two of the examples, RHEA's performance in simulations with sharp gradients is tested. First, a one dimensional consolidation problem where the hydraulic conductivity varies in four orders of magnitude between layers and a second two dimensional example with realistic heterogeneity in which the hydraulic conductivity of the geological facies varies over six orders of magnitude.

The first test, the classical Terzaghi's problem, is used as a basic benchmark of the hydro-mechanical coupling in RHEA. In later sections, we illustrate the full potential of RHEA when simulating spatially-heterogeneous systems in one and two dimensions. The four verification scenarios are described in the following subsections. All numerical solutions were calculated using an 8 core Intel i7-3770 CPU @ 3.40GHz with 32 GB DDR4 RAM memory and the results were stored on a hard disk drive.

2.4.1 Terzaghi's problem

In the one dimensional consolidation problem, also known as Terzaghi's problem (Terzaghi, 1923), a single load q is applied at $t = 0$ on the top of a fully saturated homogeneous sample with the height L. The system is only drained at the top, where the pressure of the fluid is assumed to be $p = 0$ for $t > 0$. At the moment of loading, $t = 0$, the undrained compressibility of the solid increases the pressure of the sample. For $t > 0$, the system is allowed to drain and the consolidation processes begins.

In the absence of sources and sinks, Eq. 2.1 is reduced to the basic storage equation as

$$\frac{1}{M}\frac{\partial p_f}{\partial t} + \alpha\frac{\partial \varepsilon_{zz}}{\partial t} = \frac{k}{\gamma_f}\frac{\partial^2 p_f}{\partial z^2}, \tag{2.8}$$

where the product $\rho_f \cdot g$ was written as γ_f and represents the volumetric weight of the fluid. Eq. 2.3 is used to couple the fluid discharge $\vec{q}_d$. From Hook's law, assuming one-dimensional deformation, the vertical strain equals the volume change

$$\frac{\partial \varepsilon_{zz}}{\partial t} = -m_v\frac{\partial \sigma'_{zz}}{\partial t} = -m_v\left(\frac{\partial \sigma_{zz}}{\partial t} - \alpha\frac{\partial p_f}{\partial t}\right), \tag{2.9}$$

where m_v is the confined compressibility of the porous medium

$$m_v = \frac{1}{K_s + (4/3)G_s} \tag{2.10}$$

and K_s and G_s are the bulk and shear moduli of the porous medium respectively. Substituting Eq. 2.9 into the storage equation (Eq. 2.8), the general differential equation for one dimensional consolidation is obtained:

$$\frac{\partial p_f}{\partial t} = \frac{\alpha m_v}{(1/M + \alpha^2 m_v)}\frac{\partial \sigma_{zz}}{\partial t} + \frac{k}{\gamma_f(1/M + \alpha^2 m_v)}\frac{\partial^2 p_f}{\partial z^2} \tag{2.11}$$

For $t > 0$, the total load q is kept constant and the total stress σ_{zz} is also constant. Consequently,

Eq. 2.11 reduces to

$$t > 0 : \quad \frac{\partial p_f}{\partial t} = \frac{k}{\gamma_f(1/M + \alpha^2 m_v)} \frac{\partial^2 p_f}{\partial z^2}. \tag{2.12}$$

Since the system is undrained at $t = 0$, the initial condition can be established from Eq. 2.11 as

$$t = 0 : \quad p_f = p_0 = \frac{\alpha m_v}{(1/M + \alpha^2 m_v)} q. \tag{2.13}$$

The boundary conditions at the top and bottom of the sample are

$$t > 0, \, z = L : \quad p_f = 0 \tag{2.14}$$

and

$$t > 0, \, z = 0 : \quad \frac{\partial p_f}{\partial z} = 0. \tag{2.15}$$

The analytical solution of the problem is well known and reads (Wang, 2017; Cheng, 2016; Verruijt, 2018)

$$\frac{p_f}{p_0} = \frac{4}{\pi} \sum_{k=1}^{\infty} \frac{(-1)^{k-1}}{2k - 1} \cos\left[(2k-1)\frac{\pi}{2}\frac{z}{L}\right] \exp\left[-(2k-1)^2 \frac{\pi^2}{4} \frac{kt}{\gamma_f(1/M + \alpha^2 m_v)L^2}\right]. \tag{2.16}$$

For this example, the height of the sample was set to 100 m, the hydraulic conductivity is $1 \cdot 10^{-4}$ ms^{-1}, the porosity is 0.2, the Biot coefficient is 0.9, the bulk modulus is $8.40 \cdot 10^7$ Pa and the shear modulus is $6.25 \cdot 10^7$ Pa. The performance and consistency of RHEA on the consolidation problem is shown as pore pressure versus depth profiles at discrete times in Fig. 2.2a. A comparison of the analytical and RHEA's solution reveals excellent agreement, thereby verifying the numerical solution. The total time for computing 101 time steps was 1.92 s.

2.4.2 Layered Terzaghi's problem

The objective of this test is to investigate the performance of RHEA when heterogeneity and sharp gradients are present. The consolidation experiment of the previous section is performed on a sample with multiple layers of contrasting properties. For simplicity, porosity and mechanical parameters are assumed homogeneous. Since the total load q is constant for $t > 0$, Eq. 2.11 reduces to Eq. 2.12 across n layers as follows

$$t > 0 : \quad \frac{\partial p_{fi}}{\partial t} = \frac{k_i}{\gamma_f(1/M + \alpha^2 m_v)} \frac{\partial^2 p_{fi}}{\partial z^2}, \quad i \in [1, n], \tag{2.17}$$

which describes the consolidation in each layer. Here, $z_{i-1} \leq z \leq z_i$ is the depth of the sample, p_{fi} and k_i are the fluid pressure and permeability of the solid in each layer i, respectively. The contact between layers is assumed to be perfect, i.e. the boundary conditions at the layers is represented by equivalent matching fluid pressure as

$$t > 0, \, z = z_i : \quad k_i \frac{\partial p_{fi}}{\partial z} = k_{i+1} \frac{\partial p_{fi+1}}{\partial z}. \tag{2.18}$$

The sample is drained at the top, whereas the bottom remains undrained

$$t > 0, \, z = z_0 = L : \quad p_f = 0 \tag{2.19}$$

and

$$t > 0,\ z = z_n = 0 : \ \frac{\partial p_f}{\partial z} = 0. \tag{2.20}$$

The fluid pressure produced by the external load starts to dissipate when $t > 0$, but at different rates depending on the consolidation coefficient of the layer. The height of the sample is 100 m and 10 layers are equally distributed along the sample with 10 m height. To represent sharp gradients, the selected hydraulic conductivities have four orders of magnitude difference between layers, $1 \cdot 10^{-4}$ ms^{-1} and $1 \cdot 10^{-8}$ ms^{-1}. The high and low permeability layers are alternating. The porosity is set to 0.2, the Biot coefficient is 0.9, the bulk modulus is $8.40 \cdot 10^7$ Pa and the shear modulus is $6.25 \cdot 10^7$ Pa.

A step-by-step semi-analytical solution of the diffusion problem in a layered sample was derived by Hickson et al. (2009). To solve this problem in RHEA, a mesh of 100 elements was used with a time step of $1 \cdot 10^4$ s. The total time for computing 701 time steps was 13.8 s. A comparison between the analytical solution and RHEA's numerical simulation is shown in Fig. 2.2b. In the layers with high hydraulic conductivity, the consolidation process occurs rapidly leading to faster pore pressure dissipation (vertical pore pressure profile), and therefore also faster water movement. In contrast, the consolidation process is slower in the low conductivity layers with slower pore pressure dissipation and water movement.

2.4.3 Plane strain consolidation

To evaluate the performance of RHEA for two-dimensional heterogeneity, a consolidation problem with plane strain is developed. The two-dimensional consolidation caused by a uniform load over a circular homogeneous area can be represented by the storage equation (Eq. 2.1) in two dimensional case as

$$\frac{1}{M} \frac{\partial p_f}{\partial t} + \alpha \frac{\partial \varepsilon}{\partial t} = \frac{k}{\gamma_f} \left(\frac{\partial^2 p_f}{\partial x^2} + \frac{\partial^2 p_f}{\partial z^2} \right) \tag{2.21}$$

where ε represents the volumetric strain. Including two equilibrium equations, in terms of total stress, as

$$\frac{\partial \sigma_{xx}}{\partial x} + \frac{\partial \sigma_{zx}}{\partial z} = 0 \tag{2.22}$$

and

$$\frac{\partial \sigma_{xz}}{\partial x} + \frac{\partial \sigma_{zz}}{\partial z} = 0. \tag{2.23}$$

The total stress is related to the effective stress through

$$\sigma_{xx} = \sigma'_{xx} + \alpha p \qquad \sigma_{xz} = \sigma'_{xz} \tag{2.24}$$

and

$$\sigma_{zz} = \sigma'_{zz} + \alpha p \qquad \sigma_{zx} = \sigma'_{zx}. \tag{2.25}$$

The analytical solution can be found by expressing the equilibrium Eq. 2.22 and Eq. 2.23 in terms of the displacement components u_x and u_z using Hooke's law as

$$\sigma'_{xx} = -\left(K_s - \frac{2}{3} G_s \right) \varepsilon - 2 G_s \frac{\partial u_x}{\partial x} \tag{2.26}$$

and

$$\sigma'_{zz} = -\left(K_s - \frac{2}{3} G_s \right) \varepsilon - 2 G_s \frac{\partial u_z}{\partial z} \tag{2.27}$$
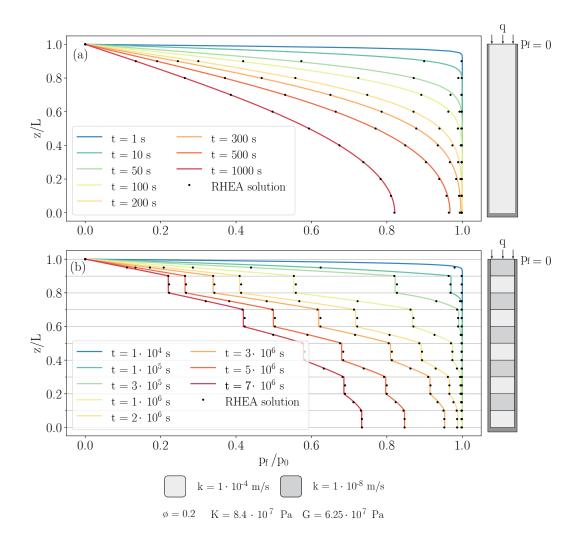
Figure 2.2: The lines represent the analytical solution whereas the dots represent the RHEA solution. (a) Homogeneous case. For this simulation, a total of 100 nodes and 99 elements were set. (b) Heterogeneous case. For this simulation, a total of 100 nodes and 99 elements were set.

and

$$\sigma'_{xz} = \sigma'_{zx} = -G_s \left(\frac{\partial u_z}{\partial x} + \frac{\partial u_x}{\partial z} \right).$$ (2.28)

Here, the assumed plane strain is the y axis, i.e. $u_y = 0$. Replacing Hooke's law in plane strain (Eq. 2.26 to 2.28) with the effective stress balance (Eq. 2.22 and Eq. 2.23 combined with Eq. 2.24 and Eq. 2.25) leads to a complete system of equations as

$$\left(K_s + \frac{1}{3} G_s \right) \frac{\partial \varepsilon}{\partial x} + G_s \nabla^2 u_x - \alpha \frac{\partial p_f}{\partial x} = 0$$ (2.29)

and

$$\left(K_s + \frac{1}{3} G_s \right) \frac{\partial \varepsilon}{\partial z} + G_s \nabla^2 u_z - \alpha \frac{\partial p_f}{\partial z} = 0,$$ (2.30)

where the elastic strain is

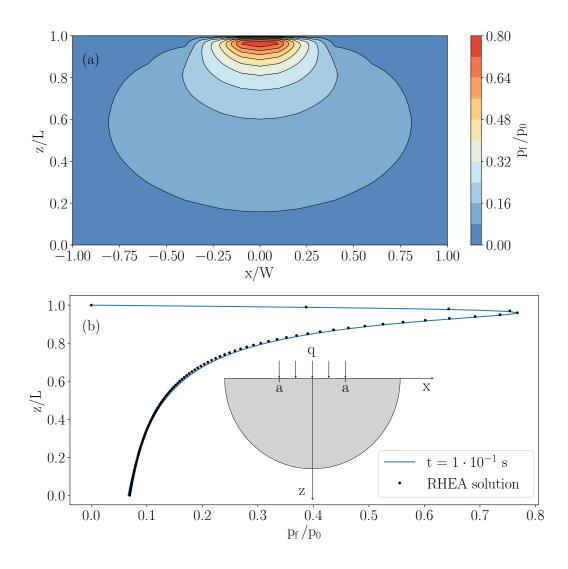$$\varepsilon = \frac{\partial u_x}{\partial x} + \frac{\partial u_z}{\partial z}.$$ (2.31)

Figure 2.3: The solution of the consolidation problem in plane strain by RHEA is shown in a sample 10 m wide and height. (a) Contour plot of the solution at time $1 \cdot 10^{-2}$ s. (b) A comparison of the semi-analytical solution (continuous line) and the RHEA solution (dotted line). The differences in pore pressure between both approaches is due to the assumption of an infinite domain in the analytical solution which is not feasible to replicate the latter with RHEA.

The boundary conditions are represented by a constant load in an area of width $2a$, applied at $t = 0$. The system is allowed to drain for $t > 0$ as

$$t > 0, \; z = 0 : \; p_f = 0 \tag{2.32}$$

and

$$t > 0, \; z = 0 : \; \sigma_{zz} = \begin{cases} q, & |x| < a \\ 0, & |x| > a \end{cases} \tag{2.33}$$

and

$$t > 0, \; z = 0 : \; \sigma_{xz} = 0. \tag{2.34}$$

When the sample is loaded, a confined pore pressure in generated which starts to drain instantaneously through the borders of the system. A semi analytical solution in the Fourier domain and Laplace transform for the given equation system and boundary conditions is presented in Verruijt (2013). The height and the width of the sample are 10 m. The load is applied

on the surface of the sample between -1 and 1 m. The hydraulic conductivity is $1 \cdot 10^{-5}$ ms^{-1}, the porosity is 0.2, the Biot coefficient is 0.9, the bulk modulus is $8.40 \cdot 10^7$ Pa and the shear modulus is $6.25 \cdot 10^7$ Pa. To solve this problem, a coarse mesh was defined, and MOOSE's native mesh adaptivity system was employed to automatically generate a finer resolution in areas where the pore pressure gradients are steep. This significantly reduces the computational time when compared with using a fine mesh throughout. The total simulation time was 312.6 s for 101 time steps and 10000 elements with 20502 nodes.

The results are illustrated in two figures, Fig. 2.3a shows a cross section of the sample as contour plot. Fig. 2.3b shows a pore pressure profile with depth at the center of the sample $x = 0$. Excellent agreement between the analytical solution and the simulated solution by RHEA is observed.

2.4.4 Modelling realistic geology

The last example aims to study and illustrate the performance of RHEA's with a real data set. This example illustrates how to generate input files using the developed workflow and demonstrates the potential of RHEA for simulating increased spatial complexity and sharp gradients. While the Herten analog is a 3D data set, the example was reduced to two dimensions to facilitate presentation. However, simulations in three dimensions are also possible and can be done using the presented workflow in unmodified form. The 2D consolidation problem was solved with RHEA, integrating the multi-facies realizations and material properties of the Herten analog (Bayer et al., 2015). Although the data set does not contain geomechanical subsurface properties, the hydraulic conductivity varies over six orders of magnitude which provides sufficient proof of RHEA's capabilities.

Herten aquifer dataset description

Realistic modelling relies not only on accurate data concerning material parameters, but also on appropriate spatial distribution of such parameters (Houben et al., 2018; Irvine et al., 2015; Kalbus et al., 2009). Typically, distributed material parameters are generated by stochastic random fields based on an *a priori* statistical distribution (Vanmarcke et al., 1986). Although random fields have proven to be useful, they do not capture the usual continuity of material parameters (Strebelle, 2002). Consequently, the use of high resolution data, such as "aquifer analogs", is preferred (Alexander, 1993; Zappa et al., 2006). Aquifer analogs consist of centimeter-resolution data obtained from detailed investigation of geological formations at outcrops. Although aquifer analogs are rare, they have been widely used in different subsurface fields (Höyng et al., 2015; Beaujean et al., 2014; Finkel et al., 2016). The Herten analog is a well-known and rigorously generated 2D outcrop (Bayer et al., 2015). It consists of a fluvial braided river deposit from the south east of Germany, which represents one of the most important drinking water resources in central Europe. Its architecture consists of sedimentary facies, and its body of unconsolidated gravel and well sorted sand. The dimensions of the 2D outcrop are 16 m wide by 7 m high, and features horizontal and vertical data resolution of $5 \cdot 10^{-2}$ m for hydraulic conductivity and porosity. Hence, the 2D cross-section has a total of 4480 measurements points. The corresponding hydraulic conductivity k, ranges from $6 \cdot 10^{-7}$ ms^{-1} to $1.30 \cdot 10^{-1}$ ms^{-1}, and porosity ϕ, from 0.17 to 0.36 (Fig. 2.4a). To represent spatial distribution of mechanical properties, typical values of bulk and shear moduli for gravel and sand were assumed to be linearly correlated with the porosity of the aquifer: similar trends have been reported in previous studies (Mondol et al., 2008; Hardin & Kalinski, 2005; Hicher, 1996). Representative geomechanical moduli can be

Material	Young's modulus (MPa)	Poisson's ratio (-)	Reference
Loose gravel	48 - 148	-	(Subramanian, 2011)
Dense gravel	96 - 192	-	(Subramanian, 2011)
Gravel	50 - 100	0.3 - 0.35	(Look, 2014)
Sand and gravel	69.0 - 172.5	0.15 - 0.35	(Das, 2019)
Gravel	68.9 - 413.7	0.4	(Xu, 2016)
Dense sand	-	0.3 - 0.4	(Lade, 2001)
Loose sand	-	0.1 - 0.3	(Lade, 2001)
Gravel	-	0.1 - 0.4	(Kulhawy & Mayne, 1990)

Table 2.1: Typical elastic properties of sand and gravel.

found in soil mechanics literature as shown in Table 4.1. The elastic tensor is assumed isotropic in this example, hence elastic moduli are related via (Wang, 2017; Cheng, 2016)

$$
\begin{aligned}
K_s &= \frac{E_s}{3(1 - 2\nu_s)} \\
G_s &= \frac{E_s}{2(1 + \nu_s)} ,
\end{aligned}
$$

(2.35)

where E_s and ν_s denote the Young's modulus and Poisson's ratio of the solid material respectively. The result is that the bulk moduli vary between $6.70 \cdot 10^7$ Pa and $1.70 \cdot 10^8$ Pa, whereas the shear moduli range between $3.0 \cdot 10^7$ Pa and $3.50 \cdot 10^8$ Pa, as shown in Fig. 2.4a. RHEA does not require the mechanical moduli to be related to the hydraulic properties in the way we have described in this particular example.

Problem and model description

The two dimensional consolidation is described by Eqs. 2.21, 2.29 and 2.30. A constant load at the top of the sample is applied at $t > 0$, which generates a confined pore pressure. After that, the system is allowed to drain through the top boundary and is subjected to the normal stress. The sample's bottom and sides are impermeable to the fluid, and subject to roller boundary conditions.

For this simulation, a quadrilateral mesh was generated with the mesh generator system of MOOSE. The mesh has 44800 elements and 44940 nodes, which matches the data set resolution. Since the material properties of the data set differs in orders of magnitude, the mesh adaptivity system of MOOSE was used to ensure accurate results. At each time step the 30% of elements with the highest pore pressure gradient were refined, which reduces the local error at contrasting facies. Hence the mesh is refined in each time step. At the end of the simulation, the number of nodes had grown to 708548 and the number of elements to 631615. The total simulation time was 0.49 hours for 70 time steps and 44341 elements with 44800 nodes.

Simulation results

The pore pressure profiles depicted in Fig. 2.5 illustrate how the physical heterogeneity of the cross-bedded data set strongly influences the fluid flow through the sample. The effect of the centimeter resolution of the data set can be studied when the initial load is applied at $t = 0$. Since the sample is not yet allowed to drain, confined porepressure is generated which depends on the geomechanical characteristics of the sand and gravel. In facies where the soil is highly compressible, the generated pore pressure is also relatively high since the total load is shared
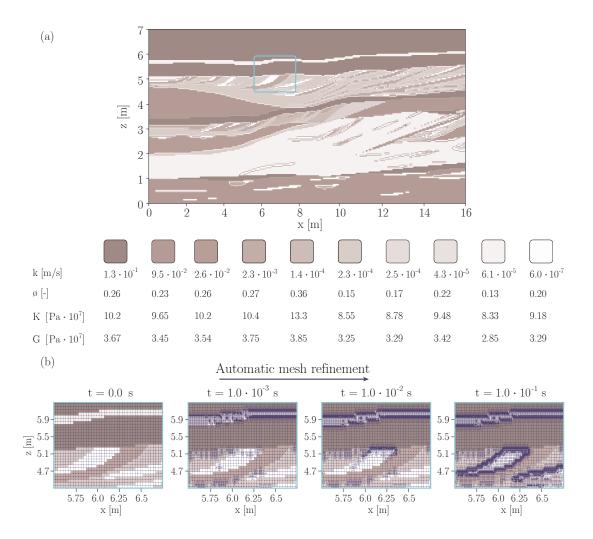
Figure 2.4: Facie architecture and properties of the Herten aquifer analog. (a) Color scale of the hydro-geomechanical properties of the aquifer imported to RHEA. (b) Shows the mesh discretization and its dynamic evolution when the mesh adaptivity system is activated. The time evolution is shown from left to right.

between the the fluid and the soil. In contrast, in facies that have higher elastic moduli values the confined pore pressure is relatively low. This effect is nicely shown in Fig. 2.5a. At time $t > 0$ the top of the sample is allowed to drain. The effect of the highly permeable units made of poorly sorted and well sorted gravel is shown in Fig. 2.5b. The top facie of the aquifer consists of a highly permeable soil ($k = 1.30 \cdot 10^{-1}$ ms^{-1}), which is divided by a thin low permeable layer ($k = 6.10 \cdot 10^{-5}$ ms^{-1}), the latter causes contrasting pore pressure profiles. Similar permeability effects have been discussed before (Choo & Lee, 2018; Peng et al., 2017; Kadeethum et al., 2019). The influence of the temporal and spatial scales on the consolidation process is shown in Fig. 2.5c and 2.5d. It can be observed that the process occurs rather quickly and is strongly influenced by the low permeability facies. This example demonstrates that RHEA can solve complex and realistic heterogenous hydro-geomechanical coupled problems.

2.5 Conclusions

In this paper we develop and verify Real HEterogeneity App (RHEA): a numerical simulation tool that allows fully coupled numerical modelling of hydro-geomechanical systems. Moreover, RHEA can easily include full heterogeneity of parameters as occurs in real subsurface systems.
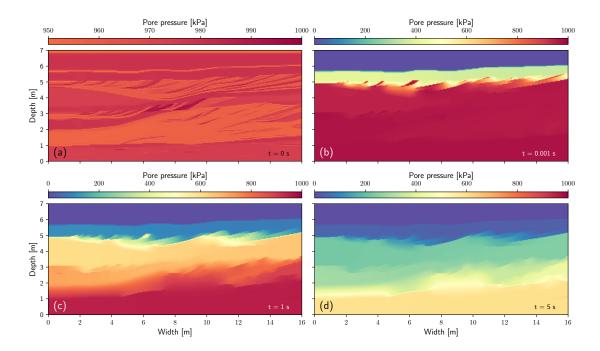
Figure 2.5: Sequence of snapshots of the consolidation process and pore pressure variation in the aquifer with time. (a) Displays the initial condition of the simulation. (b) Snapshot at time $1 \cdot 10^{-3}$ s. (c) Snapshot at time 1 s. (d) Snapshot at time 5 s. Note that (a) uses a different colour range to highlight the small variations in pore pressure.

RHEA is based on the powerful Multiphysics Object-Oriented Simulation Environment (MOOSE) open source framework. Furthermore, we provide an easy-to-understand workflow which explains how to compile the application and run a customised numerical simulation. Despite its simplicity, the workflow combines all the technical advantages provided by MOOSE and its well established framework. The latter allows the development and use of state-of-the-art and massively scalable applications backed by the unconditional support of a growing community.

Beyond unlocking the ability to include full heterogeneity of hydro-geomechanical parameters in simulations, our contribution provides examples to verify future numerical codes. Additionally, a semi-analytical benchmark problem is proposed to verify the performance of numerical code when heterogeneity and sharp gradients are present.

Our example simulations illustrate that the subsurface hydro-geomechanical properties, in particular permeability (or transmissivity), play a key role in the consolidation process. Although this insight is valuable, it can lead to an oversimplification when models assume transmissivity varies heterogeneously while mechanical parameters are assumed homogeneous. This approach can lead to biased results in systems where different geologic formations are present. For example, land surface subsidence is a process that can occur due to anthropogenically induced decrease of subsurface pore pressure causing progressive consolidation and slow downward percolation across the layers within the subsurface. This process depends on the spatial distribution of the geomechanical properties, in particular those of clay layers within the subsurface. RHEA could be used to increase our understanding of the spatial and temporal evolution of land surface subsidence. Our newly developed workflow enable such advanced numerical simulations.

RHEA has the potential to advance our understanding of real world systems that have previously been oversimplified. Further, RHEA offers the integration of high resolution data set with sophisticated numerical implementations. Potential numerical instabilities caused by highly

heterogeneous systems (i.e. settings with sharp gradients) are handled automatically by combining adaptive meshing capabilities with implicit time stepping. While this work demonstrates RHEA's capabilities for two dimensional problems, this can easily be extended to three dimensional simulations. In that case, a three dimensional mesh that is representative of the spatially distributed hydraulic and geomechanical properties of any available dataset can be generated. The tasks follow the data formatting workflow and simulation control as described in Section 3.

Our current work focuses on hydro-geomechanical coupling of heterogeneous systems. However, RHEA could potentially be extended to include also thermal processes. While it would allow fully coupled simulations of thermal-hydraulic-mechanical (THM) systems including spatially distributed heterogeneities, verification will require the development of more advanced analytical solutions, a task that however is beyond the scope of this contribution.

Chapter 3

Groundwater responses to Earth tides: Evaluation of analytic solutions using numerical simulation

Abstract

Harmonic Earth tide components in well water levels have been used to estimate hydraulic and geomechanical subsurface properties. However, the robustness of various methods based on analytical solutions has not been established. First, we review the theory and examine the latest analytical solution used to relate well water levels to Earth tides. Second, we develop and verify a novel numerical model coupling hydraulics and geomechanics to Earth tide strains. Third, we assess subsurface conditions over depth for a range of realistic properties. Fourth, we simulate the well water level response to Earth tide strains within a 2D poroelastic layered aquifer system confined by a $100\ m$ thick aquitard. We find that the non-linear inversion of analytical solutions to match two observations (amplitudes and phases) to multiple unknown parameters is sensible to the initial guess. We reveal that undrained, confined conditions are necessary for the analytical solution to be valid. This occurs for the dominant M_2 frequency at depths $> 50\ m$ and requires specific storage at constant strain of $S_\epsilon \geq 10^{-6}\ m^{-1}$, hydraulic conductivity of the aquitard of $k_l \leq 5 \cdot 10^{-5}\ ms^{-1}$ and aquifer of $k_a \geq 10^{-4}\ ms^{-1}$. We further illustrate that the analytical solution is valid in unconsolidated systems, whereas consolidated systems require additional consideration of the Biot modulus. Overall, a priori knowledge of the subsurface system supports interpretation of the groundwater response. Our results improve understanding of the effect of Earth tides on groundwater systems and its interpretation for subsurface properties.

3.1 Introduction

Earth tides have long been observed to influence groundwater systems Meinzer (1939), a phenomenon that is commonly expressed as harmonic water level fluctuations in monitoring wells Merritt (2004). Analytical solutions based on simplified concepts have been developed to enable calculation of subsurface hydraulic and geomechanical properties Cutillo & Bredehoeft (2011); Wang & Manga (2021); Rau et al. (2020a). Since Earth tides are an ubiquitous natural force, their response should be contained in the data from numerous wells around the world. In fact, a recent review found that interpreting the groundwater response to Earth tides is underutilized and that further development offers the potential for widespread application, which in turn would lead to increased knowledge of the subsurface McMillan et al. (2019a).

Changes in strain produced by Earth tides exert deformation onto the (semi-) confined subsurface resulting in pressure variations of the pore water. Such effects are embedded in the water levels measured within wells as small harmonic fluctuations with frequencies that depend on the Earth tide component (Figure 3.1). These signals have long been observed and can be used to estimate the subsurface hydro-geomechanical properties Merritt (2004); McMillan et al. (2019b). However, this requires good quality monitoring data-sets of the well water level measured at sufficient time intervals as well as predictions of Earth tide strains Rau et al. (2020c). The magnitude of Earth tide impacts on groundwater is most pronounced in well-known frequencies between 0.5 and 2.5 cycles per day (cpd) and can be extracted from groundwater measurements and Earth tide predictions Rojstaczer (1988); Rojstaczer & Riley (1990). For a given frequency, the ratio between the measured head at the observation well and the confined pore pressure produced by the change in strain is known as amplitude ratio (i.e. h_1/P_1 in Figure 3.1), whereas the time lag between these parameters is known as phase shift (i.e. $t_2 - t_1$ in Figure 3.1). If field data is available, harmonic least squares (HALS) with the main tidal components can be directly applied to the time series to obtain the amplitude ratio and phase shift between both signals Turnadge et al. (2019); Schweizer et al. (2021).

Field measurements of the groundwater response to Earth tides has resulted in negative and positive phase shifts between strain and well water levels. Negative phase shifts are interpreted as fully confined conditions and horizontal flow only Hsieh et al. (1987). For example, hydraulic conductivity and specific storage were estimated from negative phase shifts Roeloffs et al. (1989). However, positive phase shifts in the field were also observed and attributed to vertical flow through leaky aquitards Xue et al. (2016); Allègre et al. (2016). This was interpreted using the analytical solution of vertical flow in an homogeneous aquifer caused by a harmonic load or stress ignoring the effect of the observation well Wang (2017).

Early research developed and tested an analytical solution to estimate subsurface properties from the relationship between strain and water levels in observation wells in a fully confined aquifer Cooper Jr et al. (1967); Hsieh et al. (1987). This was extended to include leaky conditions and allow concurrent use of multiple frequencies Rojstaczer (1988); Rojstaczer & Riley (1990). Rojstaczer & Agnew (1989) studied the dependency of porosity and elastic parameters to a real deformation of a poroelastic medium. High sensitivity was reported when the applied strains occurs in low porosity and the increase with decreasing compressibility (inverse of the bulk modulus) of the solid matrix.

Recent research included modifications to the original analytical solution by Hsieh et al. (1987) to account for more realistic conditions. Most notable is the work by Wang et al. (2018) who developed an extended analytical solution which includes vertical leakage to model a two-
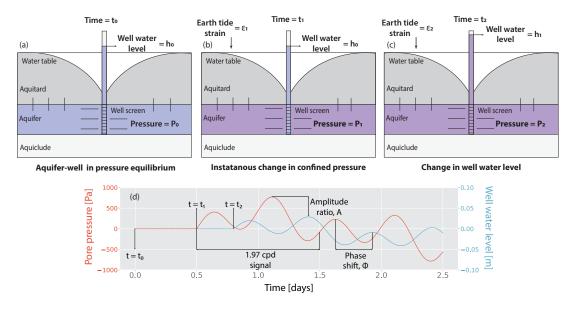
Figure 3.1: Representation of the pore pressure change and well water level in a semi-confined aquifer due to Earth tide strains. Earth tides induce subsurface stress which results in strains that generate changes in the pore water pressure. This leads to pressure gradients between the subsurface and observation wells that cause water movement in or out of the well. The ratio between the Earth tide strain and the well water level response can be expressed as amplitude ratio whereas the time difference between both signals as phase shift. (a) Aquifer and well pressure are in hydro-static equilibrium. (b) Earth tidal strain changes confined pore pressure. (c) Pressure gradients move fluid to the observation well. (d) Confined pore pressure changes due to Earth tidal forcing and well water level changes over time.

layered aquifer system. Gao et al. (2020) investigated the well skin effect which originates from the fact that the formation around a well is disturbed and well water storage on the well water level response to Earth tides. The authors found that the skin effect may significantly delay the well water level phase response to Earth tides. In addition, Guo et al. (2021) developed a model for tidal response with a fault passing through the aquifer based on a fault-guided fracture network to estimate fracture properties. They found that the hydraulic diffusivity in the fault damage zone higher than previously established values, but also that it remains below estimates based on induced seismicity migration. Sun et al. (2020) reviewed four of the most common analytical models to estimate hydraulic properties with Earth tidal analysis. They estimated hydraulic properties from a real data set and provide a range of applicability of the different models based on the transmissivity of the aquifer.

While analytical models offer a convenient approach to estimate hydraulic properties, their applicability is limited through simplifying assumptions arising from fundamental physics, conceptual model or boundary conditions. These include for example only radial flow, negligible horizontal displacement of the aquifer, confined and undrained conditions, unconsolidated materials and no gravity. Moreover, it has been reported that some of these assumptions may significantly influence the estimated subsurface properties Wang et al. (2019); Zhu & Wang (2020).

Numerical modeling of tidal effects is common in coastal Abarca et al. (2013); Zhang et al. (2021a) and adjacent settings Jardani et al. (2012); Pendiuk et al. (2020); Alcaraz et al. (2021), likely because the loading effect of ocean tides is much larger than that caused solely by Earth tide forces. So far, modeling the subsurface response to ocean tides has considered poroelastic conditions and harmonic loading by the weight of the water, therefore, solved as a consolidation problem. In contrast, the pressurization of an inland aquifer is produced by changes in the pore

space volume of the porous material due to strains (i.e., eigenstrains) caused by the gravitational influence from the movement of celestial bodies. Moreover, the change of the confined pore pressure is generally measured using an observation well which causes fluid movement.

To the best of our knowledge, only hydraulic modeling approaches neglecting any geomechanical effects, i.e., groundwater flow without coupled poroelasticity, have so far been used to investigate the groundwater response to Earth tides. For example, Wang et al. (2019) simulated the effect of capillarity of the unsaturated zone in one dimension. They found out that the assumption of fixed water table can lead to erroneous estimation of subsurface properties with analytical solutions. Zhu & Wang (2020) simulated a multi-layered system to study the effect of leakage through an aquitard and concluded that simplifications in the analytical model lead to overly conservative estimates of vertical flux between layers. Wang & Manga (2021) provide a summary of these works.

The confined pore pressure generated as result of Earth tide strains is a mechanical phenomenon caused by the elastic deformation of the porous matrix. Furthermore, unlike for traditional hydraulic testing approaches, there is a general lack of work investigating the effect of realistic conditions and assumptions on interpretations using analytical solutions. Investigating the influence of limiting assumptions and realistic subsurface conditions to better understand the applicability and robustness of analytical solutions requires development of more advance numerical models that also consider coupling with geomechanics.

The objective of this study is therefore to (1) critically examine assumptions upon which analytical solutions are based, (2) develop a numerical model for the groundwater responses to Earth tides, which couples hydraulic and geomechanical processes, (3) investigate and compare response conditions as well as the influence of geomechanical properties. Thus, our work significantly improves our understanding of the coupled physics, which controls the well response in a poroelastic medium. These results can act as a practical guide for improved estimation of aquifer properties due to the groundwater response to Earth tides.

3.2 Methodology

3.2.1 Fundamental theory of the groundwater response to Earth tides

Earth tides are displacements of the solid Earth's crust caused by the gravitational forces of celestial bodies that move in relation to the Earth. Such displacements are typically expressed as harmonic signals that can be predicted from well-known astronomical relationships. Earth tide forces are dominant at distinct frequencies within the semi-diurnal and diurnal range, e.g., M_2 at 1.97322 cycles per day (cpd) or S_1 at 1.0 cpd. Under tidal forcing, the poroelastic space and the porous material elastically deforms depending on the mechanical properties of the system resulting in a small change of volume. If the subsurface is saturated, the filling fluid has to adapt to the new available pore space which raises or lowers the pore pressure. The processes can be mathematically represented by the *Biot* consolidation theory.

Biot (1941) developed the constitutive laws which relate the applied forces (stresses) with deformation (strains) and motion within a elastically compressible porous medium. For the purpose of modeling, these laws are formulated in the form of mathematical equations which consist of four basic variables; total stress (σ_{ij}), strain (ϵ_{ij}), pore pressure (p_f) and increment of fluid content (ξ). The mechanical variables (stress or strain) can be related with one of the fluid quantity (pore pressure or fluid content) to form independent variable and therefore

mathematical equations. For the particular case of Earth tides, is convenient to express the poroelastic equations in terms of total stress and pore pressure as independent variables, also termed pure stiffness formulation. The basic relation between total stress and pore pressure is,

$$\sigma_{ij} = \sigma'_{ij} + \alpha p \delta_{ij}, \tag{3.1}$$

where σ'_{ij} is the effective stress, δ_{ij} is the Kronecker delta and α is the Biot poroelastic coefficient,

$$\alpha = 1 - \frac{K}{K_s}, \tag{3.2}$$

K_s is the solid material bulk modulus, K is the porous medium bulk modulus. The latter is related to the undrained bulk modulus, K_u, as

$$K_u = K + \alpha^2 M, \tag{3.3}$$

here, M, is the Biot modulus which is defined as,

$$\frac{1}{M} = \frac{n}{K_f} + \frac{(1-\alpha)(\alpha-n)}{K} = \frac{\alpha}{BK_u}, \tag{3.4}$$

where n is the porosity, K_f is the bulk modulus of the fluid and B is the Skempton coefficient.

The effective stress, σ'_{ij}, is related to elastic strain by the generalized Hooke's law through the compliance tensor C_{ijlk} Berryman (1999); Dropek et al. (1978),

$$\sigma'_{ij} = C_{ijlk} : \epsilon_{ij} = \left(K_u - \frac{2G}{3}\right)\delta_{ij}\epsilon + 2G\epsilon_{ij}, \tag{3.5}$$

where G is the solid material shear modulus, ϵ is the volumetric strain ($\epsilon = \epsilon_{xx} + \epsilon_{yy} + \epsilon_{zz}$). Combining equation 3.1 and 3.5 results

$$\sigma_{ij} = \left(K_u - \frac{2G}{3}\right)\delta_{ij}\epsilon + 2G\epsilon_{ij} + \alpha p_f \delta_{ij}, \tag{3.6}$$

and the dynamic property p_f can be related to the volume change as

$$p_f = M(-\alpha\epsilon + \xi), \tag{3.7}$$

Note that equation 3.6 is the effective stress equation, but for convenience is expressed in terms of total stress and the effective stress is reduce to the first and second terms of the right hand side.

Fluid transport is modeled with the fluid balance equation as

$$S_\epsilon \left(\frac{\partial p}{\partial t} + BK_u \frac{\partial \epsilon}{\partial t}\right) = \frac{k_{p,ij}}{\mu}\nabla^2 p_f + Q \tag{3.8}$$

where $k_{p,ij}$ is the porous medium permeability tensor, μ is the fluid viscosity, Q represents sinks or sources, $\epsilon_{ij} = \nabla u_i$ relates strain with displacement, often prefered in simulation codes Verruijt (2013); Kolditz et al. (2012); Flemisch et al. (2011); Keilegavlen et al. (2021), and the

effective stress can be related to the strain though the Hooke's law (i.e. equation 3.5). S_ϵ is the specific storage at constant strain and is related to the Biot modulus as

$$S_\epsilon = \frac{1}{M},\tag{3.9}$$

Equations 3.6, 3.7 and 3.8 can be solved in a coupled manner with appropriate boundary conditions and represent the elastic deformation and fluid movement in a porous medium.

3.2.2 Analytical solution

When uniaxial-vertical strain and zero incremental vertical stress are assumed (this occurs only when one of the principal stresses is non-zero and the stress does not change with depth), the subsurface is mechanically restricted to move only in the vertical direction, e.g., land surface subsidence due to consolidation occurs primarily in the vertical direction Herrera-García et al. (2021). Under such conditions $\epsilon_{xx} = \epsilon_{yy} = 0$ and $\sigma_{zz} = 0$ which leads to a simplified version of equations 3.6 and 3.7 as

$$\sigma_{zz} = 0 = \left(K + \frac{4G}{3} \right) \epsilon_{zz} - \alpha p_f \tag{3.10}$$

and

$$p_f = M(-\alpha\epsilon_{zz} + \xi). \tag{3.11}$$

Combining 3.10 and 3.11 to eliminate ϵ_{zz} gives

$$\xi = S p_f, \tag{3.12}$$

where

$$S = \frac{1}{M} + \frac{3\alpha^2}{3K + 4G}. \tag{3.13}$$

This is the definition of storage coefficient in hydrology Cheng (2016); Verruijt (2013); Wang (2017). The specific storage, S_s, is obtained when the specific weight of the fluid is considered as

$$S_s = S\rho_f g, \tag{3.14}$$

where ρ_f is the density of the filling fluid and g Earth's gravitational acceleration constant.

With this derivation, we stress the conceptual difference between the specific storage at constant strain (equation 3.9) and the storage coefficient with uniaxial strain (equation 3.13). Please note that S approaches S_ϵ when $K >> K_f$, hence the second term of equations 3.4 and 3.13 go towards zero. Physically, in such cases the amount of fluid coming out of storage will only depend on the fluid compressibility and the porosity of the porous medium, as the porous material is rigid. Verruijt & Van Baars (2007); Lambe & Whitman (1991); Freeze & Cherry (1979a).

Hydraulic head can be used as a proxy for pore pressure in equation 3.8, $h = p\rho_f^{-1}g^{-1}$. Moreover, in a confined aquifer with a constant thickness H_a, hydraulic conductivity, $k_a = k_{p,ij}\rho^{-1}g^{-1}$, can be express in terms of transmissivity ($T = k_a H_a$) and specific storage at constant strain in terms of storativity at constant strain $S_{\epsilon,t} = S_\epsilon H_a$ as Cheng (2016); Verruijt (2013); Wang (2017),

$$S_{\epsilon,t} \left(\frac{\partial h}{\partial t} + \frac{BK_u}{\rho_f g} \frac{\partial \epsilon}{\partial t} \right) = T \left[\frac{\partial^2 h}{\partial x^2} + \frac{\partial^2 h}{\partial y^2} + \frac{\partial^2 h}{\partial z^2} \right] + \frac{Q}{\rho_f g}. \tag{3.15}$$

For practical reasons, equation 3.15 can be reformulated into cylindrical coordinates assum-

ing only radial flow Jacob & Lohman (1952); Jacob (1946), also the effect of a leaky layer on top of the aquifer can be included as vertical leakage in the sink/source in terms of hydraulic conductivity of the layer on top (k_l) and thickness of such layer (H_l) expecting $k_a k_l^{-1} \gg 1$ as $Q/\rho_f g = k_l h H_l^{-1}$,

$$S_{\epsilon,t} \left(\frac{\partial h}{\partial t} + \frac{BK_u}{\rho_f g} \frac{\partial \epsilon}{\partial t} \right) = T \left[\frac{\partial^2 h}{\partial r^2} + \frac{1}{r} \frac{\partial h}{\partial r} \right] + \frac{k_l}{H_l} h. \tag{3.16}$$

In this work we use the terms aquifer and aquitard to reflect layers of higher and lower hydraulic conductivity, respectively, as is consistent with the terminology used in previous works. Equation 3.16 was used to derive analytical solutions that describe the groundwater response to Earth tides in a fully vertical and horizontal confined aquifers Hsieh et al. (1987) and in aquifers with vertical leakage Wang et al. (2018). A detailed derivation of the more versatile leaky solution is presented in Wang et al. (2018), but is also included in 3.5 of this work. The solution describes the water level in a well (h_w) in terms of the hydraulic conductivity of the aquifer (k_a), hydraulic conductivity of the aquitard (k_l), the specific storage at constant strain of the aquifer (S_ϵ) and the geometry of the well (equation 3.40, 3.41 and 3.42). In this formulation, any effects arising from well skin or storage are neglected, but such effects have been investigated in the literature Gao et al. (2020). Fluid level changes in the well are caused by forces generated at the far field (far away from the radius of influence of the observation well). Assuming undrained conditions ($\xi = 0$, in equation 3.7) and $\alpha = 1$ representing unconsolidated systems, (e.g., sands, gravels and clays) such changes can be quantified as

$$p = -M\epsilon_G, \tag{3.17}$$

where ϵ_G is a external volumetric strain. The change of water level in a well due to an areal strain is graphically shown in Figure 3.2a and 3.2b for two given times from $t_0 = 0$ to $t = t$ with gravitational strains from $\epsilon_G = 0$ to $\epsilon_G = \epsilon_G(t)$.

The amplitude ratio and phase shift between the piezometric head at a distance from the well beyond its radius of influence and the water level in the well are expressed as Hsieh et al. (1987),

$$A = \left| h_w / \frac{BK_u \epsilon_0}{\rho g} \right| = \left| h_w \alpha / \frac{M\epsilon_0}{\rho g} \right| \tag{3.18}$$

and

$$\Delta\phi = arg \left(h_w / \frac{BK_u \epsilon_0}{\rho g} \right) = arg \left(h_w \alpha / \frac{M\epsilon_0}{\rho g} \right). \tag{3.19}$$

Here, ϵ_0 is the amplitude of the volumetric strain signal, which can be obtained from software based on tidal catalogs, e.g. PyGtide Rau (2018b), ETERNA PREDICT Wenzel (1996), *TSoft* Van Camp & Vauterin (2005) and h_w is the fluid level in the well obtained by the analytical solution (equation 3.43). The analytical solution is subject to the assumptions under which it was derived: (1) undrained conditions, (2) the confining layer has negligible specific storage, (3) the flow is horizontal in the aquifer, (4) the well is represented by a line with length matching the aquifer extent, (5) the deformation is only vertical, (6) no external forces such as gravity.

Moreover, field measured amplitude ratio, A, and phase shift, $\Delta\phi$, can be obtained from applying HALS to the Earth tide strain and hydraulic head time series Schweizer et al. (2021). The obtained phase shift varies between $-\pi \geq \phi \geq \pi$, thus, only fluid capable to flow from the aquifer to the observation well within that time frame (half a day for M2) is going to contribute in a change of the amlitude and phase shift. The latter bounds the scale of the method as high

conductivity aquifers can move fluid from higher distances than low conductivity aquifers.

Using the results obtained from HALS, equations 4.12 and 4.13 can be inverted to estimate constant values of equation 3.16 using any approach suitable for non-linear algorithm estimation (gradient methods), e.g. least-squares. In fact, this approach has been used to estimate aquifer hydraulic conductivity, specific storage and aquitard leakage from the amplitude and phase response of groundwater to Earth tides Rau et al. (2020a); Zhang et al. (2021b). However, the task of solving these non-linear equations is an ill-posed problem, because the solution might not be unique. The computation of meaningful approximate solutions of inversion of equation 4.12 and 4.13, therefore, can be quite challenging and strongly dependent on the a suitable initial guess feed to the non-linear algorithm. Moreover, it is not always a simple matter to decide which initial guess to choose. We note that the implications of initial guess nor the performance of iterative methods have been investigated for practical use of this solution.

Gradient methods such as the *Levenburg-Marquardt* often use in least-squares to numerically search for the nearest (local) minimum to the given initial condition and are readily implemented in SciPy Virtanen et al. (2020). The function fitting model finds the local or global minimum, which depends on the feed initial guess. To investigate the performance of least-squares by the initial guess on the parameter estimation of Wang et al. (2018) (equation 4.12 and 4.13), we systematically explore the solution space of a fitting function. The fitting function was formulated as

$$FO_{Amplitude} = A_{obs} - A(k_a, S_\epsilon, k_l) \tag{3.20}$$

and

$$FO_{Phase} = \phi_{obs} - \Delta\phi(k_a, S_\epsilon, k_l) \tag{3.21}$$

where $A(k_a, S_\epsilon, k_l)$ and $\Delta\phi(k_a, S_\epsilon, k_l)$ are equation 4.12 and 4.13. The aquifer thickness and aquitard depth were arbitrarily defined to be $1\ m$ and $100\ m$, respectively; the radius of the well to 0.2 m, A_{obs} and ϕ_{obs} are objective amplitude ratio and phase shift values given by the user. The Earth tide frequency was set to 1.93 cpd, previous studies have suggested that by considering an extra tide frequency, for instance, 1 cpd might constrain better the minimization problem Zhang et al. (2021b). But this is not explored in this study.

The least-squares solver minimizes the difference between $A_{obs} - A(k_a, S_\epsilon, k_l)$ and $\phi_{obs} - \Delta\phi(k_a, S_\epsilon, k_l)$ of equations 3.20 and 3.21 by iterating through a combination of values of k_a, S_ϵ and k_l. An array consisting of discrete values within realistic ranges for amplitude ratio ($0.001 \leq A \leq 1$) and phase ($-90° \leq \Delta\phi \leq 90°$) where generated. For each pair of amplitude ratio and phase shift, the solution space was solved using least-squares of SciPy. The tolerance for termination by the change of the cost function was set to be $3 \cdot 10^{-6}$ and units for 3.20 and 3.21 where set to days so as to increase the numeric values and avoid errors. The sensitivity of the method was tested by generating 1000 samples of k_a, S_ϵ and k_l generated by a random log uniform distribution ranging from $1 \cdot 10^{-7} \leq k_a \leq 1 \cdot 10^{-3}\ ms^{-1}$, $1 \cdot 10^{-7} \leq S_\epsilon \leq 1 \cdot 10^{-5}\ m^{-1}$ and $1 \cdot 10^{-8} \leq k_l \leq 1 \cdot 10^{-4}\ ms^{-1}$. Each trio of samples was set as initial condition in equation 3.20 and 3.21. Starting from different initial values allows the solver to find potentially different local minima. The outputs were stored and the maximal difference between each estimated property was used as a proxy for performance of the non-linear search. This approach allows identification of values within the solution space where several local minimum might be encounter.

3.2.3 Numerical model

The generic equations presented in Section 3.2.2 can be solved analytically for specific boundary conditions (equation 3.16), but analytical solutions do not accounts for the elastic deformation of the porous medium (Section 3.2.1, equations 3.6, 3.7 and 3.8). The coupled physics between fluid movement and mechanical deformation can be solved numerically. Here, we develop a novel numerical approach for simulating the groundwater response to Earth tides. This allows a more realistic physical representation compared to the limiting assumptions of the analytical solution presented in Section 3.2.2 and advances the previous study by Wang & Manga (2021). The aim is to investigate and establish robustness of the analytical solution when interpreting the groundwater response to Earth tides.

When modeling Earth tides, an external gravitational strain $\epsilon_G(x, y, z, t)$ is applied to deform the Earth's crust and the resulting fluid pressure $p_f(x, y, z, t)$, and the displacement vector $u_{ii}(x, y, z, t)$ is calculated. Under the free surface condition, the normal stress along the radius is zero. Hence, gravitational strain can be decomposed into its vertical $\epsilon_h(x, y, t)$ and horizontal component $\epsilon_v(z, t)$ Agnew (2005),

$$\epsilon_G(x, y, t) = \epsilon_h(x, y, t) + \epsilon_v(z, t). \tag{3.22}$$

Earth tides induce an *eigenstrain*, i.e., a strain that does not result directly from an applied force. Qu & Cherkaoui (2006) describes the differences and relationships between total, elastic and eigenstrains. To simulate the effect in a realistic well-aquifer system, in which the hydraulic and geomechanical properties of the material may vary in space, we applied vertical and horizontal strain as displacement boundary conditions. This fixes the internal strain throughout the model as a function of the filling material elastic tensor as Wang (2017),

$$r = R : u_{rr} = \epsilon_h(x, y, t)\, R, \tag{3.23}$$

$$r = 0 : u_{rr} = 0, \tag{3.24}$$

and

$$z = 0 : u_{zz} = \epsilon_v(z, t)\, L, \tag{3.25}$$

$$z = -L : u_{zz} = 0, \tag{3.26}$$

where R and L are the horizontal and vertical lengths of the model, respectively. A constant atmospheric pressure (i.e. drained condition) is assumed at the top of the modelling domain and at the top of the observation well. Note that we exclude consideration of barometric variations, such as could be caused by atmospheric tides, which is a valid assumption for the $M2$ frequency discussed here Rau et al. (2020b),

$$z = 0 : p_f = 0. \tag{3.27}$$

The governing equations follow the traditional Biot (1941) theory of a linear elastic, saturated and deformable porous medium with water as the fluid Wang (2017); Cheng (2016). The strong form of the general equations in Subsection 3.2.1 can be converted into the respective weak form and discretized before solving with the finite element (FE) method. In this study, we adopt the continuum representation of an elementary volume (REV) in a porous medium. To solve the numerical system the Real Heterogeneity App (RHEA), a FE application based on the Multiphysics Object Oriented Simulation Environment (MOOSE) was used Permann et al. (2020).
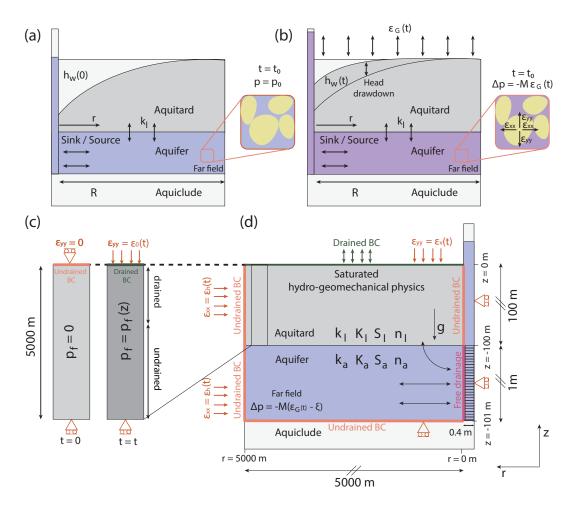
Figure 3.2: Overview of the conceptual models used in this work. (a) Analytical model of Wang et al. (2018) when no external force is applied (b) Analytical model of Wang et al. (2018) when the confined pore pressure generated at the far field is generated and fluid flow towards the well. (c) A 1D column of the subsurface representative of the aquitard to assess the type of response. At $t = 0$ the column is equilibrium, at $t > 0$ a harmonic strain is applied which results in fluid movement in and out of the column. (d) A 2D model of the aquifer bounded by a aquitard and connected to a well. Earth tide strain is applied which moves fluid towards a well that is numerically modeled.

A detailed description of the system of equations to be solved as well as further information of the tight coupling and numerical description of the FE implementation utilized in this study can be found in Bastías Espejo et al. (2021); Wilkins et al. (2021, 2020). For consistency, we keep the original notation used in Bastías Espejo et al. (2021), where the field variables are the fluid pressure p_f and the displacement vector u_{ii}.

3.2.4 Assessing the subsurface response conditions

Within the theory of linear poroelasticity (equations 3.6 to 3.8), one can distinguish between two end-members that describe the type of pore pressure response to stresses and strains: undrained and drained. When a deformation in a porous medium occurs, under drained conditions, the rate of applied distortion is slow in relation to the ability of the porous medium to allow dissipation of the pressure gradient. This results in the flow of fluid caused by the buildup of pressure differences. Under undrained conditions, the rate of applied distortion is fast enough for an instantaneous pore pressure response to external deformations and fluid cannot flow in response generating a constant confined pore pressure throughout the porous medium. The type of response is of importance as analytical solution often assume undrained systems, however most aquifers in nature are draining in at least one boundary, further its relevance has not yet been studied.

The type of subsurface response is represented by equation 3.7, in which ξ describes an increment of change in fluid content. Under undrained conditions, $\xi = 0$ and equation 3.7 reduces to equation 3.17. While under drained conditions $\xi \neq 0$. Hence, the confined pore pressure as a response to Earth tides can be obtained with equation 3.7 if the Earth tide strain (ϵ_G) is known.

For Earth tides, the applied strain depends on the frequency of the harmonic and the type of response is a function of the hydro-geomechanical subsurface properties as well as depth. To assess the type of response under realistic conditions, we numerically modeled an infinitely long 1D (5000 m) section of the subsurface (Figure 3.2c) using a harmonic function as displacement boundary condition as follows

$$z = 0, \ \epsilon_{M2} = \epsilon_0 \cdot \sin\left[2\pi f_{M_2} t\right]. \tag{3.28}$$

Here, ϵ_0 is the amplitude of the Earth strain, f_{M_2} is the frequency of the M_2 component and t is the time in days. We computed the increment of fluid content, ξ, over depth $0 \leq z \leq 1000$ m and repeated the calculations by setting assumed, but realistic discrete values of specific storage at constant strain S_ϵ, ($1 \cdot 10^{-7} \ m^{-1}$, $1 \cdot 10^{-6} \ m^{-1}$ and $1 \cdot 10^{-5} \ m^{-1}$), and bulk modulus K, ($1 \cdot 10^9$ Pa, $1 \cdot 10^{10} \ Pa$ and $1 \cdot 10^{11} \ Pa$,). These values represent realistic conditions as reported in the geoscience literature Das & Das (2008); Wang (2017); Cheng (2016); Lade (2001). We note that we use the term aquitard even though the assigned values of its hydraulic conductivity are relatively high ($1 \cdot 10^{-7} \leq k_l \leq 1 \cdot 10^{-4} \ ms^{-1}$). In our work the term aquitard reflects the fact that it is used as a layer with lower hydraulic conductivity values compared to the aquifer and its use is consistent with the terminology and values found in previous literature, e.g. Wang et al. (2018).

When analyzing the groundwater response to Earth tides, undrained conditions have to be given for the analytical solution to be valid (3.5). However, the type of response to Earth tides has not been assessed before and is therefore unknown. To assess whether the subsurface response is sufficiently undrained, we can use equation 3.7 assuming $\alpha = 1$. Under undrained

conditions $\xi = 0$, such condition can be assumed when $\epsilon \gg \xi$. Hence, the effect of ξ can be neglected in equation 3.7.

3.2.5 Numerical model of a coupled well-aquifer system

To investigate the limitations of the analytical model presented in Section 3.2.2, a 2D axial-symmetric cylindrical model was developed. The model accounts for poro elastic aquifer (Section 3.2.1) bounded by a low permeable aquitard on top and by a rigid aquiclude on the bottom. Gravity, vertical and horizontal flows are allowed (Figure 3.2d). Boundary conditions are set as described in Section 3.2.5. The applied Earth strain (ϵ_G) was calculate theoretically with PyGtide Rau (2018b), a Python wrapper for ETERNA PREDICT 3.4. We chose the city of Berlin (Germany) and a signal frequency of 2 cpd for simplicity as it closely resembles M_2 with a duration of 30 days. While the location is arbitrary, it does not change the conclusions because the context of this study is generic.

The borehole-subsurface system is modeled as a 1D element outside the 2D system. To relate the porous medium and the borehole-subsurface, the boundary at $r = 0$ is modeled as a free drainage boundary, i.e., a sink boundary where the flux is computed in function of the pressure at $r = 0$ ($p_{r=0}$) and at the bottom of the borehole-subsurface (p_w)

$$r = 0, \; -101 \leq z \leq 100, \; \dot{m}_f = C(p_f - p_{r=0}), \qquad (3.29)$$

where $\dot{m}_f$ is the mass flux, C the conductance (i.e., how efficiently fluid is transported though a boundary) between the borehole-subsurface and the model. For this study $C = 10^{-3} \; m^2 s^{-1}$ which is high enough to ensure that $p_f = p_{r=0}$ at the end of each non-linear iteration.

As a result, the mass flux through the boundary between the model and the well is computed in every non-linear iteration, which fixes the pore pressure at the boundary for the next iteration. This way, the fluid level in the well is tightly coupled to the pressure at the well boundary of the model as the fluid level in the well is computed in the same Jacobian matrix with the numerical model as,

$$\frac{dh_f}{dt} = \frac{\dot{m}_f A_c}{\rho_f A_w}. \qquad (3.30)$$

Here, h_f represents the water level in the well ($h_f = p_f g^{-1} \rho_f^{-1}$), A_c is the external area of a cylinder and A_w is the inner area of a cylinder. Since the model is linear elastic, typically, only two non-linear iterations are needed.

The model domain is $R = 5000$ m long in the r direction and $L = 101$ m in depth in the z direction. The aquitard is 100 m thick, whereas the aquifer is 1 m thick, and we assume that the well is screened throughout this unit. The 101 m long well is located at the left boundary of the modeling domain and the well has $r_w = 0.2$ m of radius (Figure 3.2d). The geometry complies with previous studies Hsieh et al. (1987); Wang et al. (2018) and therefore enables a comparison. The finite elements were discretized using the built-in mesh generator of MOOSE and the element size increases logarithmically along the r-axis away from the well. The mesh is vertically and logarithmically discretized 5 times across the aquifer, 20 times across the top layer and 100 times in the horizontal direction. The material properties of the model are summarized in Table 3.1. The values of Table 3.1 were assumed in previous studies Wang et al. (2018) and extracted from literature Das & Das (2008); Wang (2017); Cheng (2016); Lade (2001).

The initial pore pressure condition is set as $p_f^0 = -\rho_f g z$ and the effective initial stress as $\sigma_{zz}'^0 = (\rho_s - \alpha \rho_f) g z$, where $\sigma_{zz}'^0$ is the vertical component of the effective stress at time zero.

Again, we apply a harmonic displacement function with the M_2 frequency computed with a tidal catalog, the amplitude of the strain is $\epsilon_0 = 1.2 \cdot 10^{-8}$. The model runs until it reaches quasi steady-state, at which point the well physics as well as tidal forcing as boundary conditions are activated. This approach minimizes potential numerical overshooting produced by the free drainage boundary between the porous medium and the well. We verify this numerical implementation using the analytical solution of Wang et al. (2018) (Subsection 3.2.2) with the aquitard permeability set to zero, i.e., the model represents only one layer.

3.3 Results and discussion

3.3.1 Analytical solutions

Previous research has used the analytical solutions by Hsieh et al. (1987) and Wang (2000); Wang et al. (2018) to estimate hydraulic properties for negative and positive phase shifts between groundwater and Earth tides, respectively. We note that the Hsieh et al. (1987) and Wang et al. (2018) require undrained conditions, whereas Wang (2000) drained conditions. The robustness of these assumptions have not been investigated for Earth tide frequencies. For drained conditions the relationship between stress and strain is no longer linear, as pore pressure also plays a role bearing loads (see equation 3.7). Furthermore, while Wang (2000) considers vertical flow in a one dimensional poroelastic aquifer, it neglects the influence of an observation well. As shown in Figure 3.3, a well generates phase shifts between the confined far distance porepressure and the water level in the well as the fluid requires time to move in and out of the well. Strictly speaking, this solution was derived for surface loads, such as exerted from atmospheric pressure, but not for Earth tide strains. These aspects illustrate that Wang (2000) has limited use when estimating hydraulic properties from the groundwater response to Earth tides.

Wang et al. (2018) provides an extended formulation to Hsieh et al. (1987) considering vertical aquitard leakage accounting for both negative and positive phase shifts. It is useful to illustrate the solution space of Wang et al. (2018) by providing an overview of amplitude ratios and phase shifts (equations 4.12 and 4.13) as a function of realistic ranges of the aquifer hydraulic conductivity (k_a) and specific storage at constant strain (S_ϵ) as well as discrete values of leakage, see Figure 3.3. Note that this is based on the dominant harmonic signal frequency of 2 cpd, a well and screen radius of 0.2 m, a screen length of 1 m and an aquitard thickness of 100 m. The first row, Figure 3.3a and 3.3b, shows the case where there is no vertical leakage leading to negative phase shifts only. We confirm the reports by Wang et al. (2018) that the analytical solution matches the previous solution by Hsieh et al. (1987) when the aquitard hydraulic conductivity is set to zero.

The solution space shows that vertical leakage causes positive phase shifts at relatively high aquifer hydraulic conductivity, i.e., $k_a > 1 \cdot 10^{-5}\ ms^{-1}$ in Figure 3.3d. This threshold is even more clear for vertical leakage larger than $k_l > 1 \cdot 10^{-6}\ ms^{-1}$ where the transition to positive phase shift is almost linear. Moreover, in Figures 3.3d and 3.3f, the phase shift behavior is very similar for the lower part of the specific storage at constant strain under study ($S_\epsilon < 1 \cdot 10^{-5}\ m^{-1}$). A similar case is observed in Figures 3.3c and 3.3e where the amplitude response of the analytical solution shows very similar results.

The solution space illustrated in Figure 3.3 shows that the functions are non-linear and, therefore, to estimate subsurface parameters a gradient root finding method is necessary. This is based on an iterative method resulting in an approximate solution only. The search is based

Table 3.1: Overview of the hydraulic and mechanical properties of the numerical model.

Property	Acronyms	Value	Unit	Reference
Aquitard hydraulic conductivity	k_l	$1 \cdot 10^{-7} \leq k_l \leq 10^{-4}$	$m\,s^{-1}$	Wang (2017); Cheng (2016)
Aquitard specific storage at constant strain	$S_{\epsilon,l}$	$1 \cdot 10^{-7}, 1 \cdot 10^{-6}, 1 \cdot 10^{-5}$	m^{-1}	Wang (2017); Cheng (2016)
Aquitard bulk modulus	K_l	10	GPa	Das & Das (2008)
Aquitard Poisson's ratio	ν_l	0.25	-	Das & Das (2008)
Aquitard Biot coefficient	a_l	1	-	Wang (2017); Cheng (2016)
Aquifer hydraulic conductivity	k_a	$1 \cdot 10^{-3}, 1 \cdot 10^{-4}, 1 \cdot 10^{-5}$	$m\,s^{-1}$	Wang (2017); Cheng (2016)
Aquifer specific storage at constant strain	$S_{\epsilon,a}$	$1 \cdot 10^{-7}, 1 \cdot 10^{-6}, 1 \cdot 10^{-5}$	m^{-1}	Wang (2017); Cheng (2016)
Aquifer bulk modulus	K_a	10	GPa	Das & Das (2008)
Aquifer Poisson's ratio	ν_a	0.25	-	Das & Das (2008)
Aquifer Biot coefficient	a_a	1	-	Das & Das (2008)
Skeleton density	ρ_s	2000	$kg\,m^{-3}$	Wang (2017); Cheng (2016)
Bulk modulus of the water	K_f	2.2	GPa	Wang (2017); Cheng (2016)
Water density	ρ_f	1000	$kg\,m^{-3}$	Wang (2017); Cheng (2016)

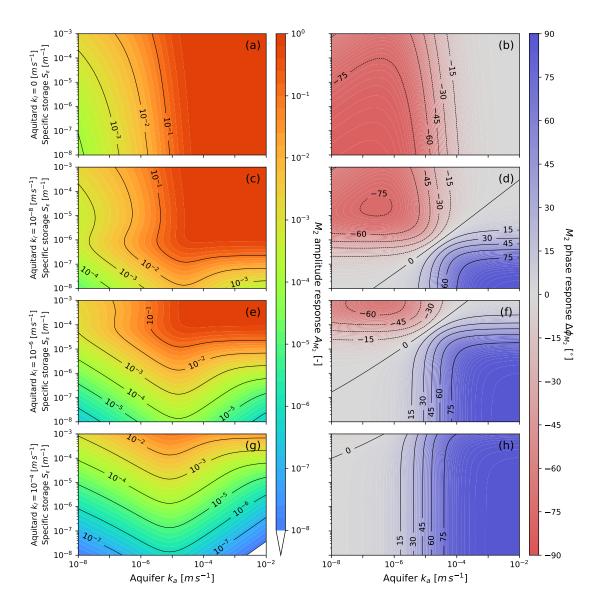The subscript l and a refer to aquitard and aquifer, respectively.

Figure 3.3: Amplitude and phase shift response of the analytical solution presented in Wang et al. (2018) for a realistic range of hydraulic conductivity and specific storage at constant strain values. (a) and (b) are representative of zero leakage through the aquitard corresponding to Hsieh et al. (1987). (c) to (f) consider distinct and increasing aquitard hydraulic conductivity values. The harmonic signal frequency is 2 cpd, the well and screen radius are $0.2\ m$, the screen length is 1 m and the aquitard has $100\ m$ thickness

on an initial guess and the method may find different potential solutions depending on the function gradients. We investigate the effect of the initial guesses on the solution space by visualizing the difference in the found local minimum. Figure 3.4 shows the variability in estimated parameters due to providing different initial guesses for least-squares solving. Blue color means less variability whereas red color shows a larger difference in the solution space and therefore higher number of local minimum.

In general, higher sensitivity to the initial values is observed in the phase shifts compared to the amplitude ratios. The sensitivity for inverting the hydraulic conductivity of the aquifer k_a is relatively low ($\Delta k_a < 5 \cdot 10^{-4} \ ms^{-1}$) at negative phases and increases as the phase shift approaches $0°$. For values higher than zero degrees the sensitivity decreases again until approximately $40°$ where it starts to increase again (Figure 3.4a). The highest sensitivity is found around amplitude ratio of one and positive phase shift. Situations where the amplitude ratio is one and the phase shift much higher than zero are not realistic and should be disregarded.

Specific storage at constant strain shows a high contrast in solution variability with values that are very close to $\Delta S_\epsilon = 1 \cdot 10^{-5} \ m^{-1}$ for most of the solution space (Figure 3.4b). At low phase shifts ($\Delta \phi < -70°$) the variability significantly reduces to $\Delta S_\epsilon = 1 \cdot 10^{-7} \ m^{-1}$. In practice, most of the realistic cases will fall within the high variability zone. Vertical leakage shows relatively low sensitivity where the phase shift is negative ($\Delta k_l < 5 \cdot 10^{-5} \ ms^{-1}$, Figure 3.4c). However, at positive phase sifts the variability increases up to two orders of magnitude, demonstrating the effect of the phase shift on vertical leakage.

In the illustrated case, the sensitivity of the specific storage at constant strain is constant throughout the solution space and therefore its initial value does not play a significant role on finding different solutions. Therefore, is likely that for each specific storage at constant strain study a local minimum was found during the minimization. We, therefore, advise special attention when selecting the initial value of the specific storage in order to obtain a meaningful result. This value can be bound if knowledge of porosity is available (Section 3.3.2). Negative phase shifts show a low sensitivity to the initial condition and will likely result in an accurate inversion of the hydraulic properties without a priori knowledge of the subsurface properties as mentioned in section 3.2.2. For positive phase shifts a handle on at least one of the properties is necessary as the vertical leakage significantly increases its variability. Further, the hydraulic conductivity increases its variability towards high amplitudes which is the range where Earth tide methods work best. Overall, this complies with the previous finding that positive phase shifts can robustly be interpreted as vertical leakage Wang et al. (2018).

3.3.2 Notes on the specific storage

An interesting implication of Section 3.2.1 arises when $\alpha = 1$. The latter refers to systems where the compressibility of porous medium is small compared to the compressibility of grains, such as is the case for unconsolidated materials. Here, the specific storage at constant strain (the inverse of the *Biot* modulus, equation 3.4) reduces to

$$S_\epsilon = \frac{1}{M} = \frac{n}{K_f}. \tag{3.31}$$

Since the bulk modulus of water is known ($K_f = 2.2 \cdot 10^9 \ Pa$), the porosity of the material can also be estimated from the groundwater response to Earth tides. However, for consolidated materials the Biot coefficient may be smaller than one. This can help to constrain the expected values of the specific storage at constant strain. For instance, if the subsurface material is
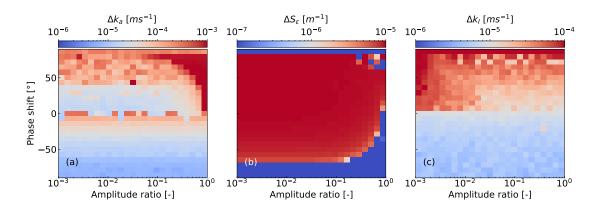
Figure 3.4: Color map exploring the solution space, i.e., the variability of parameters as a function of the initial guess, of the under-determined problem by Wang et al. (2018). Estimating three hydraulic properties out of two measured parameters: (a) aquifer hydraulic conductivity, (b) specific storage at constant strain, (c) aquitard hydraulic conductivity. Note that each color scale has a different range. Blue indicates less variability, whereas red means more variability of the results.

unconsolidated and has realistic porosity values, i.e., $0.01 \leq n \leq 0.3$, then the specific storage at constant strain is constrained to

$$4.5 \cdot 10^{-8} m^{-1} \leq S_\epsilon \leq 1 \cdot 10^{-6} m^{-1}. \tag{3.32}$$

We note that previous studies which estimated the specific storage from the groundwater response to Earth tides have not considered the appropriate context for this property. The result is referred to as "specific storage at constant strain" (S_ϵ) and it can vary significantly from the specific storage generally used in hydrogeology (S_s, see Equation 3.13) Hantush (1960). The difference between both coefficients originates from the underlying assumptions. The specific storage at constant strain is defined in conditions in which the volume of the porous frame is maintained constant but the fluid volume is not, which induces changes in the pore volume because fluid has to be accommodated. In contrast, for the specific storage used in hydrogeology the porous frame is allowed to deform in the vertical direction. This is mathematically represented by the second term of Equation 3.13. Thus, when the subsurface material is much less compressible than the filling fluid and the pore space the second term of Equation 3.13 tends to zero because no deformation of the frame takes occurs, hence $S \approx S_\epsilon$. Moreover, note that $S_\epsilon \leq S$. Thus, as demonstrated in this study, attention must be paid to the conceptual difference between these two parameters.

Analytical models typically assume that the leaky layers have zero specific storage. Zhu & Wang (2020) numerically investigated the effect of specific storage on Earth tide analysis in leaky layers. The authors concluded that the assumption of leaky layers with zero specific storage may lead to wrong estimations of subsurface properties as the specific storage changes the phase shift. As shown in this work, in unconsolidated systems the specific storage at constant strain depends on porosity only. Therefore, the porosity of the aquifer has to exceed that of the leaky layer based on the results of Zhu & Wang (2020).

3.3.3 Numerical modeling of the groundwater response to Earth tides

The fluid continuity equation (equation 3.8) has been solved in previous studies assuming that the strain term $\epsilon(t)$ is known and solely time-dependent with adequate boundary conditions.

64

This equation is an *inhomogenous* diffusion equation for which the change of volumetric strain is mathematically equivalent to a sink/source in the aquifer storage term. Therefore, changes of strain result in changes of porepressure in the entire model domain. When mechanical coupling is included, the continuity equation needs to be coupled to the state of stress, hence the strain is tightly coupled to porepressure. Thus, the strain term in equation 3.8 is no longer uniform over the entire model and may vary depending on the amount of change of fluid. For instance, changes in porepressure (for earth tides within the radius of influence of the well) induces changes in the volumetric strain, which generate drained conditions (Section 3.3.4). Therefore, assuming that the applied strain is constant within the model domain is inaccurate for our purposes since, as explained before, the strain is function of the porepressure. Another common way to express the coupling between porepressure and strain is by rearranging equations 3.6 and 3.7 as

$$\epsilon = \frac{1}{K}\sigma + \frac{\alpha}{K}p_f. \tag{3.33}$$

The relative movement of celestial bodies in relation to Earth induces variations in the gravitational force which results in small deformation of the Earth's crust. Such deformations are not caused by an applied stress. In continuum mechanics, this problem is known as *eigenstrain*, and it is very common in heat transport, e.g., dilatation caused by heating of materials. The relationship between deformation and *eigenstrain* can be obtained experimentally leading to a constitutive model Qu & Cherkaoui (2006). In this work we apply a simpler approach. As FE implementation typically requires displacement or load as boundary conditions, we set displacement as boundary condition and directly applied the strain obtained from an Earth tide catalog multiplied with the length of the model, i.e., $u_{ii} = \epsilon_{ii}L$.

While this approach is convenient it has limitations. If the mechanical properties change over the modeling domain (composite material), the displacement will not be uniformly distributed across the domain and therefore the resulting strain will also be non-uniform. This would produce larger displacements in soft layers resulting in higher pore pressure. One way to solve this problem is to assume vertical heterogeneity and to apply the total volumetric strain only at the horizontal boundaries. This would result in a uniform displacement distribution in the horizontal axis and therefore result in an appropriate pore pressure response. We note that the effects of distributed mechanical heterogeneity are not further explored in this work.

Initialization of the numerical model is not trivial since the initial hydrostatic and mechanical states (initial pore pressure and stresses) has to be in equilibrium Settari & Walters (2001). This challenge applies in particular for heterogeneous distributions of material properties and transient boundary conditions. Achieving mechanical equilibrium at time $t = 0$ is difficult and may in most cases require a separate initialization step during the simulation Chen et al. (2009). We recommend to first simulate steady-state conditions which generates the stress and pore pressure distribution within the modeling domain.

From a numerical point of view, the simulator is setting the force balance as an approximation, i.e., $\nabla\sigma = 0$. In practice, a non-linear step is finished when the force balance falls below a threshold close to zero but residual errors always remain. Earth tides generate only small changes in pore pressure which are close to the residual error. For example, if the acceptable error is $e = 1\ Pam^{-2}$, then in our case the area is 5050000 m^2 leading to total residuals up to $R \approx 5050 kPa$ at the bottom of the model. Since Earth tides generate pore pressure change in smaller magnitude, minimizing the error is an important consideration when modeling. Numerical modeling of Earth tides therefore requires attention to decreasing the tolerance of the

numerical solver (e.g., by increasing the number of linear steps), increasing space discretization (e.g., by increasing the size of the Jacobian matrix) or decreasing time discretization (e.g., by increasing the number of time steps).

3.3.4 Are conditions for the M_2 Earth tide drained or undrained?

When a stress is applied to an undrained subsurface system, the load is shared by the bulk material, the grains and the pore fluid. The balance between these three responses results in instantaneous deformation of the pore space and a change in fluid pressure. If the rate of the applied deformation is slow enough then fluid can flow out of the system which result in a change of the pore pressure. The balance between the rate of Earth tide stress and realistic hydro-geomechanical subsurface properties is rarely known. Moreover, fluid movement (i.e., drained conditions) may be given leading to $\xi \neq 0$. Under such conditions the assumptions of the analytical solutions are violated potentially leading to errors when interpreting the groundwater level response to Earth tides.

To assess the conditions under which an undrained response occurs for the M_2 frequency, we numerically simulate a 1D vertical column with depth $0 \leq z \leq 5000$ m (Figure 3.2b) and with a range of realistic hydraulic and geomechanical properties. Equation (3.7) can be solved for fluid quantity (ξ) assuming the worst scenario ($\epsilon_G = 1 \cdot 10^{-8}$ corresponding to a low tide amplitude) and $\alpha = 1$,

$$\xi = \frac{p_f}{M} - \epsilon_G = S_\epsilon p_f - \epsilon_G, \tag{3.34}$$

Figure 3.5 shows the results of our numerical model which calculates ξ up to $1000\ m$ depth and for a range of realistic hydraulic properties as well as discrete values of the bulk modulus. As typical Earth tide amplitudes vary between $1 \cdot 10^{-7} \leq \epsilon_G \leq 1 \cdot 10^{-8}$ Rojstaczer & Agnew (1989), we define

$$\xi < 5 \cdot 10^{-11} \tag{3.35}$$

as a condition for an undrained response for which the analytical solution is valid, i.e., no pore-pressure changes occur under this value. This is highlighted in Figure 3.5 and allows an assessment of the conditions for which the analytical solution should be valid.

Figure 3.5 shows that undrained conditions are more likely the deeper a system. Further, when the hydraulic conductivity of the leaky layer (k_l) increases, the system behaves more drained. This is expected as the system becomes more permeable and therefore allows flow in response to pressure gradients. This results in fluid movement which causes increased drainage. Similarly, as the specific storage at constant strain increases (rows of plots in Figure 3.5) the level of drainage decreases. This is because as S_ϵ increases the volume of fluid that the system contains due to deformation increases leading to less fluid moving out of the system. This can also be explained using equation 3.8 when dividing by S_ϵ

$$\left(\frac{\partial p}{\partial t} + B K_u \frac{\partial \epsilon}{\partial t} \right) = \frac{k_{p,ij}}{\mu S_\epsilon} \nabla^2 p_f + \frac{Q}{S_\epsilon} \tag{3.36}$$

Equation 3.36 illustrates that the hydraulic diffusivity of a system ($k_{p,ij} \mu^{-1} S_\epsilon^{-1}$) decreases with the increase of S_ϵ.

As the bulk modulus (K) increases, see columns in Figure 3.5, the system becomes more drained. An explanation for this is that as the filling material becomes stiffer, the mechanical coupling becomes less relevant and the system approaches an incompressible porous skeleton. Under such conditions, only a drained response is allowed and an instantaneous pneumatic
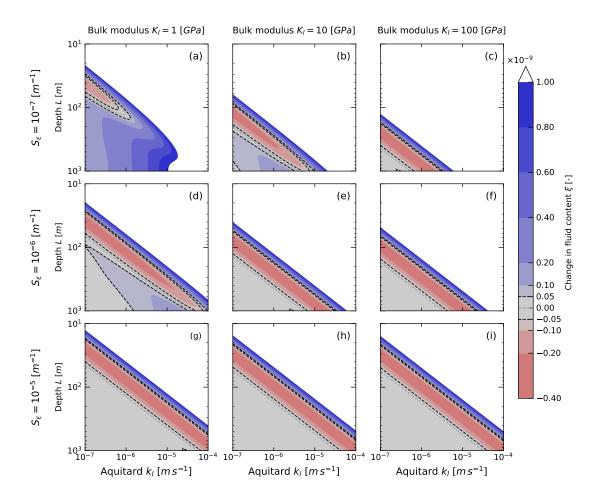
Figure 3.5: Change of fluid content ξ over depth and aquitard hydraulic conductivity for a 1D column (Figure 3.2b) and Earth tide forcing with M_2 frequency. Rows correspond to different values of specific storage whereas columns are representative for different bulk moduli, e.g., clay (a, d, g), sand (b, e, h) and hard rock (c, f, i). Values of ξ can be used to infer the depth at which the system response is undrained, i.e., where application of the analytical solution (equations 4.12 and 4.13) is valid. Value ranges of validity are delineated by the dashed line.

response of the system is no longer possible. This can also be explained by revisiting the definition of the Skempton coefficient (B). Assuming $\alpha = 1$, then

$$B = \frac{K_f}{K_f + \phi K} \tag{3.37}$$

which illustrates that when the bulk modulus increases B decreases. This results in a reduction of the overall storativity of the system and consequently also drainage. Another way to understand this result is by considering the coupling of equations. For this simulation we assumed mechanical stress balance as follows

$$\frac{\partial \sigma_{zz}}{\partial z} = 0. \tag{3.38}$$

Here, equation 3.6 must remain constant when the total stress increases (first two terms of the equation 3.6) thus the amount of fluid leaving the system must increase (third term of the equation 3.6).

In general, a larger porosity will increase the value of the specific storage at constant strain, which will decrease the level of drainage. Our assessment shows that when the hydraulic conductivity of the leaky layer exceeds $k_l > 10^{-5}\ ms^{-1}$, this leads to drained conditions and could result in errors when the analytical solution is used to estimate the properties of the aquifer. However, it is worth noting that the level of drainage depends on the geomechanical properties of the system, as well as depth and frequency of the signal. The amplitude of the signal, ϵ_0, for field measurements, as higher amplitudes will generate higher confined porepressure and facilitate detection of fluid level changes inside the observation well.

As shown in Figure 3.5, the level of confinement depends on the hydraulic and geomechanical properties of the subsurface under consideration. Consequently, defining conditions under which an undrained response exists depends on the particular field conditions, e.g., depth of the borehole and some knowledge of the subsurface properties. Figure 3.5 can be used as a preliminary guide for assessing whether or not it is appropriate to apply the analytical solution for interpreting the groundwater level response to Earth tides.

We note that Figure 3.5 represents the subsurface response to the M_2 frequency. Whether or not a porous medium is drained or undrained depends, among other things, on the frequency of the applied strain. In general, the slower the frequency the deeper the transition between drained and undrained. Consequently, if two Earth tide components were used to estimate properties (equations 3.20 and 3.21) then the observation must be deep enough to ensure undrained conditions for both components.

3.3.5 Robustness and limits of analytical Earth tide interpretations

Determining subsurface properties from Earth tide responses requires system confinement as a basic condition. To study the effects of a realistic well-aquifer system and the effect of (un)drained conditions, the level of confinement is gradually relaxed in a layered 2D model in this section. The red dots in Figure 3.6 shows the results from our numerical model (Section 3.2.5) compared to the analytical solution without vertical leakage ($k_l = 0\ ms^{-1}$) for a tidal signal with 2 cpd frequency (Section 3.2.2). The good agreement of amplitude ratios and phase differences verifies our coupled numerical modeling approach. This allows a rigorous hydraulic and geomechanical assessment of how realistic conditions (e.g., subsurface layered heterogeneity) affects the groundwater response to Earth tides.

The effect of the Biot modulus is also shown in Figure 5. Discrete values of $\alpha = 0.75$, $\alpha = 0.5$
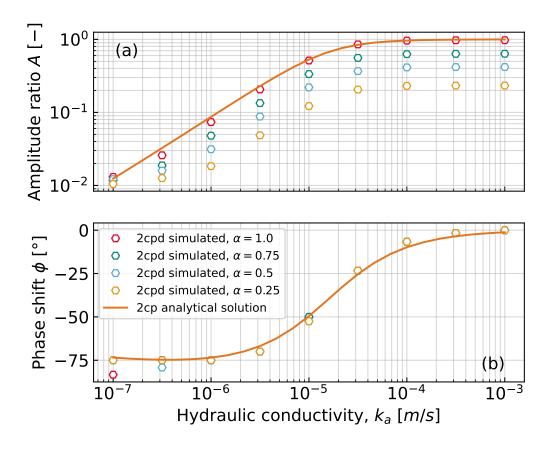
Figure 3.6: Verification of the 2D numerical model against Hsieh et al. (1987) for a harmonic forcing signal with 2 cpd frequency. Here, the simulation of the hydraulic conductivity of the leaky layer was set to zero. The figure also shows the effect of the Biot modulus on the confined pore pressure.

and $\alpha = 0.25$ were considered and show the effect over the confined pore pressure generated by a Earth tide deformation. In an undrained system, the Biot modulus represents the ratio of deformation between the porous space and the porous material. Thus it becomes relevant in situations where porous material rearrangement is not possible, such as in consolidated systems, and it usually varies between $n \leq \alpha \leq 1$ Wang (2017). As expressed in equation 2, the Biot modulus attenuates the confined pore pressure generated by a given strain. Therefore, a priori knowledge of its value is fundamental when dealing with consolidated systems.

Numerical simulations consider discrete values of the hydraulic conductivity of the aquifer (10^{-3} ms^{-1}, 10^{-4} ms^{-1} and 10^{-5} ms^{-1}) and varying values of the aquitard, $10^{-7} \leq k_l \leq 10^{-4}$ (in ms^{-1}) which is the range of values studied by Wang et al. (2018). In addition, discrete values of specific storage at constant strain (10^{-5} m^{-1}, 10^{-6} m^{-1} and 10^{-7} m^{-1}) were investigated. For detailed information of all the material parameters used in the simulation please refer to Table 3.1.

The effect of the amplitude ratio and the phase shift due to leakage of the aquitard are shown in figure 3.7. The columns represent values of aquifer hydraulic conductivity (k_a). The first row shows the effect on the amplitude ratio (A) and the second column the effect of the phase shift (ϕ) over different levels of aquitard confinement (k_l). Each line in the figure 3.7 correspond to the three discrete simulated values of the specific storage at constant strain (S_ϵ). Simulations are shown with marked lines while the analytical solution of Wang et al. (2018) is shown with
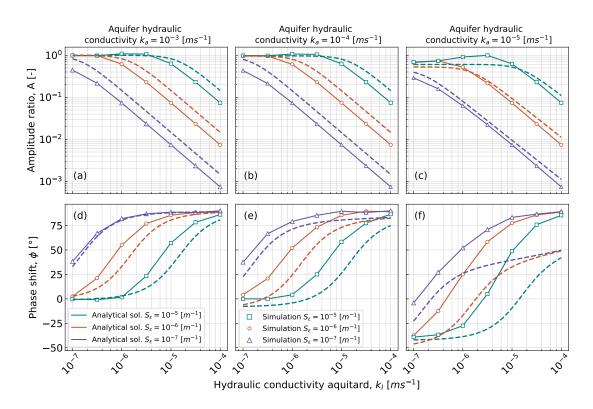
Figure 3.7: Comparison of the amplitude ratios and phase shifts obtained from numerical modeling and the analytical solution by Wang et al. (2018).

dashed lines.

The level of drained conditions can be assessed in conjunction with figure 3.5 for the three specific storage at constant strain simulated here (figure 3.5b, 3.5e and 3.5h). For example, at $100\ m$ depth (which is the thickness of the aquitard in the simulations) and $S_\epsilon = 10^{-7}\ m^{-1}$ (Figure 3.5b), the system shows drained conditions within the entire range of confinement ($10^{-7} \leq k_l \leq 10^{-4}\ ms^{-1}$, see the blue triangle markers in Figure 3.7). Therefore, the simulated amplitude under these conditions is somewhat lower and the phase shift higher compared to the analytical solution. This results in an underestimation of the hydraulic properties of the aquifer (k_a and S_ϵ) or overestimation of leakage from the aquitard (k_l) when the analytical solution is used.

When the specific storage at constant strain of the aquifer is $S_\epsilon = 10^{-6}\ m^{-1}$, at $100\ m$ depth, the system is in a transition zone between positive and negative change of fluid content when $k_l = 10^{-7}\ ms^{-1}$ (Figure 3.5e). Since the simulated amplitude ratio and phase shift match the analytical solution, the system can still be assumed as undrained within this transition zone. However, for higher levels of leakage ($k_l > 10^{-7}\ ms^{-1}$), the system is outside this transition zone and completely drained conditions prevail. The latter leads to significant differences between numerical and analytical results.

Similar results are observed when the specific storage at constant strain of the aquifer is $S_\epsilon = 10^{-5}\ m^{-1}$. When the level of leakage is $k_l \leq 5 \cdot 10^{-5}\ ms^{-1}$ the system is undrained or in the transition zone and the numerical results comply with the analytical solution. For lower levels of confinement (i.e. $k_l > 5 \cdot 10^{-5}\ ms^{-1}$), the system becomes drained and the simulation results, once again, differ compared to the analytical solution.

In the particular case when the hydraulic conductivity of the aquifer is $k_a = 10^{-5}\ ms^{-1}$, the numerical result do not comply with the ones obtained with the analytical solution even

under undrained conditions (Figure 3.7c and 3.7f). As the hydraulic conductivity of the aquifer decreases, the finite time to move fluid in or out of the well increases. Hence, it is likely that the fluid velocity is much more influenced by high gradients generated by the drained top boundary rather than by the gradients produce inside the open well under such conditions.

In all three columns of Figure 3.5, as the level of confinement provided by the aquitard decreases, the simulated results of phase shift tend towards the same value ($90°$ for the simulated system). This means that, as the drainage from the aquitard increases, the effect of the top drained boundary over the pore pressure in the aquifer increases. The same effect is observable on the amplitude ratio, where the final value of the amplitude ratio is the same in every specific storage at constant strain under study. This effect indicates that the hydraulic conductivity of the aquifer loses relevance as the drainage from the aquitard increases. And, therefore, if the system is draining, at low levels of confinements ($k_l > 5 \cdot 10^{-5} \ ms^{-1}$), the groundwater level measured in the field can potentially result in very similar values regardless of the aquifer hydraulic conductivity.

The effect of drained conditions on the amplitude ratio and phase shift can be better understood when streamlines (i.e., the Darcy velocity field) of the system are plotted. Figure 3.8 shows streamlines in an area close to the open well when the amplitude of the Earth tide strain is at maximum. This provides understanding of how flow paths change as the level of confinement decreases at fixed aquifer specific storage at constant strain ($S_\epsilon = 10^{-6} \ m^{-1}$) and hydraulic conductivity ($k_a = 10^{-4} \ ms^{-1}$). At the high confinement ($k_l = 10^{-7} \ ms^{-1}$) the flow within the aquifer is horizontal and porepressure gradients are directed towards the well. This complies with the assumption of horizontal flow inherent to the analytical solution. As confinement decreases (i.e., increasing leakage of the aquitard), the velocity field shows increasing flow in the vertical direction through layers which reduces the radius of influence of the well. With the smallest confinement investigated (Figure 6c), vertical flow dominates in the aquifer and almost no horizontal flow is observable. This shows that the pressure wave produced by the open top boundary has strong effects on the amplitude ratio and phase shift at low confinement and dampens the porepressure signal generated by Earth tides.

Figure 3.3 can be used in conjunction with the results shown in Figure 3.7 to assess the potential error due to requiring undrained conditions when the analytical solution is utilized. For example, assuming a typical specific storage at constant strain of $S_\epsilon = 10^{-6} \ m^{-1}$, leakage of $k_l = 10^{-6} \ ms^{-1}$ and hydraulic conductivity of the aquifer $k_a = 10^{-3} \ ms^{-1}$, the simulated amplitude ratio is 0.61 and the phase shift is $55.0 °$ (Figure 6a and 6d). Since the phase shift is positive there is leakage from and to the aquifer to the aquifer is occurring (i.e. $k_l \neq 0 \ ms^{-1}$ Figure 2c to 2h). When the hydraulic conductivity of the aquitard is between $0 \leq k_l \leq 10^{-8} \ ms^{-1}$ (Figure 2c and 2d) the positive phase shifts occur only at low amplitude $0 \leq A \leq 0.1$. When k_l is $10^{-4} \ ms^{-1}$ (Figure 2g and 2h) the amplitude is smaller than 0.1 in the studied range. Thus, k_l should range between $10^{-8} < k_l < 10^{-4} \ ms^{-1}$, $10^{-4} \leq k_a \leq 10^{-2} \ ms^{-1}$ and the specific storage at constant strain between $10^{-5} \leq S_\epsilon \leq 10^{-4} \ m^{-1}$ (Figure 2e and 2f).

Our results show that a high specific storage at constant strain ($S_\epsilon \geq 10^{-6} \ m^{-1}$) in combination with a high confinement ($k_l \leq 5 \cdot 10^{-5} \ ms^{-1}$) and hydraulic conductivity of the aquifer ($k_a \geq 10^{-4} \ ms^{-1}$) allow application of the analytical solution. Application to real world system further requires a high contrast in hydraulic conductivity between the layers ($k_a k_l^{-1} \geq 10^3$) with specific storage values that are typical ($\approx 10^{-6} \ m^{-1}$). In reality, the confined porepressure is damped by the movement of fluid and fully undrained conditions may be rare. Any a priori knowledge of the formation (e.g., thicknesses and hydraulic properties) is key in the assessment of
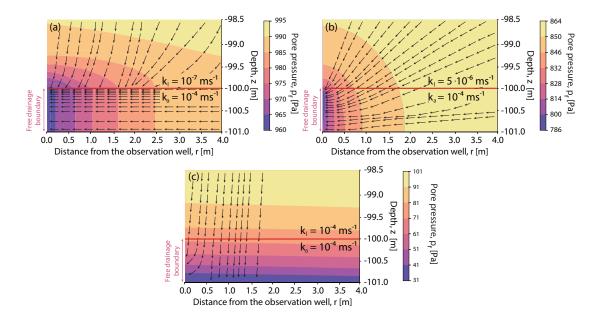
Figure 3.8: Streamlines show the velocity field towards the observation well during maximum Earth tide strain for three different aquitards with varying hydraulic conductivities: (a) low, (b) medium, (c) high. This illustrates that the flow direction changes from horizontal to vertical as the leakage increases.

Earth tidal analysis, not only to have a good approximation when inverting equations, but also to approximate the level of drainage and therefore assess potential errors when the analytical solutions are utilized.

For unconsolidated systems the soil matrix is more compressible than the grains (i.e., an unconsolidated subsurface) which leads to $\alpha = 1$. Moreover, hydraulic conductivity and porosity for what can be considered an aquifer varies between $10^{-2}\ ms^{-1} \leq k_a \leq 10^{-4}\ ms^{-1}$ and $0.2 \leq n \leq 0.3$, respectively. This means that the specific storage at constant strain varies between $9.1 \cdot 10^{-7}\ m^{-1} \leq S_\epsilon \leq 1.4 \cdot 10^{-6}\ m^{-1}$ (with the bulk modulus of water, $K_f = 2.2 \cdot 10^{-9}\ Pa$). Considering these ranges and given sufficiently high confinement between layers, application of the analytical solution to well fluid levels is valid. For example, this would be the case for hydraulic properties of sands and gravels overlain by clays or silts.

For consolidated systems, Earth tidal analysis poses a challenge as the Biot coefficient generally is $\alpha < 1$. In order to use the groundwater response to Earth tides, the Biot coefficient has to be known as it directly attenuates the porepressure response to strain (equation 3.7). Although some values of the Biot coefficient have been reported for different rock types varying from 0.1 to 1 Cheng (2016), real world measurements are difficult to find in the literature Wang & Zeng (2011); Cosenza et al. (2002). Our work shows that the Biot coefficient requires estimation when the groundwater response to Earth tides is quantitatively evaluated for wells screened in consolidated systems. Hence, for real systems, this leads to the following trade-off: As deeper wells are more likely to contain Earth tide influences because undrained conditions exists, but they are also more likely consolidated, in which case an estimate of the Biot modulus is required. Overall, our results show that a presence of Earth tide components in wells that are screened in deep and unconsolidated systems are likely to have undrained conditions and are therefore suitable for interpretation.

3.4 Conclusions

The amplitude and phase of the groundwater response to harmonic Earth tide components can be used to estimate hydraulic conductivity and specific storage values of aquifer systems. However, this approach is based on simplified analytical solutions to the groundwater flow equation, which has various assumptions that have not been tested yet. To assess the effect of such assumptions, we present a numerical method to simulate the groundwater response to Earth tides by coupling compressible flow to geomechanics. We demonstrated that this can be solved numerically using the *Multi Object Oriented Simulation Environment* (MOOSE) and verify this using a simplified analytical solution of the groundwater flow equation. We further use simulations to assess the conditions of validity for simplified analytical solutions when estimating hydraulic properties from the groundwater response to Earth tides.

By first focusing on the aquitard layer, we assess the subsurface response type, i.e., drained or undrained conditions, to the dominant harmonic Earth tide component at M_2 with frequency of 1.93227 cycles per day (cpd) for depths up to $5\ km$ and a range of hydraulic conductivities. Based on typical Earth tide strains, we define that undrained conditions exist when the incremental of fluid content is smaller than $5 \cdot 10^{-11}$ for which the groundwater equation and associated analytical solution should be valid. Our results show that this is the case for specific storage at constant strain larger than $1 \cdot 10^{-6}\ m^{-1}$ and depths higher than $50\ m$ for low conductivity systems ($k_a < 10^{-7}\ ms^{-1}$) and depths up to 1 km for high conductivity systems ($k_a \geq 10^{-3}\ ms^{-1}$).

We revisited previously interpretations based on analytical solutions and showed that the specific storage has been often misinterpreted. Moreover, only an approximation of the exact solution of the non-linear analytical models can be obtained. Obtaining physically plausible results for (1) aquifer hydraulic conductivity, (2) specific storage at constant strain and (3) aquitard hydraulic conductivity requires constraints, e.g. through additional information. A comparison between the analytical solution and a 2D two-layered aquitard-aquifer system coupled to a well shows that amplitudes and phases diverge when the hydraulic conductivity contrast between aquifer and aquitard reduces. This is caused by decreasing confinement leading to flow paths that change from horizontal to vertical as the vertical leakage increases. Applicability of the analytical solution to real-world problems requires a hydraulic conductivity contrast of at least 3 orders of magnitude.

Overall, the confined porepressure generated by Earth tide strains can be significantly attenuated by the movement of fluid through boundaries (i.e., drained conditions). Furthermore, any additional a priori knowledge about the hydraulic or geomechanical properties of the subsurface formation is crucial, if the groundwater response to Earth tides is evaluated using analytical solutions. Our numerical approach developed and documented can be extended to investigate the influence of other variables on results from analytical solutions. Finally, results obtained from the groundwater response to Earth tides should be validated with established hydraulic and geophysical methods.

3.5 Appendix

3.5.1 Response of well water levels to harmonic forcing

Hsieh et al. (1987) assumed unidirectional radial flow to a well which changes the water level in a well located at a boundary of the aquifer. The head gradient in the aquifer is given by the

volumetric strain of an Earth tide which is assumed to be known. Later on, Wang et al. (2018) complemented Hsieh et al. (1987) work by considering a two layered system by adding a leaking term to the equation 3.16 expressed by

$$Q = -\frac{k_l}{H_l}h,$$ (3.39)

with boundary conditions given by

$$t > 0, r = r_\infty : h(r, t) = h_\infty$$ (3.40)

$$t > 0, r = r_w : h(r, t) = h_w(t)$$ (3.41)

$$t > 0, r = r_w : 2\pi r_w T(\partial h/\partial r) = \pi r_c^2(\partial h_w/\partial t)$$ (3.42)

where k_l is the hydraulic conductivity of the leaky layer and H_l the thickness of the leaky layer. Wang et al. (2018) presented a solution for changes in well water levels are given by

$$h_w = \frac{i\omega S_t}{(i\omega S_t + k_l/H_l)\gamma}\left(\frac{BK_u\epsilon_0}{\rho g}\right),$$ (3.43)

where ω is the angular frequency, $h_{w,e}$ is the change in water level in the well caused by Earth tides, ϵ_0 the amplitude of the Earth strain

$$\gamma = 1 + \left(\frac{r_c}{r_w}\right)^2 \frac{i\omega r_w}{2T\beta}\frac{K_0(\beta r_w)}{K_1(\beta r_w)},$$ (3.44)

where r_w is the well radius, r_c is the radius of the well case, K_0 and K_1 are the modified Bessel functions of the first and second kind respectively and

$$\beta = \left(\frac{k_l}{TH_l} + \frac{i\omega S_t}{T}\right)^{0.5}.$$ (3.45)

Chapter 4

Technical note: Novel analytical solution for groundwater response to atmospheric tides

Abstract

Subsurface hydraulic and geomechanical properties can be estimated from well water level responses to Earth and atmospheric tides. However, the limited availability of analytical solutions restricts the applicability of this approach to realistic field conditions. We present a new and rigorous analytical solution for modelling flow between a subsurface-well system caused by harmonic atmospheric loading. We integrate this into a comprehensive workflow that also estimates subsurface properties using a well-established Earth tide method. When applied to groundwater monitoring datasets obtained from two boreholes screened in a sand aquifer in the Mary-Wildman Rivers region (Northern Territory, Australia), estimated hydraulic conductivity and specific storage agree. Results also indicate that small vertical leakage occurs in the vicinity of both boreholes. Furthermore, the estimated geomechanical properties were within the values reported in literature for similar lithological settings. Our new solution extends the capabilities of existing approaches, and our results demonstrate that analysing the groundwater response to natural tidal forces is a low-cost and readily available solution for unconsolidated, hydraulically confined, and undrained subsurface conditions. This approach can support well-established characterisation methods, increasing the amount of subsurface information.

4.1 Introduction

Knowledge of subsurface hydro-geomechanical properties is crucial for Earth resource development and management. Such properties determine the capacity of hydrostratigraphic units to

store and transmit groundwater. Traditional, active hydraulic testing methods such as pumping, slug, pressure and packer tests or laboratory analyses of cores involve considerable logistical expenses (Maliva, 2016). In contrast, passive methods (e.g. *Tidal Subsurface Analysis*, TSA), which are used to estimate hydraulic properties from well water level responses to ubiquitous periodic forces (Merritt, 2004; Cutillo & Bredehoeft, 2011), are relatively low cost to implement and derive additional value from commonly measured datasets (McMillan et al., 2019b; Rau et al., 2020b, 2022). The effect of gravitational effects and atmospheric loading on the subsurface has been long observed and reported (Meinzer, 1939) and is contained in routine groundwater pressure measurements made in countless observation wells around the world (McMillan et al., 2019b). The influence of natural forces such as tides on groundwater pressures are ubiquitous allowing widespread application reducing effort and cost of investigations. Since passive approaches rely on natural signals and do not require any active perturbation of the subsurface system, we will refer to them collectively as *Passive Subsurface Characterisation* (PSC) in our work.

Earth and atmospheric tides act at as harmonic forces at various frequencies (McMillan et al., 2019b). For groundwater investigation the most informative frequencies range from 0.8 to 2.0 cycles per day (cpd) (Merritt, 2004). Dominant frequencies present in groundwater pressure measurements are the S_1 (1.0 cpd), M_2 (1.93 cpd) and the S_2 (2.00 cpd). These components generally show a higher amplitude in comparison with other tidal harmonics and are, therefore, more likely to be contained in field datasets (McMillan et al., 2019b).

Loading forces cause mechanical deformation of the water-saturated porous medium, leading to an instantaneous pore pressure response and a hydraulic gradient towards the nearby observation well. This gradient drives groundwater exchange between the subsurface and the well until re-equilibrium is achieved (Cheng, 2016; Verruijt, 2013; Wang, 2017). The amplitude ratio between the magnitude of well water level variation and subsurface pore pressure variation, as well as the time delay required for groundwater exchange, expressed as a phase shift or phase lag, can be used to estimate subsurface hydro-geomechanical properties (Hsieh et al., 1987). Positive phase shifts (i.e., when well water levels respond before subsurface water pressures to Earth tide-induced strain variations) have been linked to vertical connectivity with adjoining hydrostratigraphic units (Roeloffs et al., 1989). Amplitude ratios and phase shifts can be readily extracted from measurements and inverted using established analytical solutions (McMillan et al., 2019b).

Cooper Jr et al. (1965) derived an analytical solution for the movement of groundwater caused by seismic waves in fully confined aquifers. Bredehoeft (1967) proposed a method to interpret the effect of Earth tides on observation wells based on classic solid mechanics, which allowed the estimation of specific storage of the aquifer if the Poisson's ratio of the porous medium was known. However, this method did not comply with Biot consolidation theory (Biot, 1941) as it did not couple fluid dynamics with mechanical deformation. Subsequently, many studies described the effect of Earth tides in poroelastic systems (Bodvarsson, 1970; Robinson & Bell, 1971; Arditty et al., 1978; Van der Kamp & Gale, 1983), but did not consider the damping effect of the observation well on the amplitude and phase. To address the signal diminishing effect of a well, Hsieh et al. (1987) combined the poroelastic response of a confined aquifer with Cooper Jr et al. (1965)'s work and derived an analytical solution to model flow to wells due to Earth tides.

Rojstaczer (1988) proposed an analytical solution for modelling flow to wells induced by atmospheric tides. However, the solution requires knowledge of vadose properties which are

often unknown, and it does not account for the effect of barometric efficiency on confined pore pressure (also known as tidal efficiency). To address this, Rojstaczer & Riley (1990) developed an analytical solution that includes the barometric effects on confined pore pressure, but it does not consider the effects on amplitude and phase shift of a well. Additionally, the mean stress in their formulation only considers the vertical direction and neglects lateral directions, which can lead to significant errors for typical Poisson's ratio values (Cheng, 2016; Verruijt, 2013; Wang, 2017).

Several studies have estimated subsurface properties using Earth tide analysis (Le Borgne et al., 2004; Doan et al., 2006; Cutillo & Bredehoeft, 2011; Lai et al., 2013, 2014; Rahi & Halihan, 2013; Xue et al., 2016; Shi & Wang, 2016; Acworth et al., 2016). However, many of the analytical solutions used to derive estimates assume oversimplified settings, which can lead to inaccurate results. To address this, Wang et al. (2018) recently developed an analytical solution that describes flow in and out of a well caused by Earth tides in a two-layered flow system. Gao et al. (2020) accounted for the well skin effect, which occurs when the physical properties of the formation in a larger area around a borehole are affected by drilling, leading to reduced amplitude ratio and phase shift. Additionally, Guo et al. (2021) derived an analytical solution to describe flow in fractures caused by Earth tides and estimated hydraulic properties. Finally, Liang et al. (2022) solved Richards equation (Freeze & Cherry, 1979b) to include the effect of the unsaturated zone, finding that it delays the phase shift response of the borehole pressure.

Xue et al. (2016) and Rau et al. (2020b) used the analytical solution of Wang (2017) to model the barometric effect of atmospheric tides with vertical leakage, but it lacks the damping effect of an observation well. Recently, Rau et al. (2022) proposed a new approach based on the work of Acworth et al. (2017) that combines poroelastic relations for one-dimensional Earth and atmospheric tide deformation to obtain a system of equations with poroelastic properties. However, their approach is based on an analytical model that does not correctly represent vertical leakage. To the best of our knowledge, there is no rigorous analytical solution in the literature to model flow to wells induced harmonically from atmospheric tides based on the mean stress flow equation while considering a semi-confined aquifer.

The objective of this work is twofold. Firstly, we introduce a new analytical solution based on the Biot theory of consolidation that describes the flow between a subsurface-well system caused by the harmonic loading of atmospheric tides. Secondly, we demonstrate its usefulness by applying it to well water levels from two boreholes in the Northern Territory of Australia and comparing the results with established Earth tide methods and existing knowledge of the groundwater system. Our study demonstrates that our new analytical solution extends the range of properties that can be accurately estimated and provides a better understanding of subsurface processes and properties.

4.2 Analytical solution

In this section, a new analytical solution based on the mean stress flow equation is derived to simulate flow to wells resulting from atmospheric tides loading the surface. The fluid continuity equation in the mean stress form can be used to describe the water flow from a semi confined aquifer towards an observation well. If only radial flow is assumed and small vertical fluid exchange from the semi confined layer occurs, the equation reads (Cheng, 2016; Verruijt, 2013; Wang, 2017)

$$S_\sigma H_a \left(\frac{\partial h}{\partial t} - \frac{\alpha}{3KS_\sigma} \frac{\partial \sigma}{\partial t} \right) = T \left[\frac{\partial^2 h}{\partial r^2} + \frac{1}{r} \frac{\partial h}{\partial r} \right] - \frac{k_l}{H_l} h. \tag{4.1}$$

Here, σ is the mean stress; K is the drained bulk modulus of the solid material; r radius; hydraulic head of the fluid (groundwater for this study), h is being used as a proxy for pore pressure $p_f = \rho g h$; T is the transmissivity of the aquifer with $T = k_a H_a$, where k_a is the hydraulic conductivity and H_a the aquifer thickness. If the aquifer is overlain by a leaky aquitard, then the downward leakage flux can be described as $k_l h H_l^{-1}$, where k_l is the vertical hydraulic conductivity and H_l is the aquitard saturated thickness. Note that this approximation is only valid when $k_a k_l^{-1} \gg 1$. α is the Biot coefficient which is equal to one for unconsolidated systems (e.g., gravels, sands and clays), and ranges between $n \le \alpha \le 1$ for consolidated systems (e.g. bedrock); where n is effective porosity. S_σ is the Biot modulus at constant stress (also known as three dimensional storage coefficient) (Cheng, 2016; Verruijt, 2013; Wang, 2017)

$$S_\sigma = \frac{\rho g}{R}, \tag{4.2}$$

where g is gravitational acceleration and ρ the fluid density. R is the Biot modulus at constant stress defined as (Cheng, 2016; Verruijt, 2013; Wang, 2017)

$$\frac{1}{R} = \frac{n}{K_f} + \frac{\alpha - n(1 - \alpha)}{K}, \tag{4.3}$$

where K_f is the bulk modulus of the fluid ($K_f = 2.2 \cdot 10^9 \ Pa$ for freshwater).

Barometric pressure fluctuations cause loading at the ground surface which results in vertical deformation of the subsurface and, therefore, changes to the internal stress balance of the fluid-solid skeleton system. For example, when atmospheric pressure rises and, the formation undergoes compressive stress resulting in an increased in the confined pore pressure (Domenico & Schwartz, 1997).

In a fully saturated porous medium, this effect can be described by Biot consolidation theory as follows (Cheng, 2016; Verruijt, 2013; Wang, 2017)

$$p_f = R\left(-\frac{\alpha}{K}\sigma + \xi\right). \tag{4.4}$$

Here, p_f is the fluid (i.e., water in this study) pore pressure; σ is the mean stress; K is the drained bulk modulus of the solid material; ξ is the change in fluid content, can be used to quantify changes in pore pressure resulting from hydraulic gradients (Cheng, 2016; Verruijt, 2013; Wang, 2017). The sign of this parameter indicates whether a fluid is leaving or entering a given porous medium.

Biot's consolidation theory assumes $\xi = 0$ when undrained conditions apply within the porous medium. Conversely, system conditions are drained when $\xi \ne 0$. Note here that a drained porous medium conceptually differs from a confined aquifer and these concepts that are often mixed up in the literature. For example, a confined aquifer may exchange fluid via one of its horizontal boundaries such as a confined aquifer bounded by a river.

We solved Eq. 4.1 for steady state conditions to obtain the periodic water level in an open borehole $h_w^{AT} = h_{w,o}^{AT} e^{i\omega t}$ due to atmospheric loading, where ω is the angular frequency of the tide signal and superscript AT stands for atmospheric tides, for example S_1 at 1 cycle per day (CPD) or the atmospheric response to S_2 at 2 cpd (Merritt, 2004; McMillan et al., 2019b).

As boundary condition, the hydraulic head far away from the radius of influence of the borehole is given only by the mechanical response of the system

$$t > 0, r = r_\infty : h(r,t) = h_\infty = \frac{p_{f,\infty}}{\rho g}, \tag{4.5}$$

where r_∞ is a distance far away from the radius of influence of the borehole and the hydraulic head at the borehole screen, h_w, should be the water level in the bore

$$t > 0, r = r_w : h(r,t) = h_w^{AT}(t), \tag{4.6}$$

the bore and the aquifer are free to exchange groundwater, i.e.,

$$t > 0, r = r_w : 2\pi r_w T(\partial h/\partial r) = \pi r_c^2 (\partial h_w^{AT}/\partial t). \tag{4.7}$$

With these boundary conditions the solution of the water level in the borehole is derived as

$$h_{w,o}^{AT} = \frac{i\omega H_a}{(i\omega(S_\epsilon + \frac{\rho g}{K})H_a + k_l/H_l)\gamma_a} \left(\frac{\sigma}{3K}\right), \tag{4.8}$$

where the periodic atmospheric loading is assumed only vertical (i.e. $\sigma = \sigma_{zz}$) modelled as $\sigma = \sigma_{atm}e^{i\omega t}$, thus σ_{atm} represents the amplitude of the atmospheric tide, and

$$\gamma = 1 + \left(\frac{r_c}{r_w}\right)^2 \frac{i\omega r_w}{2T\beta} \frac{K_0(\beta r_w)}{K_1(\beta r_w)}. \tag{4.9}$$

Here, K_0 and K_1 are the modified Bessel functions of the second kind and order zero and one, respectively, and

$$\beta = \left(\frac{k_l}{TH_l} + \frac{i\omega(S_\epsilon + \frac{\rho g}{K})H_a}{T}\right)^{0.5}. \tag{4.10}$$

Note that S_ϵ, the specific storage at constant strain, and S_σ are related as (Cheng, 2016; Verruijt, 2013; Wang, 2017)

$$S_\epsilon = S_\sigma - \frac{\rho g}{K}. \tag{4.11}$$

Since it is assumed that the borehole is open to the atmosphere, any change in barometric pressure will also play a role in the hydrostatic pressure inside the borehole. Thus, the amplitude ratio between the atmospheric loading and the confined pore pressure due to atmospheric tides, A^{AT}, has to be expressed as the balance between the far field pore pressure ($p_{f,\infty}(\rho g)^{-1}$, Eq. 4.4), the amplitude of the atmospheric load ($\sigma_{atm}(\rho g)^{-1}$) and the change of fluid level in the well, $h_{w,o}$, such as

$$A^{AT} = \left|\frac{p_{f,\infty} - \sigma_{atm} - (\rho g)h_{w,o}^{AT}}{\sigma_{atm}}\right|. \tag{4.12}$$

The time lag between the far field confined pore pressure and the actual change of fluid in an open well is given by

$$\Delta\phi^{AT} = arg\left(\frac{p_{f,\infty} - \sigma_{atm} - (\rho g)h_{w,o}^{AT}}{\sigma_{atm}}\right). \tag{4.13}$$

Note that the applied amplitude of the periodic stress at a boundary has to be equal to the atmospheric pressure

$$\sigma_{atm} = -P_{atm}, \tag{4.14}$$

where P_{atm} is the barometric pressure measured in the field. In this convention, the compression stress is opposite in sign compared to the atmospheric pressure as an increase compresses the subsurface.

We have named our novel analytical solution as the *mean stress solution*. Drawing an anal-

ogy to the established Earth tide methods (Hsieh et al., 1987; Wang et al., 2018, e.g.,), our new solution enables the estimation of subsurface hydraulic and geomechanical properties from atmospheric tidal components that are ubiquitous in standard field measurements of well water levels. This innovative solution expands the scope of existing approaches that passively characterise subsurface processes and properties (McMillan et al., 2019b).

4.3 Field application
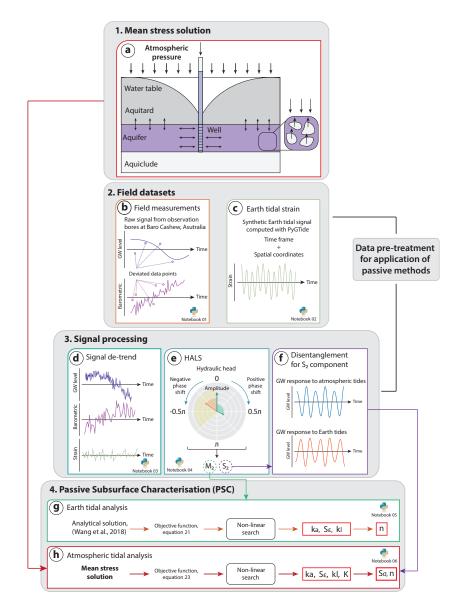
4.3.1 Field site and groundwater monitoring

Figure 4.1: Overview of the workflow applied to estimate subsurface hydraulic and geomechanical properties using the groundwater response to Earth and atmospheric tides. The data set and Python scripts developed for this work are available in an external repository (see Code and Data Availability statements).

In this section, we apply our analytical solution to field data, compare the results with those derived from established Earth tide methods and consider the results in the context of existing knowledge such as from lithological logs and hydraulic testing. The overall workflow applied in

this section is shown in Fig. 4.1 which incorporates established Earth tide methods alongside our new solution.

The study area is bounded by the Mary River National Park in the west and by the Kakadu National Park in the east. The intervening area has been of interest for irrigated agricultural development since the 1980s. The area features a sub-equatorial climate, with the dry season occurring between May and September and the wet season occurring between October and April. The highest annual mean air temperatures are recorded between October and December at around $35°C$ and the lowest in July at around $16°C$ (Tickell, 2017).

Two main hydrostratigraphic units are present as layers in the study area: (1) Mesozoic/Cenozoic sediments underlain by (2) the Proterozoic Koolpinyah Dolostone, and silt- and sandstones (Fig. 4.2a) (Tickell, 2017). Groundwater and mineral exploration wells are the main source of geological information as outcrops are rare. Mesozoic/Cenozoic sediments consist of unconsolidated to poorly consolidated sands, clayey sands, and clays. Lithological logs indicate that this unit is laterally extensive across the study area (Tickell, 2017). A leaky sandy clay aquitard partially confines a second semi-confined sand aquifer (B1 and B2 in Fig. 4.2c). This aquifer is sufficiently permeable to allow recharge to the semi-confined sand aquifer, as observed by increases in the groundwater level during each wet season. The Proterozoic strata consist primarily of Koolpinyah Dolostone and Wildman Siltstone. The hydrological behaviour of this unit is conceptually a fractured aquifer (Tickell, 2017). Constant rate discharge pumping tests indicate that the hydraulic conductivity of the Mesozoic/Cenozoic strata ranges from $8.0 \cdot 10^{-5}$ to $6.3 \cdot 10^{-4}$ ms^{-1} (Appendix 4.5.2).

Groundwater monitoring datasets from two boreholes B1 and B2 were analysed in this work (Fig. 4.2b and Table 4.1). Note that the original nomenclature from the Australian Northern Territory (NT) was modified (Table 4.1). The lithological logs indicate that the boreholes are screened in the upper strata (Fig. 4.2c). In general, the upper two thirds of the profile are clays and sandy clays that confines the underlying aquifer. The lower third often consists of sands, clayey sands and gravels. Sands are mostly present as fine-grained quartz with limited occurrences of coarse sands to pebbles.

Well water levels were monitored hourly between June 2016 and September 2019 in each borehole using InSitu Level TROLL 400 data loggers (InSitu Inc., USA). The measured pressure heads were converted to hydraulic head values by referencing the dips of depth to water level manually to the surveyed top of casing elevations. Concurrently, barometric pressure was recorded from September 2016 to October 2017 using an InSitu BaroTROLL 500 data logger (InSitu Inc., USA).

Table 4.1: Groundwater well construction information, reference datum Geocentric Datum Of Australia (GDA) 1994. DD stands for *decimal degrees*.

Borehole NT ID	Borehole	Latitude $[DD]$	Longitude $[DD]$	Total depth $[m]$	Screen length $[m]$	Radius $[m]$
RN039769	B1	-12.6077	131.8295	43.0	4	0.156
RN024762	B2	-12.6259	131.8801	61.1	6	0.203

4.3.2 Extraction of tidal responses

Earth tide strains, barometric pressure and hydraulic heads in wells B1 and B2, are shown in Fig. 4.3. Outliers were identified using Pearson's rule, i.e., values that deviate more than three times the *Median Absolute Deviation* (MAD) (Pham-Gia & Hung, 2001), and removed from the
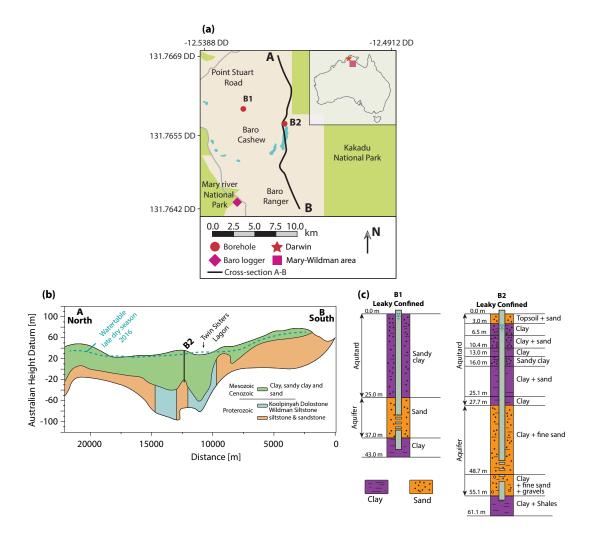
Figure 4.2: (a) Map of the study site, including surface water features, borehole locations and, location of the transect from A-B, (b) transect showing simplified geology adapted from (Tickell, 2017) and (c) lithological logs from both studied boreholes. DD stands for decimal degrees.

data (Fig. 4.1b and 4.6). Note that the overall head varies by about 2 m reflecting the wet and dry seasons that are typical for tropical Australia. Earth tide strains were calculated using *PyGTide* (Rau, 2018a) which is based on the widely used ETERNA PREDICT software Wenzel (1996) (Fig. 4.1c).

Harmonic tidal components of the ten dominant target frequencies between 0.33 and 2.2 cycles per day (cpd) (Merritt, 2004; McMillan et al., 2019b) were extracted from all time series and locations following the methods outlined in Schweizer et al. (2021) and Rau et al. (2020b):

- The measured well water levels were de-trended using a moving linear regression filter with a 3-day window (Fig. 4.1d) and the results are shown in Fig. 4.7.

- Amplitudes and phases of ten tidal harmonic constituents were jointly estimated using *Harmonic Least Squares* (HALS) (Fig. 4.1e).

- From HALS, amplitudes and phases of the M_2 and S_2 tidal components were obtained for the Earth tide strains (Fig. 4.4a), barometric pressure (Fig. 4.4b) and hydraulic heads (Fig. 4.4c,d).

- Complete disentanglement of the groundwater response to Earth and atmospheric tide influences was done for S_2 following the method established by Rau et al. (2020b) (Fig.
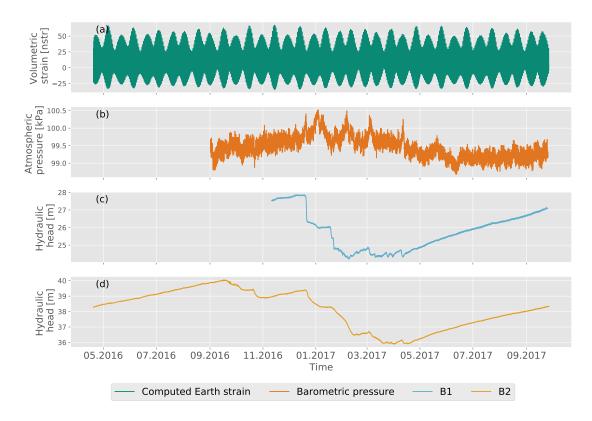
Figure 4.3: Time series of: (a) computed Earth tide strain in nano-strain (nstr), (b) measurements of barometric pressure, and hydraulic head time series measured in boreholes B1 (c) and B2 (d).

4.1f).

The resulting amplitude of the hydraulic head (abbreviated as GW for groundwater) A^{GW} can be divided by the Earth tide strain amplitude (abbreviated as ETP for Earth tides) A^{ETP}, to obtain the amplitude ratio (Fig. 4.4e)

$$A_o^{ET} = \frac{A^{GW}}{A^{ETP}}.$$ (4.15)

The phase shift $\Delta\phi_o^{ET}$, can be obtained as the difference between the obtained phase of the hydraulic head measurements ϕ^{GW} and the computed Earth tide strain prediction, ϕ^{ETP} as

$$\Delta\phi_o^{ET} = \phi^{GW} - \phi^{ETP}.$$ (4.16)

Resulting A_o^{ET} and $\Delta\phi_o^{ET}$ for hydraulic head and areal Earth tide strain for borehole B1 and B2 are presented in Fig. 4.4e and Table 4.4.

Analogously, the ratio between the resulting amplitude of HALS of the hydraulic head A^{GW} can be divided by the measured (time series) barometric pressure (abbreviated as ATP for atmospheric tides) A_{ATP} to obtain the amplitude ratio

$$A_o^{AT} = \frac{A^{GW}}{A^{ATP}}\rho g.$$ (4.17)

The phase shift $\Delta\phi_o^{AT}$, can be obtained as the difference between the obtained phase of the hydraulic head measurements ϕ^{GW} and the measured barometric pressure, ϕ^{ATP} as

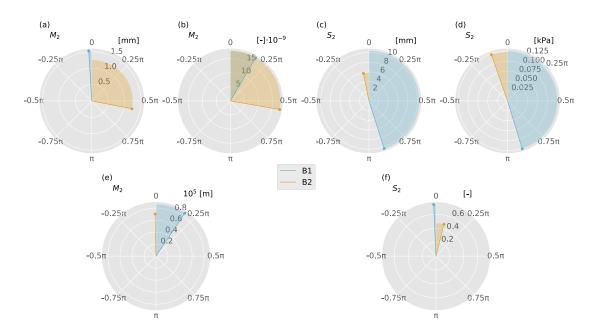$$\Delta\phi_o^{AT} = \phi^{GW} - \phi^{ATP}.$$ (4.18)

Figure 4.4: Polar plots showing the M_2 and S_2 harmonics estimated from hydraulic heads in response to Earth and atmospheric tides for boreholes B1 and B2. (a) M_2 constituent in measured well water levels. (b) M_2 constituent in Earth tide strain data calculated at well locations. (c) S_2 constituent in well water levels. (d) S_2 constituent in Earth tide strain data calculated at well locations. (e) Amplitude and phase shift of the M_2 constituent, equations 4.15 and 4.16. (f) Amplitude ratio and phase shift of the S_2 constituent, equations 4.17 and 4.18 .

Resulting A_o^{AT} and $\Delta\phi_o^{AT}$ for hydraulic head and areal Earth tide strain for borehole B1 and B2 are presented in Fig. 4.4f and Table 4.5.

4.3.3 Estimation of subsurface properties

To estimate subsurface parameters from the groundwater response to Earth tides, the analytical solution by Wang et al. (2018) was fitted to the M_2 harmonic component extracted from field data. This analytical describes the well water level fluctuations, $h_{w,o}^{ET}$, caused by the harmonic compression of the subsurface from Earth tides (abbreviated as ET).

The reduction in amplitude of an harmonic signal is described by the ratio between the far field pressure generated by Earth tide strain and the fluid level in the borehole and is known as amplitude ratio(Hsieh et al., 1987)

$$A^{ET} = \frac{h_{w,o}^{ET}}{\epsilon},$$

(4.19)

where ϵ is the unit-less areal strain. The time lag between the far field pressure and the fluid level in the borehole is known as phase shift Hsieh et al. (1987)

$$\Delta\phi^{ET} = arg\left(\frac{h_{w,o}^{ET}S_\epsilon}{\epsilon}\right).$$

(4.20)

In theory, the obtained amplitude and phase shift from field measurements (equations 4.15 and 4.16) should be the same as those obtained using the analytical solution (Eq. 4.19 and 4.20). Since the observed amplitude, A_o^{ET}, and phase shift, $\Delta\phi_o^{ET}$, are measurable in the field, they can be used to fit parameters of the analytical solution of Wang et al. (2018) with a non-linear

solver to find roots (Fig. 4.1g). To do so, the following objective function has to be minimised

$$OF^{ET} = \left| \frac{A_o^{ET} - A^{ET}}{A_o^{ET}} \right| + \left| \frac{\Delta\phi_o^{ET} - \Delta\phi^{ET}}{\Delta\phi_o^{ET}} \right|.$$ (4.21)

Since phase shifts can be orders of magnitude grater than amplitude ratio, OF^{ET}, is nor-malised to avoid that one term dominates the solution. Assuming that the borehole construction parameters are known (H_a, H_l, r_c and r_w), three parameters can be estimated, i.e., hydraulic conductivity of the aquifer (k_a), vertical hydraulic conductivity of the leaky layer (k_l), and specific storage at constant strain (S_ϵ). Once S_ϵ is obtained, effective porosity can be computed if the material is unconsolidated using (Cheng, 2016; Verruijt, 2013; Wang, 2017)

$$n = \frac{S_\epsilon K_f}{\rho g},$$ (4.22)

where K_f is the bulk modulus of the fluid ($K_f = 2.2 \cdot 10^9 \ Pa$ for freshwater).

In analogy to Earth tides, the field measurements of barometric pressure and well water levels in the field should match the those obtained by analytical methods. Thus, the obtained amplitude ratio, A_o^{AT}, and phase shift, $\Delta\phi_o^{AT}$, in the field (computed later with Eq. 4.17 and 4.18, respectively) can be used to estimate subsurface parameters by iterative non-linear numerical methods (Fig. 4.1h). The function to minimise is

$$OF^{AT} = \left| \frac{A_o^{AT} - A^{AT}}{A_o^{AT}} \right| + \left| \frac{\Delta\phi_o^{AT} - \Delta\phi^{AT}}{\Delta\phi_o^{AT}} \right|.$$ (4.23)

The non-linear search allows for the iterative fitting of four parameters: hydraulic conductivity of the aquifer (k_a), vertical hydraulic conductivity of the leaky layer (k_l), bulk modulus (K), and specific storage at constant strain (S_ϵ). Additionally, specific storage at constant stress (S_σ) can be estimated using Eq. 4.11.

Once S_ϵ is estimated, porosity can be computed with Eq. 4.22. If values of specific storage, S are known (i.e., from a different characterisation method such as pumping tests), then shear modulus can also be estimated as (Cheng, 2016; Verruijt, 2013; Wang, 2017)

$$G = \frac{3}{4} \frac{(1 - K(S - S_\epsilon/\rho g))}{S - S_\epsilon/\rho g}.$$ (4.24)

By effectively combining hydraulic and poroelastic theory, this approach expands the number of parameters that can be estimated.

By solving Eq. 4.21, aquifer hydraulic conductivity k_a, specific storage at constant strain S_ϵ, and vertical hydraulic conductivity of the aquitard k_l can be estimated. Eq. 4.23 allows estimation of aquifer hydraulic conductivity k_a, specific storage at constant strain S_σ, vertical hydraulic conductivity of the aquitard k_l, and bulk modulus K. Once specific storage at constant strain is quantified, porosity n, can be estimated with Eq. 4.22. If the specific storage is known, shear modulus G, can be estimated with equation Eq. 4.24. Equations 4.21 and 4.23 can be solved using non-linear iteration (Fig. 4.1g and 4.1h).

The non-linear inversion was performed in two steps to help the iterative method converge to a global minimum instead of a local one. Firstly, the solution space of the objective function was divided into intervals within feasible ranges of subsurface properties, creating a feasible objec-tive space, thus bounding the initial conditions for the least-squares algorithm. Secondly, 1,000 randomly generated values following a log-normal distribution were fed as initial conditions to

the least-squares algorithm, the array of parameters that converges to the best fit among them, was considered to be the global minimum of the non-linear search (Aster et al., 2018).

4.3.4 Hydraulic and geomechanical properties

Values from Earth tide analysis and atmospheric tide analysis are presented in Tables 4.2 and 4.3. Further, the estimated aquifer hydraulic conductivity, specific storage at constant strain and aquitard vertical hydraulic conductivity for boreholes B1 and B2 are shown Fig. 4.5.

Table 4.2: Estimated subsurface parameters from Earth tide analysis.

| Borehole | Non-linear search results | | | |
	k_a [ms^{-1}]	S_ϵ [m^{-1}]	k_l [ms^{-1}]	n [-]
B1	$1.1 \cdot 10^{-5}$	$1.8 \cdot 10^{-6}$	$5.4 \cdot 10^{-8}$	0.37
B2	$1.0 \cdot 10^{-4}$	$3.8 \cdot 10^{-7}$	$1.1 \cdot 10^{-8}$	0.08

Table 4.3: Estimated subsurface parameters from atmospheric tide analysis.

| Borehole | Non-linear search results | | | | | |
	k_a [ms^{-1}]	S_ϵ [m^{-1}]	k_l [ms^{-1}]	K [GPa]	S_σ [m^{-1}]	n [-]
B1	$1.6 \cdot 10^{-5}$	$1.8 \cdot 10^{-6}$	$8.0 \cdot 10^{-10}$	0.3	$3.5 \cdot 10^{-5}$	0.4
B2	$1.0 \cdot 10^{-4}$	$5.0 \cdot 10^{-7}$	$6.0 \cdot 10^{-8}$	10.0	$1.5 \cdot 10^{-6}$	0.11

The basic assumption of undrained conditions applies to the analytical solutions by Wang et al. (2018) and this study (Eq. 4.8). To assess whether this condition is fulfilled, both Earth and atmospheric tide analyses, were assessed separately:

1. For Earth tide analysis, Bastias et al. (2022) numerically computed the level of drainage over depth for different arrays of subsurface properties. Despite the estimated k_l being outside the range presented by Bastias et al. (2022), it can be extrapolated. At borehole B1, the aquifer is within undrained conditions. At borehole B2, it is within the transition zone between drained and undrained.

2. For atmospheric tide analysis, Wang (2017) defined the depth of undrained conditions as

$$\delta = \sqrt{\frac{2c}{\omega}}, \tag{4.25}$$

where c is the consolidation coefficient. For boreholes B1 and B2, undrained conditions are found at depths higher than 2.3 and $40.6\ m$, respectively, under atmospheric tide loading.

Consequently, for the estimated parameters in this study, B2 borders drained conditions, and the generated confined pore pressure by tidal forcing is being diminished. This may influence the estimated properties.

The aquifer hydraulic conductivity estimated with PSC complies with previous values of poorly consolidated sands and gravel aquifers in the literature ($5 \cdot 10^{-6} \leq k_a \leq 10^{-3}\ ms^{-1}$) (Freeze & Cherry, 1979b; Tickell, 2017) (Fig. 4.5a, Tables 4.2 and 4.3). Note that the estimated value of k_a is lower compared to the pumping tests in the study site (Table 4.6). Bastias et al. (2022) studied the area of influence of PSC and concluded that PSC is a small-scale characterisation technique where parameters are estimated in the vicinity of the well screen. This might explain the difference between values presented in this study and the ones obtained with pumping tests (Appendix 4.5.2), as estimates parameters with small-scale methods will tend to
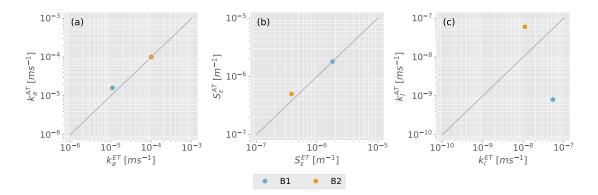
Figure 4.5: Comparison of the subsurface parameters estimated independently using the well water level response to Earth tides and atmospheric tides: (a) hydraulic conductivity of the aquifer, (b) specific storage at constant strain, (c) vertical hydraulic conductivity of the aquitard.

give much lower values than obtained from a full-well or packer pumping test, because small-scale analyses may miss the most permeable intervals that make the greatest contribution to the transmissivity (Maliva, 2016). This idea is supported by previous studies that reported several orders of magnitude differences between traditional hydraulic characterisation methods and PSC (Allègre et al., 2016; Zhang et al., 2019; Valois et al., 2022; Qi et al., 2023). The difference was attributed to issues such as the borehole skin effect (Zhang et al., 2019; Valois et al., 2022) and differing model assumptions (Qi et al., 2023). Furthermore, Zhang et al. (2021b) showed good agreement between hydraulic parameters of a consolidated subsurface system derived using PSC and laboratory measurements. This supports our observation that PSC results are representative of a smaller sample volume close to the well screen. However, determining the extent of the area around the well screen affected by flow from tidal forces is outside the scope of this work and requires further investigation. Additionally, reconciling the properties derived from both active and passive approaches will require more research.

The estimated values of specific storage at constant strain for B1 are within the previously reported values in the literature for sand aquifers, $1.13 \cdot 10^{-6} \leq S_\epsilon \leq 2.27 \cdot 10^{-6} \ m^{-1}$ (Freeze & Cherry, 1979b) (Fig. 4.5b). Porosity, computed with Eq. 4.22, is also within the reported range, $0.25 \leq n \leq 0.5$ (Freeze & Cherry, 1979b). Conversely, borehole B2 shows values of specific storage at constant strain and porosity are below the expected range Tables 4.2 and 4.3. There are several potential causes for this, such as the presence of flow paths that create undrained conditions, leading to a reduction in the generated confined pore pressure and exposing the limitations of passive methods for this borehole. Furthermore, the degree of aquifer consolidation is limited, and the length of the well screen is not representative of the full depth of the aquifer. These factors were not explored in this study and should be the focus of future numerical investigations to better understand their effects on the results.

The estimated aquifer bulk modulus values (Table 4.3) were consistent with literature values for sands and gravels, typically between $5 \cdot 10^{-2} \ GPa$ and $3 \cdot 10^1 \ GPa$ (Das & Das, 2008; Look, 2007). If it is assumed that the average variability of the hydraulic properties in the aquifer is low (Fig. 4.8b), the values presented in Table 4.6 (wells W7, W8, W9 and W10) can be used to estimate shear modulus using Eq. 4.24. Estimated shear modulus values were 0.7 and 0.03 GPa for B1 and B2 respectively. We note that these values are consistent with expectations reported in the literature for similar lithological settings, e.g., typically between $8 \cdot 10^{-3} \ GPa$ and $9 \cdot 10^3 \ GPa$ (Das & Das, 2008; Look, 2007).

Compared to the previous analytical solution presented by Rojstaczer & Riley (1990), which

describes flow to wells due to barometric loading, the derived analytical solution in this study simplifies the pore pressure wave generated in the vadose zone by assuming that only small vertical flow occurs in the confined layer. Moreover, the solution of Rojstaczer & Riley (1990) requires knowledge of vadose zone properties that are difficult to determine. Furthermore, the continuity equation is solved in terms of the mean stress equation, allowing for the estimation of mechanical parameters such as bulk modulus and specific storage at constant stress. As shown in our work, this extends the current range of parameters that can be estimated passively (McMillan et al., 2019b).

While we present a new analytical solution, we are unable to compare or validate geomechanical results due to a lack of independent measurements. Additionally, the literature comparing subsurface properties using PSC from different methods is sparse and contains somewhat conflicting conclusions (Allègre et al., 2016; Zhang et al., 2019; Valois et al., 2022; Qi et al., 2023; Zhang et al., 2021b). This is likely due to the fact that subsurface investigations often focus on determining hydraulic properties such as hydraulic conductivity and specific storage, which are critical for understanding subsurface fluid flow. Obtaining geomechanical information such as bulk modulus, shear modulus, and stress state can be challenging and may require additional investigation techniques. However, Rau et al. (2022) noted that in-situ stress conditions, stress anisotropy and scale differences complicate comparisons with laboratory methods. We believe that systematic investigations in different archetypes of formations, including the use of borehole geophysical investigation techniques and careful laboratory testing of material samples, could help to clarify scale and heterogeneity influences, reconcile the different theories, and provide further confidence in values derived from PSC.

4.4 Conclusions

We have introduced a novel analytical solution based on the mean stress flow equation for modelling flow to wells induced by atmospheric loading. We integrate this mean stress solution into a comprehensive workflow for estimating subsurface hydraulic and geomechanical properties using the groundwater response to Earth and atmospheric tides, applied this to a standard groundwater monitoring data set from the Northern Territory (Australia) and discussed the results with hydraulic properties from pumping tests and geomechanical literature values for similar lithological settings. Our new solution allows estimation of hydraulic conductivity of the aquifer, vertical hydraulic conductivity of the aquitard, porosity, specific storage at constant strain, specific storage at constant stress and bulk modulus. The advantages are estimation of additional subsurface properties without the need for knowledge of vadose zone properties.

We compared the hydraulic properties estimated independently using the groundwater response to Earth tides and atmospheric pressure. The estimated values of aquifer hydraulic conductivity with Earth tidal analysis were $1.1 \cdot 10^{-5}\ ms^{-1}$ and $1.1 \cdot 10^{-4}\ ms^{-1}$ for borehole B1 and B2, respectively. Meanwhile, with the mean stress solution, the estimated values of aquifer hydraulic conductivity were $1.6 \cdot 10^{-5}\ ms^{-1}$ and $1.0 \cdot 10^{-4}\ ms^{-1}$ for borehole B1 and B2, respectively. These estimated values were lower than those estimated using pumping tests for the region between Mary River National Park and Kakadu National Park (ranging from $6 \cdot 10^{-4}$ to $8 \cdot 10^{-5}\ ms^{-1}$). This difference is consistent with the literature and supports the idea that PSC is a small-scale characterisation method.

The estimated specific storage at constant strain for borehole B2 was $3.8 \cdot 10^{-7}$ and $5.0 \cdot 10^{-7}\ m^{-1}$ with Earth tidal analysis and the mean stress equation, respectively. This indicates

that the response near borehole B2 is drained since the estimated values are lower than the reported bounds in the literature. Consequently, the drained conditions reduce the confined pore pressure generated by tides. The estimated values of aquitard vertical hydraulic conductivity differed from the pumping tests by orders of magnitude but suggest that the aquifer in both boreholes is semi-confined with small leakage.

The bulk and shear moduli aligned with literature values for the formation type, confirming that PSC has the potential to enhance field investigations. However, for PSC to be applied successfully, it is necessary for the basic physical assumptions underlying the analytical solutions to be valid. This can be challenging to determine in situations such as confined and undrained hydraulic conditions or an unconsolidated system where the Biot coefficient is unknown. As a result, PSC can only be applied in hydrogeological settings that adhere to the theoretical framework.

Compared to established methods like hydraulic testing, using PSC requires a better understanding of hydraulic and hydro-geomechanical theory as well as signal processing. However, PSC is less costly and effort-intensive because it only requires monitoring datasets that typically meet standard practice criteria. The literature reflects confusion about the suitability of theory and a lack of geomechanical testing alongside hydraulic testing, making it challenging to validate poroelastic properties. Systematic investigations involving a range of archetypal formations with a combination of hydraulic, geophysical, geotechnical field and laboratory tests are needed to validate PSC. This would help compare properties from rigid and elastic formations, reconcile theories, and support groundwater and geotechnical investigations.

4.5 Appendix

4.5.1 Appendix A

The hydraulic head measurements in borehole B1 and B2 are shown in Fig. 4.6. Outliers were detected and eliminated with the procedure described in Section 4.3.2.

Figure 4.6: Hydraulic head time series and outliers measured in boreholes (a) B1 and (b) B2.

Computed areal Earth tide strain, measured barometric pressure and hydraulic head of borehole B1 and B2 were de-trended using a moving meadian filter with 3-day window, Sec. 4.3.2 and Fig. 4.7.
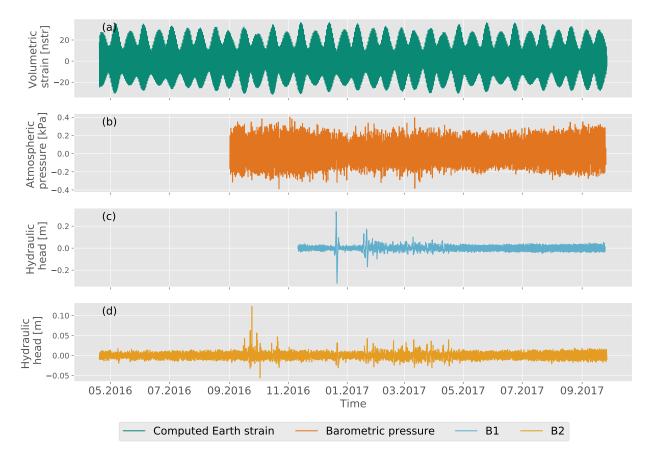

Figure 4.7: The corresponding de-trended time series showing only components with frequencies up to 3 cpd; (a) computed Earth strain, (b) measured atmospheric pressure, hydraulic head (c) B1 and (d) B2.

Harmonic constituents were obtained applying harmonic least squares (HALS), results of amplitude and phase shift to the M_2 signal are shown in Table 4.4. Analogously, the amplitude and phase shift to the S_2 signal are shown in Table 4.5.

Table 4.4: Amplitude ratio and phase shift obtained with HALS for the M_2 constituent.

Borehole	A^{ETP} [-]	$\Delta\phi^{ETP}$ [°]	A^{GW} [m]	$\Delta\phi^{GW}$ [°]	A_o^{ET} [m]	$\Delta\phi_o^{ET}$ [°]
B1	$26.57 \cdot 10^{-9}$	0.52	0.0015	-0.061	57386.49	0.59
B2	$26.65 \cdot 10^{-9}$	1.74	0.0012	1.76	46710.38	-0.02

Table 4.5: Amplitude ratio and phase shift obtained with HALS for the S_2 constituent.

Borehole	A^{ATP} [kPa]	$\Delta\phi^{ATP}$ [°]	A^{GW} [m]	$\Delta\phi^{GW}$ [°]	A_o^{AT} [-]	$\Delta\phi_o^{AT}$ [°]
B1	0.12	2.84	$1.0 \cdot 10^{-2}$	2.83	0.82	-0.71
B2	0.12	-0.33	$0.58 \cdot 10^{-3}$	-0.20	0.47	7.83

4.5.2 Appendix B

Time–drawdown data from five two-well pumping tests in the Mary–Wildman rivers area were reinterpreted using appropriate drawdown solutions using a two-step process (see Table 4.6

and W1 to W10 in Figure 4.8a) (Turnadge et al., 2018). The time–drawdown data, were used to identify appropriate pumping test analysis solutions. These included: the solutions of Barker (1988) for fractured rock flow under confined conditions; Hantush (1960) for leaky conditions; and Neuman (1974) for unconfined conditions.
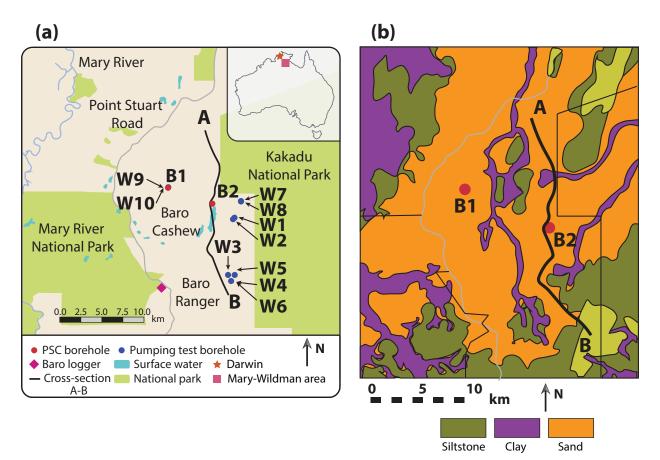

Figure 4.8: Map of the study site. (a) shows PSC boreholes, barometric sensor and location of the wells were pumping tests were performed (wells W1 to W10). (b) shows the surface geology of the Mesozoic/Cenozoic strata (modified from NT Geological Survey digital data, (Tickell, 2017))

Table 4.6: Details of five historical two-well pumping tests undertaken in the Mary–Wildman rivers area, including aquifer types interpreted from time–drawdown responses and forward solutions used to estimate aquifer hydraulic properties via model inversion. Hydraulic property values are displayed with root mean square error of optimised least squares solution. For each estimated parameter, the optimal value derived from least squares estimation is provided, as well as the approximate 95 % confidence interval.

Production well ID	Observation well ID	Attributed aquifer	Confinement type	Inversion solution	RMSE [m]	$k_a \cdot 10^{-4}$ [$m.s^{-1}$]	$S_s \cdot 10^{-5}$ [m^{-1}]	$S_y \cdot 10^{-3}$ [-]
W1 RN023158	W2 - RN023230	Cretaceous sand	Unconfined	Neuman (1974)	$1 \cdot 10^{-2}$	4.1 ± 0.3	N/A	1.0 ± 0.4
W3 RN024668	W4 - RN024596	Wildman Silt-stone	Confined	Barker (1988)	$9 \cdot 10^{-4}$	4.6 ± 0.9	8.0 ± 0.6	N/A
W5 RN024669	W6 - RN024228	Wildman Silt-stone	Confined	Barker (1988)	$2 \cdot 10^{-3}$	0.8 ± 0.2	1.0 ± 0.8	N/A
W7 RN024763	W8 - RN024764	Cretaceous sand	Leaky	Hantush (1960)	$1 \cdot 10^{-4}$	6.3 ± 0.3	5.0 ± 0.5	N/A
W9 RN039769	W10 - RN039768	Cretaceous sand	Leaky	Hantush (1960)	$1 \cdot 10^{-3}$	4.1 ± 0.4	7.0 ± 0.8	N/A

Chapter 5

Synthesis

5.1 Aim

Passive Subsurface Characterization (PSC) is a cost-effective method for estimating subsurface properties. PSC is based on the deformation caused by both celestial bodies (i.e., Earth tides) and changes in barometric pressure (e.g., atmospheric tides). Tidal forces create stresses that lead to hydraulic head gradients in the subsurface, allowing fluid exchange with a groundwater observation well. Therefore, the underlying physics of PSC can be described by subsurface flow and linear elastic solid mechanics. Despite its promise, PSC still faces several challenges, including: (1) a lack of understanding of the underlying physics, (2) the need to invert analytical solutions to estimate subsurface parameters, with limited knowledge of their robustness under realistic conditions, and (3) an analytical solution based on the mean stress flow equation, which models the flow to wells caused by atmospheric tides, and the need for validation against field data.

5.2 Workflow

To address the aforementioned challenges, three separate studies were conducted. In the first study, a flexible numerical code was designed, developed, and verified to simulate the effects of tides on the subsurface. The second study revisited the theory behind PSC and tested the robustness of the analytical solutions against numerical models. The third study focused on deriving an analytical solution to model groundwater flow due to atmospheric tides. Field data were then used to estimate subsurface parameters with both atmospheric tidal analysis and Earth tidal analysis. The objectives, methodology, and findings of the described studies are concisely presented in Figure 5.1. These studies have a strong interdependence and grow in complexity.

5.3 Novelties

This section highlights the main novelties of each of the three studies presented in this thesis.

1. The first study (Chapter 2) presents the development and verification of RHEA, a hydro-geomechanical numerical simulator based on the finite element framework MOOSE. RHEA provides a powerful tool for geoscientists to simulate complex geomechanical problems were realistic heterogenous systems can be integrated with ease. The study
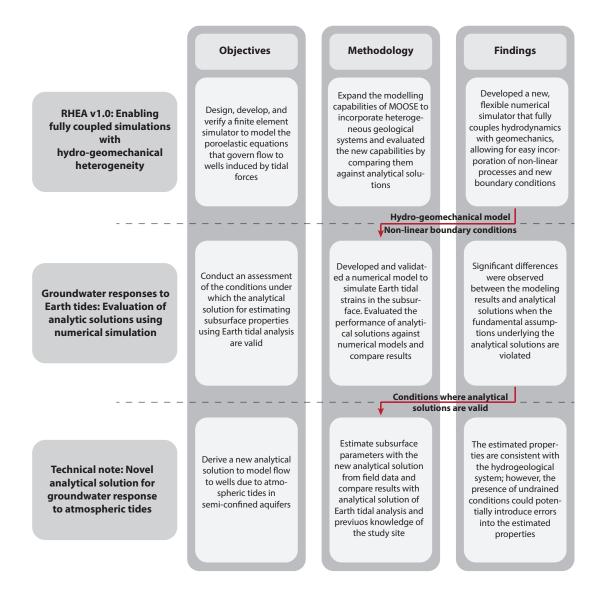
Figure 5.1: Summary of the three studies presented in this thesis. The figure shows the relation between studies.

highlights the benefits of using open source numerical frameworks with advanced features, and how they can be customized to meet specific needs. Additionally, the study includes a new test that verifies, for the first time, fully distributed hydraulic and geomechanical heterogeneity. To support modeling and data integration, the study provides a Python interface that formats field data to be incorporated into RHEA. The work serves as a great example of how numerical codes can be optimized and repurposed for geoscientific applications.

2. In the second (Chapter 3) study presents the theory behind PSC was revisited and analyzed based on the Biot consolidation theory. The fundamental equations that describe the hydraulic and mechanical coupling under Earth tidal deformation of a porous medium were systematically formulated. This study identifies suitable hydrogeological systems where PSC is applicable based on the fundamental equations of state. Additionally, a novel numerical model, capable of simulating the effect of Earth tides on the subsurface, was developed and verified using analytical solutions. For the first time, this study integrates Earth tidal strains into a subsurface geomechanical model. The model was utilized to investigate the robustness of analytical solutions that predict flow to wells due to Earth tides

and revealed significant discrepancies between numerical results and analytical solutions when the fundamental assumptions underlying the analytical solutions were violated.

3. The third study (chapter 4) presents a new analytical solution that models the flow to wells induced by the harmonic effect of atmospheric tides on a semi-confined aquifer. This new analytical solution is novel in that it integrates the pneumatic effect on pore pressure caused by atmospheric loading, expanding the range of parameters that can be estimated using PSC. The study shows that six hydro-geomechanical parameters can be estimated using atmospheric tidal analysis. The solution was validated using field data and compared to other established subsurface characterization methods. In addition, this study offers Python-based scripts that enhance the efficiency of applying PSC. The results show general agreement between well PSC and hydraulic tests. Overall, study underscore the potential of PSC in supporting characterization campaigns by providing additional information.

5.4 Methodology and findings

The change in hydraulic head produced by tides in aquifers has been modeled using analytical solutions that solve for the hydraulic physics of water in a steady state Hsieh et al. (1987); Rojstaczer (1988); Wang et al. (2018). These analytical solutions can be inverted through iterative methods to fit observed field data and estimate subsurface parameters Wang & Manga (2021). However, this approach has limitations as the analytical solutions are based on simplified assumptions of the fundamental physics of Passive Subsurface Characterization (PSC) McMillan et al. (2019b). Specifically, the analytical solutions do not account for the tight coupling between water hydraulics and the mechanical response of the porous medium under tidal deformation Bastias et al. (2022).

The elastic deformation of the porous medium caused by Earth and atmospheric tides can be described by the consolidation theory, also known as poroelastic theory Biot (1941). Many physical concepts have been historically misunderstood when deriving analytical solutions in compliance with the poroelastic theory. Furthermore, these analytical solutions have been applied in systems where the underlying assumptions, on which they were derived, are not valid. This ultimately introduces the potential for significant errors in the estimation of subsurface parameters Bastias et al. (2022).

To assess the potential errors caused by violating the fundamental assumptions on which the analytical solutions were derived, a novel and flexible finite element numerical simulator named Real Heterogeneity App (RHEA) was designed, coded, and verified. RHEA has the capability to integrate highly heterogeneous geological formations, providing a reliable tool for assessing the impact of these heterogeneities on the accuracy of subsurface characterization.

RHEA is based on the fundamental equations of the Biot consolidation theory and has been implemented on top of the Multi-physics Object-Oriented Simulation Environment framework (MOOSE) (Gaston et al., 2009; Permann et al., 2020). RHEA extends the capabilities of MOOSE to simulate transport and deformation in heterogeneous hydro-geomechanical systems. Within RHEA, material parameters can be spatially distributed by loading external datasets or defining them manually.

The performance of RHEA was verified against three analytical solutions: (1) Terzaghi's problem, a consolidation problem in a one-dimensional soil column (Terzaghi, 1923); (2) a novel consolidation problem in a one-dimensional multi-layer soil column; and (3) a two-dimensional

plane strain consolidation problem. Additionally, a high-resolution multi-facies realization of a sedimentary aquifer was imported into RHEA to model a consolidation problem, where all physical parameters (e.g., hydraulic conductivity, porosity, Young's modulus, and Poisson's ratio) varied spatially.

The study provides insights into the design of RHEA, including the equations of state and simulation procedures. Moreover, a workflow is presented for importing large external datasets into the simulator using a Python interface, which integrates various data structures with RHEA.

RHEA demonstrates great potential as it leverages the capabilities of the state-of-the-art open-source framework MOOSE. It allows for the addition of new coded objects to simulate different physics in a plug-and-play architecture. MOOSE also offers advanced numerical Jacobian solvers (PESTc) and mesh capabilities, including adaptivity provided by the numerical library LibMesh.

In RHEA, a novel numerical model was developed and verified to simulate small strain changes due to Earth tides in a porous medium. The numerical model was designed to test the robustness of analytical solutions in modeling water movement due to Earth tides under realistic scenarios, where water hydraulics are tightly coupled with the mechanics and hydraulics of the porous medium and observation well. This allows testing the fundamental assumptions on which the analytical solutions were obtained under different scenarios.

When deriving analytical solutions, hydraulic physics are decoupled from geomechanics, relying on two assumptions: (1) the system is completely undrained, with no fluid exchange at any boundary; and (2) the compressibility of the porous medium is much smaller than that of the grains, assuming an unconsolidated system (Biot, 1941).

To define the required material properties for achieving undrained conditions, a one-dimensional soil column numerical model was utilized. It was found that undrained conditions occur for an Earth tidal frequency M_2 at depths greater than 50 meters, requiring a specific storage at constant strain of $S_\epsilon \geq 10^{-6}\ m^{-1}$, an aquitard hydraulic conductivity $k_l \leq 5 \times 10^{-5}\ ms^{-1}$, and an aquifer hydraulic conductivity $k_a \geq 10^{-4}\ ms^{-1}$.

Simulation results indicate that deeper wells are more susceptible to the effects of Earth tides due to the presence of undrained conditions. However, these wells are also more likely to be consolidated, which necessitates estimating the Biot modulus. Overall, the findings suggest that wells located in deep and unconsolidated systems exhibiting Earth tide components are likely to possess undrained conditions, making them suitable for Earth tidal interpretation.

To rigorously compare the robustness of the analytical solutions, a second numerical model was developed to describe flow exchange with a well and boundaries in a two-layered system. This model consists of a leaky aquitard layer with a thickness of 100 meters, bounded by a 1-meter-thick aquifer, as described in previous literature Wang et al. (2018).

As the level of confinement decreases, the numerical results deviate from the analytical solution due to two reasons: (1) low confinement allows fluid exchange between the top boundary and the aquitard, reducing the confined pore pressure generated by Earth tides; and (2) vertical flow quickly prevails, causing the well to exchange fluid with the aquitard rather than the aquifer. For the simulated setup, the aquitard's hydraulic conductivity must be $k_l < 10^{-6}\ ms^{-1}$, the aquifer's hydraulic conductivity must be $k_a > 10^{-3}\ ms^{-1}$, and the ratio between the two conductivities must be $k_l/k_a < 10^{-3}$.

The effect of the ratio between the compressibility of the porous material and the porous medium (i.e., degree of consolidation) was also studied. As the compressibility of the porous

material approaches that of the porous medium, the generated pore pressure by tides decreases, attenuating the confined pore pressure and making PSC less feasible. However, a rigorous quantification of this effect was beyond the scope of this work.

Numerical models reveal that Passive Subsurface Characterization (PSC) is primarily a local characterization method that estimates properties of an area near the screened observation well. This finding is interesting considering that PSC was historically regarded as a large-scale characterization method (Maliva, 2016). Groundwater has limited time for exchange between the aquifer and the well, and the hydraulic gradients generated by tides are relatively small, resulting in low groundwater velocity. The available time for exchange is determined by the frequency of the tidal signal. For example, numerical models show that for a 2 cycles per day (cpd) signal, only water in the nearby area of the well screen can be exchanged.

The solution space of the analytical solutions in PSC is nonlinear. For a given subsurface system, multiple potential solutions can be found when using an iterative method to fit field data. Optimization based on iterative methods typically searches for changes in the gradient of the objective function, which can often result in unrealistic estimations of subsurface parameters. It is important for the user to properly constrain the problem within a realistic expected range where a solution might be found. Additional information about the subsurface, such as well logs or pumping tests in the area, can facilitate this task.

Although various analytical solutions exist to model the hydraulic behavior of water caused by Earth tides, the subsurface effects of atmospheric tides have historically been neglected in analytical solutions. Previous solutions focused solely on vertical flow resulting from pressure waves caused by atmospheric changes at the surface, without considering the confined pore pressure generated by the mechanical equilibrium between the solid media and the groundwater Rojstaczer (1988).

To address this limitation, a new analytical solution based on poroelastic principles was derived to model steady-state flow to wells induced by the harmonic loading of atmospheric tides. The analytical solution incorporates a two-layered system, where an aquitard confines an aquifer and small leakage occurs between the layers. Unlike previous solutions, the new analytical solution accounts for the harmonic load exerted by atmospheric tides and incorporates the change in mechanical equilibrium between the porous media and the filling fluid under applied forces. Consequently, elastic mechanical properties such as bulk modulus can be estimated. This novel analytical solution represents a significant advancement in modeling the subsurface effects of atmospheric tides.

The derived analytical solution was inverted to fit data from two boreholes located in a study site in northern Australia. The hydrostratigraphic units under investigation consist of unconsolidated sediments, where a leaky sandy clay aquitard partially confines a second semi-confined sand aquifer.

Two dominant tidal signals (M2 and S1 frequencies) were extracted from the dataset and used to estimate parameters using Earth tidal analysis and atmospheric tidal analysis, respectively. From the analysis, six hydrogeomechanical properties were estimated: aquifer hydraulic conductivity (k_a), specific storage at constant strain (S_ϵ), specific storage at constant stress (S_σ), porosity (n), vertical hydraulic conductivity (k_l) of the aquitard, and bulk modulus (K).

In addition, Python-based scripts were provided to facilitate the workflow used in this study for estimating subsurface properties using Passive Subsurface Characterization (PSC). PSC involves three fundamental steps: (1) calculation of areal tidal strain from celestial catalogs, (2)

computation of harmonic components of the tidal signals using harmonic least squares, and (3) inversion of analytical solutions using iterative methods. The provided scripts automate these steps, streamlining the overall process and improving analysis efficiency.

The estimated hydraulic conductivity (k_a) values for two boreholes, B1 and B2, were 10^{-4} ms^{-1} and 10^{-5} ms^{-1}, respectively. These values align with literature values for sand. The specific storage at constant strain (S_ϵ) values were estimated to be approximately $1.8 \cdot 10^{-6}$ m^{-1} and $5.0 \cdot 10^{-7}$ m^{-1} for B1 and B2, respectively, resulting in effective porosity estimates of 0.4 and 0.1. The lower value of S_ϵ observed in B2 can be attributed to identified undrained conditions, which were determined through subsequent analysis of the estimated hydraulic properties. The estimated vertical hydraulic conductivity (k_l) of the aquitard was $5.8 \cdot 10^{-8}$ ms^{-1} and $1.1 \cdot 10^{-8}$ ms^{-1} for B1 and B2, respectively, indicating minor leakage in the aquifer. The estimated bulk modulus (K) was found to be 0.3 Pa and 10 Pa, in agreement with literature values for the hydrogeological system (Cheng, 2016; Verruijt, 2013; Wang, 2017; Freeze & Cherry, 1979a).

Reinterpreting previous pumping tests conducted in the study area provided hydraulic conductivity estimates for the aquifer ranging from $8.0 \cdot 10^{-5}$ ms^{-1} to $4.6 \cdot 10^{-4}$ ms^{-1}. Discrepancies in the determined hydraulic properties between the two methods can be attributed to the fact that passive methods evaluate a smaller area surrounding the well screen compared to hydraulic testing analysis (Maliva, 2016). Passive methods induce slight hydraulic gradients, allowing only fluid in the immediate proximity of the well screen to flow towards the well, while hydraulic testing influences a larger area, resulting in average hydraulic properties within that zone of influence. Although determining the precise area of influence for passive methods is challenging, it can be accomplished through numerical modeling in future investigations.

Consistent hydrogeomechanical property results were obtained through both Earth tidal analysis and atmospheric tidal analysis for boreholes B1 and B2. However, undrained conditions were identified in B2, which reduced the generated confined pore pressure and could lead to deviated results. Further assessment of the causes of drainage cannot be performed with the available data, but it may be explored in future research. Comparisons between literature studies on passive methods and hydraulic testing have resulted in different conclusions. Generally, hydraulic conductivity estimates obtained using passive methods tend to be smaller than those obtained through hydraulic testing. This difference has been attributed to the skin effect of the well (Zhang et al., 2019; Valois et al., 2022).

5.5 Conclusions

RHEA is a simulation tool that enables fully coupled simulations in hydrogeomechanical systems. It utilizes the well-established numerical framework MOOSE to handle numerical technicalities. Users can incorporate new physics and material properties, such as soil or rock nonlinearities, by plugging new pieces of code into its object-oriented architecture. This approach allows users to focus on modeling, which is highly complex in geosciences as it involves defining the geometry, boundaries, and material properties of natural systems.

To evaluate the performance of RHEA in hydrogeomechanical systems, the framework was tested against established analytical solutions and a novel analytical solution specifically designed to assess RHEA's performance in heterogeneous systems. Additionally, a workflow was developed to facilitate the incorporation of field data into RHEA. The effectiveness of this workflow was demonstrated by successfully applying RHEA to a high-resolution dataset, solving a consolidation problem. These tests and demonstrations establish the robustness and flexibility

of RHEA as a simulation tool for hydrogeomechanical systems.

One numerical challenge that arises when modeling flow to wells due to small pore pressure gradients is ensuring that the water level in the well matches the hydraulic head of the aquifer at the shared boundary. Typically, small time steps are required to maintain numerical stability due to the loose coupling between them. In RHEA, the code is fully coupled, and the water level in the well is treated as a state variable, allowing it to be solved simultaneously with pore pressure and displacements in the same Jacobian matrix in each nonlinear step. This feature enables larger time steps to be used, making RHEA useful in various subsurface applications that involve coupling external variables with porous media transport physics, such as civil structures built around soil pits.

The approach in this thesis was to model Earth tides as a uniform deformation throughout the model, which is only valid in homogeneous systems. In heterogeneous systems, where the mechanical properties of the filling material may vary spatially and temporally, a different modeling strategy is required. Earth tides mechanically deform the subsurface, which is not caused by external mechanical forces (e.g., small changes in gravity). Therefore, a heterogeneous model must consider the additional physics of eigenstrains. Although this approach introduces new nonlinearities with potentially unknown properties, they can easily be incorporated into RHEA with just a few lines of code.

This study provides a comprehensive documentation of the physics underlying PSC, demonstrating the tight coupling between hydraulics and geomechanics under tidal stress. To apply PSC with analytical solutions that simplify this coupling, it is crucial to ensure that the assumptions under which they are derived are valid. However, determining the suitability of analytical solutions for a given subsurface condition and data set is not straightforward. In general, knowledge of the subsurface, such as well logs, can significantly improve the estimation of subsurface parameters using PSC by addressing potential errors that may arise when applying PSC.

The parameter fitting process for analytical solutions must be performed with constraints on the realistic limits of parameter values. Since analytical solutions are highly nonlinear functions, they may have multiple critical points. At these points, gradient-based equation inversion may exhibit poor performance, where convergence criteria may be met, but the obtained solution may not represent the true solution of the system.

Overall, the confined pore pressure generated by Earth tide strains can be significantly attenuated by fluid movement through boundaries (i.e., drained conditions). Additionally, any a priori knowledge about hydraulic or geomechanical properties of the subsurface formation is crucial when evaluating the groundwater response to Earth tides using analytical solutions. The numerical approach developed and documented in this study can be extended to investigate the influence of other variables on results obtained from analytical solutions. Furthermore, the results obtained from the groundwater response to Earth tides should be validated using established hydraulic and geophysical methods.

The effect of Earth tides on the subsurface was modeled, and the results showed significant differences between numerical and analytical results when the assumptions underlying the analytical solution were violated. Thus, this study provides simple guidelines for bounding the appropriate conditions where analytical solutions can safely be applied to estimate subsurface parameters. Future work can focus on developing more advanced models to study various scenarios, such as different types of well construction and aquifer setups, and investigate the potential impact of aquifer facies on the estimated properties using PSC. The mechanical characterization of the subsurface may also have a significant impact, as the mechanical prop-

erties of the confining layer may contrast in orders of magnitude with those of the semi-confined aquifer. For instance, a relatively soft layer can generate higher confined pore pressure when a load is applied, resulting in larger gradients that may ultimately affect the estimated parameters.

A comparison between the analytical solution and a two-dimensional two-layered aquitard-aquifer system coupled to a well showed that amplitudes and phases diverge as the hydraulic conductivity contrast between the aquifer and aquitard decreases. This divergence is caused by decreasing confinement, leading to flow paths that transition from horizontal to vertical as the vertical leakage increases. The applicability of the analytical solution to real-world problems requires a hydraulic conductivity contrast of at least three orders of magnitude.

A new analytical solution based on Biot's consolidation theory was proposed to estimate subsurface properties using the passive effects of atmospheric tides. This analytical solution models flow to wells caused by the deformation of a two-layered system by atmospheric tides and was tested with field data from two boreholes located in the north of Australia. The study outlines how six hydro-geomechanical properties can be estimated using the newly derived analytical solution, and a comprehensive workflow is provided for efficiently estimating subsurface properties using passive methods.

The estimated properties from both boreholes were compared with Earth tidal analysis, and the results were found to be consistent between the two methods, except for the observation of undrained conditions in one of the boreholes. The level of drainage is challenging to assess with the currently available data, but it can potentially be analyzed using advanced numerical models or more advanced analytical solutions that include displacements as boundary conditions.

The pumping tests conducted at the studied boreholes were also reinterpreted, revealing relatively small variability in the hydraulic properties, which aligns with previous studies conducted at the site. The results of storativity were combined with the estimated values obtained through PSC to estimate shear moduli. This combination of information from passive methods and hydraulic testing demonstrates the potential to enhance subsurface information and improve the assessment of a study site.

Passive seismic characterization (PSC) is an elegant and cost-effective method that provides valuable subsurface information through a simple process. Additionally, the influence of gravitational effects from Earth tides and atmospheric loading on the subsurface has long been observed and documented, making it detectable through routine groundwater pressure measurements in numerous observation wells worldwide. This widespread availability further enhances the potential of PSC. Although several challenges remain unresolved, this study emphasizes the significant advantages of PSC. Not only does it offer more comprehensive subsurface information compared to other methods such as pumping tests, but it can also be combined with these methods to further enhance subsurface characterization.

5.6 Outlook

There are still many challenges and unanswered questions that must be addressed to establish PSC as a reliable and widely adopted subsurface characterization method. Therefore, future efforts should prioritize addressing the following key points:

- **Potential of PSC:** While PSC has shown promising results in isolated study cases, a large-scale study on various hydrogeological architectures would provide a more holistic perspective. Analytical solutions currently allow PSC to be applied in confined or semi-

confined unconsolidated systems (such as sands, gravels, and clays) with an aquifer hydraulic conductivity of $k_a > 1 \cdot 10^{-5}\ ms^{-1}$ and a ratio in hydraulic conductivity between the aquifer and aquitard of $k_a k_l^{-1} > 10^3$. Although these conductivity constraints vary with the borehole's construction properties, they can be used as general specifications. This can help determine, on a large scale, the subsurface formations where PSC is suitable. For instance, a large-scale study could identify unconsolidated aquifers made of sand and gravel with high levels of confinement. This will assess the potential of PSC and help define its economic viability.

PSC has a lower cost than pumping tests since it does not require expert practitioners and associated hydraulic testing costs. However, there is no clear quantification of the associated costs to apply PSC. A cost analysis would involve two things: (1) drilling the borehole and (2) treating the data and inverting analytical solutions. Drilling costs are typically much higher than data treatment costs. Still, since PSC can only estimate properties from a small area near the well screen, a rigorous study of the subsurface would require drilling several boreholes in the area to generate a better statistical representation of the subsurface, thereby increasing the study's costs.

One clear advantage of pumping tests over PSC is that they require a shorter recording time series to estimate subsurface properties (one to two days). Studies based on PSC have used time series of lengths ranging from 6 months to 2 years. Therefore, if subsurface properties need to be estimated in the short term, PSC is not suitable. The minimum recording time series required to apply PSC in a reliable way has not been validated with field data. The associated costs of monitoring water levels in the borehole for a long time have not been reported.

A lab-scale study can help determine the minimum length of the time series required for PSC. In such a setup, the errors when estimating properties with PSC versus laboratory analysis of cores can also be obtained. This can be done in a sandbox where the porous media is saturated and completely sealed, ensuring fluid exchange does not occur at any boundary (i.e., undrained conditions). A well can be located, where hydraulic head and barometric pressure can be monitored, and a comparison between the properties of laboratory samples and PSC can be obtained and compared.

- **Numerical models:** Numerical models offer versatility in answering different types of questions, which can help to better understand PSC in complex and realistic scenarios. For example, a RHEA model can be used to create heterogeneous numerical models that integrate realistic aquifer configurations into the simulation. This analysis can help to clarify the effects of flow paths from the aquifer to the observation well and determine if PSC estimates properties from the flow path or is a statistical average of the well's area of influence.

  Numerical models can be utilized to evaluate the impact of borehole construction properties on pumped well capture zones (PSC). Particularly, two crucial factors can be analyzed: (1) the PSC performance under partial penetration of the well into the aquifer, and (2) the influence of borehole screen length and surface area on groundwater exchange. Analytical solutions presuppose complete borehole screen penetration of the pertinent aquifer. However, this may not always be accurate in real-world scenarios, such as wells that screen multiple aquifers or aquifers with continuously changing lithology variations.

  Ultimately, numerical models can be enhanced by integrating more realistic physics, such as the representation of Earth tides as eigenstrains, which can increase model complexity.

This approach may have the potential to evaluate the influence of mechanical properties on PSC. For instance, in scenarios where an aquifer is restrained by a highly yielding layer, that layer may generate more significant hydraulic gradients during tidal deformation than the aquifer. Numerical models can investigate the impact of this configuration on PSC, although additional parameters must be defined for this nonlinear model.

- **New analytical solutions:** The inclusion of physics coupling between hydraulics and geomechanics in analytical solutions can lead to a more realistic approximation of the physics underlying PSC. This has the potential to address questions such as pore pressure loss due to drained conditions, enabling practitioners to assess the suitability of a given site for PSC.

Interestingly, the incorporation of physics coupling does not lead to a significant increase in analysis complexity. The coupling can be achieved by utilizing a force balance, which introduces new displacement boundary conditions and establishes a relationship between stress and pore pressure via effective stress.

In analytical solutions of PSC, water velocity is determined by the ratio between hydraulic conductivity and specific storage or hydraulic diffusivity. However, when considering mechanical coupling, this parameter should also account for the mechanical properties of the system, resulting in a change from hydraulic diffusivity to consolidation coefficient. Mechanical boundary conditions can be established by defining a load and setting zero displacement. After developing a new solution, an interesting study would be to compare the existing analytical solutions with the new hydro-geomechanically coupled one.

Following the derivation of new analytical solutions, it is necessary to test new inversion methods. In this case, up to four parameters must be fitted from a single analytical solution, often leading to a poorly posed system of equations. New searching algorithms, such as Broyden's method, which weights the residuals of each parameter individually, can be explored to potentially improve fitting accuracy. Additionally, solving a system of equations that includes both Earth tidal analysis and atmospheric tidal analysis simultaneously can be investigated. This approach would enable fitting of both objective functions concurrently, potentially yielding more robust results.

Bibliography

Abarca, E., Karam, H., Hemond, H. F., & Harvey, C. F. (2013). Transient groundwater dynamics in a coastal aquifer: The effects of tides, the lunar cycle, and the beach profile. *Water Resources Research*, 49(5), 2473–2488.

Acworth, R. I., Halloran, L. J., Rau, G. C., Cuthbert, M. O., & Bernardi, T. L. (2016). An objective frequency domain method for quantifying confined aquifer compressible storage using Earth and atmospheric tides. *Geophysical Research Letters*, 43(22), 11–671.

Acworth, R. I., Rau, G. C., Halloran, L. J., & Timms, W. A. (2017). Vertical groundwater storage properties and changes in confinement determined using hydraulic head response to atmospheric tides. *Water Resources Research*, 53(4), 2983–2997.

Agnew, D. C. (2005). Earth tides: an introduction. *University of California, San Diego*.

Ahmed, E., Jaffré, J., & Roberts, J. E. (2017). A reduced fracture model for two-phase flow with different rock types. *Mathematics and Computers in Simulation*, 137, 49–70.

Alcaraz, M., Carrera, J., Cuello, J., Guarracino, L., & Vives, L. (2021). Determining hydraulic connectivity of the coastal aquifer system of La Plata river estuary (Argentina) to the ocean by analysis of aquifer response to low-frequency tidal components. *Hydrogeology Journal*, 29(4), 1587–1599.

Alexander, J. (1993). A discussion on the use of analogues for reservoir geology. *Geological Society, London, Special Publications*, 69(1), 175–194.

Allègre, V., Brodsky, E. E., Xue, L., Nale, S. M., Parker, B. L., & Cherry, J. A. (2016). Using Earth-tide induced water pressure changes to measure in situ permeability: A comparison with long-term pumping tests. *Water Resources Research*, 52(4), 3113–3126.

Allègre, V., Brodsky, E. E., Xue, L., Nale, S. M., Parker, B. L., & Cherry, J. A. (2016). Using earth-tide induced water pressure changes to measure in situ permeability: A comparison with long-term pumping tests. *Water Resources Research*, 52(4), 3113–3126.

Alnæs, M., Blechta, J., Hake, J., Johansson, A., Kehlet, B., Logg, A., Richardson, C., Ring, J., Rognes, M. E., & Wells, G. N. (2015). The fenics project version 1.5. *Archive of Numerical Software*, 3(100).

Arditty, P. C., Ramey, H. J., & Nur, A. M. (1978). Response of a closed well-reservoir system to stress induced by earth tides. In *Spe annual fall technical conference and exhibition*: OnePetro.

Aster, R. C., Borchers, B., & Thurber, C. H. (2018). *Parameter estimation and inverse problems*. Elsevier.

Atkinson, B. K. (2015). *Fracture mechanics of rock*. Elsevier.

Balay, S., Abhyankar, S., Adams, M., Brown, J., Brune, P., Buschelman, K., Dalcin, L., Dener, A., Eijkhout, V., Gropp, W., et al. (2019). Petsc users manual.

Barker, J. (1988). A generalized radial flow model for hydraulic tests in fractured rock. *Water Resources Research*, 24(10), 1796–1804.

Bastias, J., Rau, G. C., & Blum, P. (2022). Groundwater responses to earth tides: Evaluation

of analytical solutions using numerical simulation. *Journal of Geophysical Research: Solid Earth*, 127(10).

Bastías Espejo, J. M., Wilkins, A., Rau, G., & Blum, P. (2021). Rhea v1. 0: Enabling fully coupled simulations with hydro-geomechanical heterogeneity. *Geoscientific Model Development Discussions*, (pp. 1–21).

Bayer, P., Comunian, A., Höyng, D., & Mariethoz, G. (2015). High resolution multi-facies realizations of sedimentary reservoir and aquifer analogs. *Scientific data*, 2(1), 1–10.

Bear, J. & Cheng, A. H.-D. (2010). *Modeling groundwater flow and contaminant transport*, volume 23. Springer.

Bear, J. & Verruijt, A. (1987). *Modeling groundwater flow and pollution*, volume 2. Springer Science & Business Media.

Beaujean, J., Lemieux, J.-M., Dassargues, A., Therrien, R., & Brouyère, S. (2014). Physically based groundwater vulnerability assessment using sensitivity analysis methods. *Groundwater*, 52(6), 864–874.

Beck, M., Rinaldi, A., Flemisch, B., & Class, H. (2020). Accuracy of fully coupled and sequential approaches for modeling hydro-and geomechanical processes. *Computational Geosciences*, 24(4), 1707–1723.

Berre, I., Doster, F., & Keilegavlen, E. (2019). Flow in fractured porous media: A review of conceptual models and discretization approaches. *Transport in Porous Media*, 130(1), 215–236.

Berryman, J. G. (1999). Origin of Gassmann's equations. *Geophysics*, 64(5), 1627–1629.

Biot, M. A. (1941). General theory of three-dimensional consolidation. *Journal of applied physics*, 12(2), 155–164.

Birdsell, D. T. & Saar, M. O. (2020). Modeling ground surface deformation at the swiss heatstore underground thermal energy storage sites. In *World Geothermal Congress (2020)(online)*: ETH Zurich, Institute of Geophysics.

Birkholzer, J. T., Tsang, C.-F., Bond, A. E., Hudson, J. A., Jing, L., & Stephansson, O. (2019). 25 years of decovalex-scientific advances and lessons learned from an international research collaboration in coupled subsurface processes. *International Journal of Rock Mechanics and Mining Sciences*, 122, 103995.

Blum, P., Mackay, R., Riley, M., & Knight, J. (2005). Performance assessment of a nuclear waste repository: upscaling coupled hydro-mechanical properties for far-field transport analysis. *International Journal of Rock Mechanics and Mining Sciences*, 42(5-6), 781–792.

Blum, P., Mackay, R., & Riley, M. S. (2009). Stochastic simulations of regional scale advective transport in fractured rock masses using block upscaled hydro-mechanical rock property data. *Journal of Hydrology*, 369(3-4), 318–325.

Bodvarsson, G. (1970). Confined fluids as strain meters. *Journal of Geophysical Research*, 75(14), 2711–2718.

Boone, T. J. & Ingraffea, A. R. (1990). A numerical procedure for simulation of hydraulically-driven fracture propagation in poroelastic media. *International Journal for Numerical and Analytical Methods in Geomechanics*, 14(1), 27–47.

Bredehoeft, J. D. (1967). Response of well-aquifer systems to Earth tides. *Journal of Geophysical Research*, 72(12), 3075–3087.

Bridge, J. S. & Hyndman, D. W. (2004). Aquifer characterization.

Cacace, M. & Jacquey, A. B. (2017). Flexible parallel implicit modelling of coupled thermal–hydraulic–mechanical processes in fractured rocks. *Solid Earth*, 8, 921–941.

Chen, Y., Zhou, C., & Jing, L. (2009). Modeling coupled THM processes of geological porous

media with multiphase flow: theory and validation against laboratory and field scale experiments. *Computers and Geotechnics*, 36(8), 1308–1329.

Cheng, A. H.-D. (2016). *Poroelasticity*, volume 27. Springer.

Chitsazan, M., Rahmani, G., & Neyamadpour, A. (2015). Forecasting groundwater level by artificial neural networks as an alternative approach to groundwater modeling. *Journal of the Geological Society of India*, 85, 98–106.

Choo, J. & Lee, S. (2018). Enriched galerkin finite elements for coupled poromechanics with local mass conservation. *Computer Methods in Applied Mechanics and Engineering*, 341, 311–332.

Condon, L. E., Kollet, S., Bierkens, M. F., Fogg, G. E., Maxwell, R. M., Hill, M. C., Fransen, H.-J. H., Verhoef, A., Van Loon, A. F., Sulis, M., et al. (2021). Global groundwater modeling and monitoring: Opportunities and challenges. *Water Resources Research*, 57(12), e2020WR029500.

Cooper Jr, H. H., Bredehoeft, J. D., & Papadopulos, I. S. (1967). Response of a finite-diameter well to an instantaneous charge of water. *Water Resources Research*, 3(1), 263–269.

Cooper Jr, H. H., Bredehoeft, J. D., Papadopulos, I. S., & Bennett, R. R. (1965). The response of well-aquifer systems to seismic waves. *Journal of Geophysical Research*, 70(16), 3915–3926.

Cosenza, P., Ghoreychi, M., De Marsily, G., Vasseur, G., & Violette, S. (2002). Theoretical prediction of poroelastic properties of argillaceous rocks from in situ specific storage coefficient. *Water Resources Research*, 38(10), 25–1.

Cundall, P. A. & Hart, R. D. (1993). Numerical modeling of discontinua. In *Analysis and design methods* (pp. 231–243). Elsevier.

Cutillo, P. A. & Bredehoeft, J. D. (2011). Estimating aquifer properties from the water level response to earth tides. *Groundwater*, 49(4), 600–610.

Dang, H.-L. & Do, D.-P. (2021). Finite element implementation of coupled hydro-mechanical modeling of transversely isotropic porous media in deal. ii. *International Journal of Modeling, Simulation, and Scientific Computing*, 12(01), 2150003.

Das, B. M. (2019). *Advanced soil mechanics*. Crc Press.

Das, B. M. & Das, B. (2008). *Advanced soil mechanics*, volume 270. Taylor & Francis New York.

de Graaf, I. d., Sutanudjaja, E., Van Beek, L., & Bierkens, M. (2015). A high-resolution global-scale groundwater model. *Hydrology and Earth System Sciences*, 19(2), 823–837.

Doan, M.-L., Brodsky, E. E., Prioul, R., & Signer, C. (2006). Tidal analysis of borehole pressure-A tutorial. *University of California, Santa Cruz*, 25, 27.

Domenico, P. A. & Schwartz, F. W. (1997). *Physical and chemical hydrogeology*. John wiley & sons.

Dropek, R., Johnson, J., & Walsh, J. (1978). The influence of pore pressure on the mechanical properties of Kayenta sandstone. *Journal of Geophysical Research: Solid Earth*, 83(B6), 2817–2824.

Eaton, T. T. (2006). On the importance of geological heterogeneity for flow simulation. *Sedimentary Geology*, 184(3-4), 187–201.

Edwards, R. W., Doster, F., Celia, M. A., & Bandilla, K. W. (2017). Numerical modeling of gas and water flow in shale gas formations with a focus on the fate of hydraulic fracturing fluid. *Environmental science & technology*, 51(23), 13779–13787.

Famiglietti, J. S. (2014). The global groundwater crisis. *Nature Climate Change*, 4(11), 945–948.

Finkel, M., Grathwohl, P., & Cirpka, O. A. (2016). A travel time-based approach to model kinetic

sorption in highly heterogeneous porous media via reactive hydrofacies. *Water Resources Research*, 52(12), 9390–9411.

Flemisch, B., Darcis, M., Erbertseder, K., Faigle, B., Lauser, A., Mosthaf, K., Müthing, S., Nuske, P., Tatomir, A., Wolff, M., et al. (2011). Dumux: Dune for multi-{phase, component, scale, physics,…} flow and transport in porous media. *Advances in Water Resources*, 34(9), 1102–1112.

Freeze, R. A. & Cherry, J. A. (1979a). *Groundwater*.

Freeze, R. A. & Cherry, J. A. (1979b). *Groundwater*. Upper Saddle River, NJ 07458: Prentice Hall, Inc.

Freymark, J., Bott, J., Cacace, M., Ziegler, M., & Scheck-Wenderoth, M. (2019). Influence of the main border faults on the 3d hydraulic field of the central upper rhine graben. *Geofluids*, 2019.

Frih, N., Martin, V., Roberts, J. E., & Saâda, A. (2012). Modeling fractures as interfaces with nonmatching grids. *Computational Geosciences*, 16(4), 1043–1060.

Gao, X., Sato, K., & Horne, R. N. (2020). General solution for tidal behavior in confined and semiconfined aquifers considering skin and wellbore storage effects. *Water Resources Research*, 56(6), e2020WR027195.

Gariano, S. L. & Guzzetti, F. (2016). Landslides in a changing climate. *Earth-Science Reviews*, 162, 227–252.

Garipov, T. T., Tomin, P., Rin, R., Voskov, D. V., & Tchelepi, H. A. (2018). Unified thermo-compositional-mechanical framework for reservoir simulation. *Computational Geosciences*, 22(4), 1039–1057.

Gaston, D., Newman, C., Hansen, G., & Lebrun-Grandie, D. (2009). Moose: A parallel computational framework for coupled systems of nonlinear equations. *Nuclear Engineering and Design*, 239(10), 1768–1778.

Graupner, B. J., Li, D., & Bauer, S. (2011). The coupled simulator eclipse–opengeosys for the simulation of co2 storage in saline formations. *Energy Procedia*, 4, 3794–3800.

Green, C., Wilkins, A., La Force, T., & Ennis-King, J. (2018). Community code for simulating co2 storage: Modelling multiphase flow with coupled geomechanics and geochemistry using the open-source multiphysics framework moose. In *14th Greenhouse Gas Control Technologies Conference Melbourne* (pp. 21–26).

Grigoli, F., Cesca, S., Priolo, E., Rinaldi, A. P., Clinton, J. F., Stabile, T. A., Dost, B., Fernandez, M. G., Wiemer, S., & Dahm, T. (2017). Current challenges in monitoring, discrimination, and management of induced seismicity related to underground industrial activities: A european perspective. *Reviews of Geophysics*, 55(2), 310–340.

Guo, H., Brodsky, E., Goebel, T., & Cladouhos, T. (2021). Measuring Fault Zone and Host Rock Hydraulic Properties Using Tidal Responses. *Geophysical Research Letters*, 48(13), e2021GL093986.

Gupta, S. K. (2011). *Modern hydrology and sustainable water development*. John Wiley & Sons.

Haagenson, R., Rajaram, H., & Allen, J. (2020). A generalized poroelastic model using fenics with insights into the noordbergum effect. *Computers & Geosciences*, 135, 104399.

Hammond, G. E., Lichtner, P. C., & Mills, R. (2014). Evaluating the performance of parallel subsurface simulators: An illustrative example with pflotran. *Water resources research*, 50(1), 208–228.

Hantush, M. S. (1960). Modification of the theory of leaky aquifers. *Journal of Geophysical Research*, 65(11), 3713–3725.

Hantush, M. S. & Jacob, C. E. (1955). Non-steady radial flow in an infinite leaky aquifer. *Eos, Transactions American Geophysical Union*, 36(1), 95–100.

Haque, U., Blum, P., Da Silva, P. F., Andersen, P., Pilz, J., Chalov, S. R., Malet, J.-P., Auflič, M. J., Andres, N., Poyiadji, E., et al. (2016). Fatal landslides in europe. *Landslides*, 13(6), 1545–1554.

Hardin, B. O. & Kalinski, M. E. (2005). Estimating the shear modulus of gravelly soils. *Journal of geotechnical and geoenvironmental engineering*, 131(7), 867–875.

He, L., Huang, G., & Lu, H. (2010). A stochastic optimization model under modeling uncertainty and parameter certainty for groundwater remediation design—part i. model development. *Journal of Hazardous Materials*, 176(1-3), 521–526.

Hein, P., Kolditz, O., Görke, U.-J., Bucher, A., & Shao, H. (2016). A numerical study on the sustainability and efficiency of borehole heat exchanger coupled ground source heat pump systems. *Applied Thermal Engineering*, 100, 421–433.

Herrera-García, G., Ezquerro, P., Tomás, R., Béjar-Pizarro, M., López-Vinielles, J., Rossi, M., Mateos, R. M., Carreón-Freyre, D., Lambert, J., Teatini, P., et al. (2021). Mapping the global threat of land subsidence. *Science*, 371(6524), 34–36.

Herron, N., Peeters, L., Crosbie, R., Marvanek, S., Ramage, A., Rachakonda, P., & Wilkins, A. (2018). Groundwater numerical modelling for the hunter subregion. product 2.6. 2 for the hunter subregion from the northern sydney basin bioregional assessment.

Hicher, P.-Y. (1996). Elastic properties of soils. *Journal of Geotechnical Engineering*, 122(8), 641–648.

Hickson, R., Barry, S., & Mercer, G. (2009). Critical times in multilayer diffusion. part 1: Exact solutions. *International Journal of Heat and Mass Transfer*, 52(25-26), 5776–5783.

Hiscock, K. M. & Bense, V. F. (2021). *Hydrogeology: principles and practice*. John Wiley & Sons.

Holzbecher, E. (2013). Poroelasticity benchmarking for fem on analytical solutions. In *Excerpt from the Proceedings of the COMSOL Conference Rotterdam* (pp. 1–7).

Houben, G. J., Stoeckl, L., Mariner, K. E., & Choudhury, A. S. (2018). The influence of heterogeneity on coastal groundwater flow-physical and numerical modeling of fringing reefs, dykes and structured conductivity fields. *Advances in Water Resources*, 113, 155–166.

Höyng, D., Prommer, H., Blum, P., Grathwohl, P., & D'Affonseca, F. M. (2015). Evolution of carbon isotope signatures during reactive transport of hydrocarbons in heterogeneous aquifers. *Journal of contaminant hydrology*, 174, 10–27.

Hsieh, P. A., Bredehoeft, J. D., & Farr, J. M. (1987). Determination of aquifer transmissivity from Earth tide analysis. *Water resources research*, 23(10), 1824–1832.

Hsieh, P. A., Bredehoeft, J. D., & Rojstaczer, S. A. (1988). Response of well aquifer systems to earth tides: Problem revisited. *Water Resources Research*, 24(3), 468–472.

Hu, R. (2017). A fully-implicit high-order system thermal-hydraulics model for advanced non-lwr safety analyses. *Annals of Nuclear Energy*, 101, 174–181.

Huysmans, M. & Dassargues, A. (2009). Application of multiple-point geostatistics on modelling groundwater flow and transport in a cross-bedded aquifer. *Hydrogeology Journal*, 17(8).

Irvine, D. J., Cranswick, R. H., Simmons, C. T., Shanafield, M. A., & Lautz, L. K. (2015). The effect of streambed heterogeneity on groundwater-surface water exchange fluxes inferred from temperature time series. *Water Resources Research*, 51(1), 198–212.

Jacob, C. & Lohman, S. (1952). Nonsteady flow to a well of constant drawdown in an extensive aquifer. *Eos, Transactions American Geophysical Union*, 33(4), 559–569.

Jacob, C. E. (1946). Radial flow in a leaky artesian aquifer. *Eos, Transactions American Geophysical Union*, 27(2), 198–208.

Jacob, F. & Ted, B. (2007). *A first course in finite elements*. Wiley.

Jardani, A., Dupont, J.-P., Revil, A., Massei, N., Fournier, M., & Laignel, B. (2012). Geostatistical inverse modeling of the transmissivity field of a heterogeneous alluvial aquifer under tidal influence. *Journal of Hydrology*, 472, 287–300.

Kadeethum, T., Nick, H., Lee, S., Richardson, C., Salimzadeh, S., Ballarin, F., et al. (2019). A novel enriched galerkin method for modelling coupled mechanical deformation in heterogeneous porous media. In *53rd US Rock Mechanics/Geomechanics Symposium*: American Rock Mechanics Association.

Kalbus, E., Schmidt, C., Molson, J., Reinstorf, F., & Schirmer, M. (2009). Influence of aquifer and streambed heterogeneity on the distribution of groundwater discharge. *Hydrology & Earth System Sciences*, 13(1).

Kavetski, D., Binning, P., & Sloan, S. W. (2002). Adaptive backward euler time stepping with truncation error control for numerical modelling of unsaturated fluid flow. *International Journal for Numerical Methods in Engineering*, 53(6), 1301–1322.

Keilegavlen, E., Berge, R., Fumagalli, A., Starnoni, M., Stefansson, I., Varela, J., & Berre, I. (2021). Porepy: An open-source software for simulation of multiphysics processes in fractured porous media. *Computational Geosciences*, 25(1), 243–265.

Keilegavlen, E., Fumagalli, A., Berge, R., Stefansson, I., & Berre, I. (2017). Porepy: an open-source simulation tool for flow and transport in deformable fractured rocks. *arXiv preprint arXiv:1712.00460*.

Kim, J., Tchelepi, H. A., & Juanes, R. (2011). Stability and convergence of sequential methods for coupled flow and geomechanics: Fixed-stress and fixed-strain splits. *Computer Methods in Applied Mechanics and Engineering*, 200(13-16), 1591–1606.

Kirk, B. S., Peterson, J. W., Stogner, R. H., & Carey, G. F. (2006). libmesh: a c++ library for parallel adaptive mesh refinement/coarsening simulations. *Engineering with Computers*, 22(3-4), 237–254.

Koch, T., Gläser, D., Weishaupt, K., Ackermann, S., Beck, M., Becker, B., Burbulla, S., Class, H., Coltman, E., Emmert, S., et al. (2021). Dumux 3–an open-source simulator for solving flow and transport problems in porous media with a focus on model coupling. *Computers & Mathematics with Applications*, 81, 423–443.

Kolditz, O., Bauer, S., Bilke, L., Böttcher, N., Delfs, J.-O., Fischer, T., Görke, U. J., Kalbacher, T., Kosakowski, G., McDermott, C., et al. (2012). Opengeosys: an open-source initiative for numerical simulation of thermo-hydro-mechanical/chemical (thm/c) processes in porous media. *Environmental Earth Sciences*, 67(2), 589–599.

Konikow, L. F. & Kendy, E. (2005). Groundwater depletion: A global problem. *Hydrogeology Journal*, 13, 317–320.

Kosakowski, G. & Watanabe, N. (2014). Opengeosys-gem: a numerical tool for calculating geochemical and porosity changes in saturated and partially saturated media. *Physics and Chemistry of the Earth, Parts A/B/C*, 70, 138–149.

Kulhawy, F. H. & Mayne, P. W. (1990). *Manual on estimating soil properties for foundation design*. Technical report, Electric Power Research Inst., Palo Alto, CA (USA); Cornell Univ., Ithaca, NY (USA).

Kumar, C. (2019). An overview of commonly used groundwater modelling software.

LaBolle, E. M., Ahmed, A. A., & Fogg, G. E. (2003). Review of the integrated groundwater and surface-water model (igsm). *Groundwater*, 41(2), 238–246.

Lade, P. V. (2001). Engineering properties of soils and typical correlations. In *Geotechnical and geoenvironmental engineering handbook* (pp. 43–67). Springer.

Lai, G., Ge, H., & Wang, W. (2013). Transfer functions of the well-aquifer systems response to

atmospheric loading and earth tide from low to high-frequency band. *Journal of Geophysical Research: Solid Earth*, 118(5), 1904–1924.

Lai, G., Ge, H., Xue, L., Brodsky, E. E., Huang, F., & Wang, W. (2014). Tidal response variation and recovery following the wenchuan earthquake from water level data of multiple wells in the nearfield. *Tectonophysics*, 619, 115–122.

Lambe, T. W. & Whitman, R. V. (1991). *Soil mechanics*, volume 10. John Wiley & Sons.

Le Borgne, T., Bour, O., De Dreuzy, J., Davy, P., & Touchard, F. (2004). Equivalent mean flow models for fractured aquifers: Insights from a pumping tests scaling interpretation. *Water Resources Research*, 40(3).

Lecampion, B., Bunger, A., & Zhang, X. (2018). Numerical methods for hydraulic fracture propagation: a review of recent trends. *Journal of natural gas science and engineering*, 49, 66–83.

Lee, J., Kim, K.-I., Min, K.-B., & Rutqvist, J. (2019). Tough-udec: A simulator for coupled multiphase fluid flows, heat transfers and discontinuous deformations in fractured porous media. *Computers & Geosciences*, 126, 120–130.

Lei, H., Xu, T., & Jin, G. (2015). Tough2biot–a simulator for coupled thermal–hydrodynamic–mechanical processes in subsurface flow systems: Application to co2 geological storage and geothermal development. *Computers & Geosciences*, 77, 8–19.

Li, D., Bauer, S., Benisch, K., Graupner, B., & Beyer, C. (2014). Opengeosys-chemapp: a coupled simulator for reactive transport in multiphase systems and application to co 2 storage formation in northern germany. *Acta Geotechnica*, 9(1), 67–79.

Li, Z. & Jeng, D.-S. (2023). Dynamic soil response around two-layered detached breakwaters: Three-dimensional openfoam model. *Ocean Engineering*, 268, 113582.

Liang, X., Wang, C.-Y., Ma, E., & Zhang, Y.-K. (2022). Effects of unsaturated flow on hydraulic head response to earth tides–an analytical model. *Water Resources Research*, 58(2), e2021WR030337.

Lichtner, P. C. & Karra, S. (2014). Modeling multiscale-multiphase-multicomponent reactive flows in porous media: Application to co2 sequestration and enhanced geothermal energy using pflotran. In *Computational Models for CO2 Geo-sequestration & Compressed Air Energy Storage* (pp. 121–176). CRC Press.

Lie, K.-A. (2019). *An introduction to reservoir simulation using MATLAB/GNU Octave: User guide for the MATLAB Reservoir Simulation Toolbox (MRST)*. Cambridge University Press.

Look, B. G. (2007). *Handbook of geotechnical investigation and design tables*. Taylor & Francis.

Look, B. G. (2014). *Handbook of geotechnical investigation and design tables*. CRC Press.

Maliva, R. G. (2016). *Aquifer characterization techniques*, volume 10. Springer.

Manzini, G. & Ferraris, S. (2004). Mass-conservative finite volume methods on 2-d unstructured grids for the richards' equation. *Advances in Water Resources*, 27(12), 1199–1215.

Martin, V., Jaffré, J., & Roberts, J. E. (2005). Modeling fractures and barriers as interfaces for flow in porous media. *SIAM Journal on Scientific Computing*, 26(5), 1667–1691.

Martineau, R., Andrs, D., Carlsen, R., Gaston, D., Hansel, J., Kong, F., Lindsay, A., Permann, C., Slaughter, A., Merzari, E., et al. (2020). Multiphysics for nuclear energy applications using a cohesive computational framework. *Nuclear Engineering and Design*, 367, 110751.

McMillan, T. C., Rau, G. C., Timms, W. A., & Andersen, M. S. (2019a). Utilizing the Impact of Earth and Atmospheric Tides on Groundwater Systems: A Review Reveals the Future Potential. *Reviews of Geophysics*, 57(2), 281–315.

McMillan, T. C., Rau, G. C., Timms, W. A., & Andersen, M. S. (2019b). Utilizing the impact of earth and atmospheric tides on groundwater systems: A review reveals the future potential. *Reviews of Geophysics*, 57(2), 281–315.

Meinzer, O. E. (1939). *Ground water in the United States, a summary of ground-water conditions and resources, utilization of water from wells and springs, methods of scientific investigation, and literature relating to the subject*. Technical report, U.S. G.P.O.

Merritt, M. L. (2004). *Estimating hydraulic properties of the Floridan aquifer system by analysis of earth-tide, ocean-tide, and barometric effects, Collier and Hendry Counties, Florida*. Number 3. US Department of the Interior, US Geological Survey.

Mikelić, A. & Wheeler, M. F. (2013). Convergence of iterative coupling for coupled flow and geomechanics. *Computational Geosciences*, 17(3), 455–461.

Mondol, N. H., Jahren, J., Bjørlykke, K., & Brevik, I. (2008). Elastic properties of clay minerals. *The Leading Edge*, 27(6), 758–770.

Morris, J. P., Rubin, M., Block, G., & Bonner, M. (2006). Simulations of fracture and fragmentation of geologic materials using combined fem/dem analysis. *International Journal of Impact Engineering*, 33(1-12), 463–473.

Neuman, S. P. (1974). Effect of partial penetration on flow in unconfined aquifers considering delayed gravity response. *Water resources research*, 10(2), 303–312.

Nghiem, L., Sammon, P., Grabenstetter, J., Ohkuma, H., et al. (2004). Modeling co2 storage in aquifers with a fully-coupled geochemical eos compositional simulator. In *SPE/DOE symposium on improved oil recovery*: Society of Petroleum Engineers.

Pandey, S., Vishal, V., & Chaudhuri, A. (2018). Geothermal reservoir modeling in a coupled thermo-hydro-mechanical-chemical approach: A review. *Earth-Science Reviews*, 185, 1157–1169.

Pawlowicz, R., Beardsley, B., & Lentz, S. (2002). Classical tidal harmonic analysis including error estimates in matlab using t_tide. *Computers & geosciences*, 28(8), 929–937.

Pendiuk, J. E., Guarracino, L., Reich, M., Brunini, C., & Güntner, A. (2020). Estimating the specific yield of the Pampeano aquifer, Argentina, using superconducting gravimeter data. *Hydrogeology Journal*, 28(7), 2303–2313.

Peng, S. (2020). *Surface Subsidence Engineering: Theory and Practice*. CSIRO PUBLISHING.

Peng, X., Zhang, L., Jeng, D., Chen, L., Liao, C., & Yang, H. (2017). Effects of cross-correlated multiple spatially random soil properties on wave-induced oscillatory seabed response. *Applied Ocean Research*, 62, 57–69.

Permann, C. J., Gaston, D. R., Andrš, D., Carlsen, R. W., Kong, F., Lindsay, A. D., Miller, J. M., Peterson, J. W., Slaughter, A. E., Stogner, R. H., et al. (2020). Moose: Enabling massively parallel multiphysics simulation. *SoftwareX*, 11, 100430.

Pham, H. T., Rühaak, W., Schuster, V., & Sass, I. (2019). Fully hydro-mechanical coupled plug-in (sub+) in feflow for analysis of land subsidence due to groundwater extraction. *SoftwareX*, 9, 15–19.

Pham-Gia, T. & Hung, T. L. (2001). The mean and median absolute deviations. *Mathematical and Computer Modelling*, 34(7-8), 921–936.

Pruess, K., Oldenburg, C. M., & Moridis, G. (1999). *TOUGH2 user's guide version 2*. Technical report, Lawrence Berkeley National Lab.(LBNL), Berkeley, CA (United States).

Qi, Z., Shi, Z., & Rasmussen, T. C. (2023). Time- and frequency-domain determination of aquifer hydraulic properties using water-level responses to natural perturbations: A case study of the rongchang well, chongqing, southwestern china. *Journal of Hydrology*, 617, 128820.

Qu, J. & Cherkaoui, M. (2006). *Fundamentals of micromechanics of solids*, volume 735. Wiley Online Library.

Rahi, K. A. & Halihan, T. (2013). Identifying aquifer type in fractured rock aquifers using harmonic analysis. *Groundwater*, 51(1), 76–82.

Rau, G. (2018a). Pygtide: A python module and wrapper for eterna predict to compute synthetic model tides on earth, zenodo [code].

Rau, G. & Blum, P. (2021). Passive subsurface characterisation (psc): Using the groundwater response to earth tides and atmospheric pressure. In *Conference presentation @ GeoKarlsruhe (online)* (pp. 19–24).

Rau, G. C. (2018b). PyGTide: A Python module and wrapper for ETERNA PREDICT to compute synthetic model tides on Earth.

Rau, G. C., Cuthbert, M. O., Acworth, R. I., & Blum, P. (2020a). Disentangling the groundwater response to Earth and atmospheric tides to improve subsurface characterisation. *Hydrology and earth system sciences*, 24(12), 6033–6046.

Rau, G. C., Cuthbert, M. O., Acworth, R. I., & Blum, P. (2020b). Technical note: Disentangling the groundwater response to Earth and atmospheric tides to improve subsurface characterisation. *Hydrology and Earth System Sciences*, 24(12), 6033–6046.

Rau, G. C., Cuthbert, M. O., Post, V. E., Schweizer, D., & Acworth (2020c). Future-proofing hydrogeology by revising groundwater monitoring practice. *Hydrogeology Journal*, 28(8), 2963–2969.

Rau, G. C., McMillan, T. C., Andersen, M. S., & Timms, W. A. (2022). In situ estimation of subsurface hydro-geomechanical properties using the groundwater response to semi-diurnal earth and atmospheric tides. *Hydrology and Earth System Sciences*, 26(16), 4301–4321.

Rau, G. C., Post, V. E., Shanafield, M., Krekeler, T., Banks, E. W., & Blum, P. (2019). Error in hydraulic head and gradient time-series measurements: a quantitative appraisal. *Hydrology and Earth System Sciences*, 23(9), 3603–3629.

Reichenberger, V. (2003). *Numerical simulation of multiphase flow in fractured porous media*. PhD thesis.

Robinson, E. S. & Bell, R. T. (1971). Tides in confined well-aquifer systems. *Journal of Geophysical Research*, 76(8), 1857–1869.

Roeloffs, E. A., Burford, S. S., Riley, F. S., & Records, A. W. (1989). Hydrologic effects on water level changes associated with episodic fault creep near Parkfield, California. *Journal of Geophysical Research*, 94(B9), 12387.

Rogers, L. L. & Dowla, F. U. (1994). Optimization of groundwater remediation using artificial neural networks with parallel solute transport modeling. *Water Resources Research*, 30(2), 457–481.

Rojas, R., Feyen, L., & Dassargues, A. (2008). Conceptual model uncertainty in groundwater modeling: Combining generalized likelihood uncertainty estimation and bayesian model averaging. *Water Resources Research*, 44(12).

Rojstaczer, S. (1988). Determination of fluid flow properties from the response of water levels in wells to atmospheric loading. *Water Resources Research*, 24(11), 1927–1938.

Rojstaczer, S. & Agnew, D. C. (1989). The influence of formation material properties on the response of water levels in wells to Earth tides and atmospheric loading. *Journal of Geophysical Research: Solid Earth*, 94(B9), 12403–12411.

Rojstaczer, S. & Riley, F. S. (1990). Response of the water level in a well to earth tides and atmospheric loading under unconfined conditions. *Water Resources Research*, 26(8), 1803–1817.

Rutqvist, J. (2017). An overview of tough-based geomechanics models. *Computers & Geosciences*, 108, 56–63.

Schweizer, D., Ried, V., Rau, G. C., Tuck, J. E., & Stoica, P. (2021). Comparing Methods and Defining Practical Requirements for Extracting Harmonic Tidal Components from Groundwater Level Measurements. *Mathematical Geosciences*.

Settari, A. & Walters, D. A. (2001). Advances in coupled geomechanical and reservoir modeling with applications to reservoir compaction. *Spe Journal*, 6(03), 334–342.

Shi, Z. & Wang, G. (2016). Aquifers switched from confined to semiconfined by earthquakes. *Geophysical Research Letters*, 43(21), 11–166.

Siebert, S., Burke, J., Faures, J.-M., Frenken, K., Hoogeveen, J., Döll, P., & Portmann, F. T. (2010). Groundwater use for irrigation–a global inventory. *Hydrology and earth system sciences*, 14(10), 1863–1880.

Stoica, P., Li, J., & He, H. (2008). Spectral analysis of nonuniformly sampled data: A new approach versus the periodogram. *IEEE Transactions on Signal Processing*, 57(3), 843–858.

Strebelle, S. (2002). Conditional simulation of complex geological structures using multiple-point statistics. *Mathematical geology*, 34(1), 1–21.

Subramanian, N. (2011). *Steel structures-Design and practice*. Oxford University Press.

Sun, X., Shi, Z., & Xiang, Y. (2020). Frequency Dependence of In Situ transmissivity Estimation of Well-Aquifer Systems From Periodic Loadings. *Water Resources Research*, 56(11), e2020WR027536.

Tamura, Y. & Agnew, D. (2008). Baytap08 user's manual.

Tarkowski, R. (2019). Underground hydrogen storage: Characteristics and prospects. *Renewable and Sustainable Energy Reviews*, 105, 86–94.

Terzaghi, K. (1923). Die berechnug der durchlassigkeit des tones aus dem verlauf der hydromechanischen spannungserscheinungen. *Sitzungsber. Akad. Wiss.(Wien). Math.-Naturwiss. Kl., Abt. Iia*, 132, 125–138.

Tickell, Z. (2017). Water resources of the wildman river area. northern territory government.

Tran, M. & Jha, B. (2020). Coupling between transport and geomechanics affects spreading and mixing during viscous fingering in deformable aquifers. *Advances in Water Resources*, 136, 103485.

Turnadge, C., Crosbie, R., Tickell, S., Zaar, U., Smith, S., Dawes, W., Davies, P., Harrington, G., & Taylor, A. (2018). Hydrogeological characterisation of the mary–wildman rivers area, northern territory.

Turnadge, C., Crosbie, R. S., Barron, O., & Rau, G. C. (2019). Comparing methods of barometric efficiency characterization for specific storage estimation. *Groundwater*, 57(6), 844–859.

Unpingco, J. (2016). *Python for Signal Processing*. Springer.

Valois, R., Rau, G. C., Vouillamoz, J.-M., & Derode, B. (2022). Estimating hydraulic properties of the shallow subsurface using the groundwater response to earth and atmospheric tides: a comparison with pumping tests. *Water Resources Research*, 58(5), e2021WR031666.

Van Camp, M. & Vauterin, P. (2005). Tsoft: graphical and interactive software for the analysis of time series and Earth tides. *Computers & Geosciences*, 31(5), 631–640.

Van der Kamp, G. & Gale, J. (1983). Theory of earth tide and barometric effects in porous formations with compressible grains. *Water Resources Research*, 19(2), 538–544.

Vanmarcke, E., Shinozuka, M., Nakagiri, S., Schueller, G., & Grigoriu, M. (1986). Random fields and stochastic finite elements. *Structural safety*, 3(3-4), 143–166.

Verruijt, A. (1995). *Computational geomechanics*, volume 7. Springer Science & Business Media.

Verruijt, A. (2013). Theory and problems of poroelasticity. *Delft University of Technology*, 71.

Verruijt, A. (2018). Numerical and analytical solutions of poroelastic problems. *Geotechnical Research*, 5(1), 39–50.

Verruijt, A. & Van Baars, S. (2007). *Soil mechanics*. VSSD Delft, the Netherlands.

Virtanen, P., Gommers, R., Oliphant, T. E., Haberland, M., Reddy, T., Cournapeau, D., Burovski, E., Peterson, P., Weckesser, W., Bright, J., et al. (2020). SciPy 1.0: fundamental algorithms for scientific computing in Python. *Nature methods*, 17(3), 261–272.

Wang & Manga, M. (2021). Response to Tides, Barometric Pressure and Seismic Waves. *Water and Earthquakes*, (pp. 83–153).

Wang, Zhu, A.-Y., Liao, X., Manga, M., & Wang, L.-P. (2019). Capillary effects on groundwater response to Earth tides. *Water Resources Research*, 55(8), 6886–6895.

Wang, C. & Zeng, Z. (2011). Overview of geomechical properties of Bakken formation in Williston Basin, North Dakota. In *45th US Rock Mechanics/Geomechanics Symposium*: OnePetro.

Wang, C. Y., Doan, M. L., Xue, L., & Barbour, A. J. (2018). Tidal response of groundwater in a leaky aquifer—Application to Oklahoma. *Water Resources Research*, 54(10), 8019–8033.

Wang, H. F. (2000). *Theory of Linear Poroelasticity with Applications to Geomechanics and Hydrogeology*. Princeton University Press.

Wang, H. F. (2017). *Theory of linear poroelasticity with applications to geomechanics and hydrogeology*. Princeton University Press.

Wang, Q., Zhan, H., & Tang, Z. (2015). Two-dimensional flow response to tidal fluctuation in a heterogeneous aquifer-aquitard system. *Hydrological Processes*, 29(6), 927–935.

Weng, X. (2015). Modeling of complex hydraulic fractures in naturally fractured formation. *Journal of Unconventional Oil and Gas Resources*, 9, 114–135.

Wenzel, H.-G. (1996). The nanoGal software: Earth tide data processing package: Eterna 3.3. *Bulletin d'Informations des Marées Terrestres*, 124, 9425–9439.

White, M., Fu, P., McClure, M., Danko, G., Elsworth, D., Sonnenthal, E., Kelkar, S., & Podgorney, R. (2018). A suite of benchmark and challenge problems for enhanced geothermal systems. *Geomechanics and Geophysics for Geo-Energy and Geo-Resources*, 4(1), 79–117.

Wilkins, A., Green, C. P., & Ennis-King, J. (2020). Porousflow: a multiphysics simulation code for coupled problems in porous media. *Journal of Open Source Software*, 5(55), 2176.

Wilkins, A., Green, C. P., & Ennis-King, J. (2021). An open-source multiphysics simulation code for coupled problems in porous media. *Computers & Geosciences*, 154, 104820.

Wu, J. & Zeng, X. (2013). Review of the uncertainty analysis of groundwater numerical simulation. *Chinese Science Bulletin*, 58, 3044–3052.

Xu, L. (2016). Typical values of young's elastic modulus and poisson's ratio for pavement materials.

Xu, T., Sonnenthal, E., Spycher, N., & Pruess, K. (2006). Toughreact—a simulation program for non-isothermal multiphase reactive geochemical transport in variably saturated geologic media: applications to geothermal injectivity and co2 geological sequestration. *Computers & geosciences*, 32(2), 145–165.

Xue, L., Brodsky, E. E., Erskine, J., Fulton, P. M., & Carter, R. (2016). A permeability and compliance contrast measured hydrogeologically on the san andreas fault. *Geochemistry, Geophysics, Geosystems*, 17(3), 858–871.

Yang, D., Koukouzas, N., Green, M., & Sheng, Y. (2016). Recent development on underground coal gasification and subsequent co2 storage. *Journal of the energy institute*, 89(4), 469–484.

Ye, M., Pohlmann, K. F., Chapman, J. B., Pohll, G. M., & Reeves, D. M. (2010). A model-averaging method for assessing groundwater conceptual model uncertainty. *Groundwater*, 48(5), 716–728.

Ye, S., Xue, Y., Wu, J., Yan, X., & Yu, J. (2016). Progression and mitigation of land subsidence in china. *Hydrogeology Journal*, 24(3), 685–693.

Zappa, G., Bersezio, R., Felletti, F., & Giudici, M. (2006). Modeling heterogeneity of gravel-sand, braided stream, alluvial aquifers at the facies scale. *Journal of Hydrology*, 325(1-4), 134–153.

Zaruba, Q. & Mencl, V. (2014). *Landslides and their control*. Elsevier.

Zhang, M., Hao, Y., Zhao, Z., Wang, T., & Yang, L. (2021a). Estimation of coastal aquifer properties: A review of the tidal method based on theoretical solutions. *Wiley Interdisciplinary Reviews: Water*, 8(1), e1498.

Zhang, Q., Zhu, W., Gao, B., Ye, G., Jeng, D.-s., & Wang, T. (2022). Numerical investigation on horizontal deformation of large diameter monopile under cyclic wave loading with local scour holes. *Ocean Engineering*, 266, 113059.

Zhang, S., Shi, Z., & Wang, G. (2019). Comparison of aquifer parameters inferred from water level changes induced by slug test, earth tide and earthquake – A case study in the three Gorges area. *Journal of Hydrology*, 579, 124169.

Zhang, Y., Wang, C. Y., Fu, L. Y., & Yang, Q. Y. (2021b). Are deep aquifers really confined? Insights from deep groundwater tidal responses in the north China platform. *Water Resources Research*, 57(11), e2021WR030195.

Zhao, H., Jeng, D.-S., Liao, C., & Zhu, J. (2017). Three-dimensional modeling of wave-induced residual seabed response around a mono-pile foundation. *Coastal Engineering*, 128, 1–21.

Zhao, X. & Jha, B. (2019). Role of well operations and multiphase geomechanics in controlling fault stability during co2 storage and enhanced oil recovery. *Journal of Geophysical Research: Solid Earth*, 124(7), 6359–6375.

Zhu, A. Y. & Wang (2020). Response of leaky aquifers to Earth tides–Interpreted with numerical simulation. *Journal of Hydrology*, 581, 124458.

Acknowledgements

General

I would like to thank those that taught me how to "do science" and showed me its beauty:

- **Dr. Gabriel C. Rau** (formerly at KIT, now at the University of Newcastle in Australia) for supervising me with unconditional support. For the trust and freedom to develop my own research, for keeping me motivated even in the hardest times, for teaching me how to formulate ideas and how to tell a story. For not only teaching me how to do science, but also for advising me in several aspects of my personal life. For always being available and open to discuss any topic. Just for being the best doctorate supervisor possible.

- **Prof. Dr. Philipp Blum** (KIT, Germany) for being the first that thrust in my work, for his encouragement to develop my carrier in geosciences, for teaching me his *keep it short and simple* philosophy and for giving me blind freedom. For all the discussions outside science and research. For teaching me how to communicate effectively and efficiently. For always being available to solve problems.

- **Dr. Daniel Schweizer** (KIT, Germany) for constant advise and support during the first steps of my PhD and all the non work related conversations.

- **Dr. Andy Wilkins** (CSIRO, Brisbane) for guiding me into numerical modeling and taking the time to teach me the basics.

- **Dr. Chris Turnadge** (CSIRO, Adelaide) for being willing to collaborate, sharing his amazing data sets and helping me to improve my work thorough great feedback and insightful ideas.

- **Dr. Russell S. Crosbie** (CSIRO, Adelaide) for sharing data sets, give positive feedback to my work and for his amazing team work.

- **Dr. Tomas Cassanelli** (UCh, Santiago de Chile) for introducing me into Python, coding and constant support during my PhD.

Funding

Authorship Declaration

Chapter 1: José M. Bastías Espejo (JMBE) wrote this chapter.

Chapter 2: *Bastías Espejo, J. M., Wilkins, A., Rau, G. C., and Blum, P.: RHEA v1.0: Enabling fully coupled simulations with hydro-geomechanical heterogeneity, Geosci. Model Dev., 14, 6257–6272, https://doi.org/10.5194/gmd-14-6257-2021, 2021.*

JMBE developed RHEA, the analytical solutions used for verification, made the figures and tables and wrote the first manuscript draft. Gabriel C. Rau (GCR) closely supervised JMBE. Andy Wilkins (AW) provided JMBE with technical support. Philipp Blum (PB) reviewed the manuscript and provided suggestions.

Chapter 3: *Bastias Espejo, Jose M., Gabriel C. Rau, and Philipp Blum. "Groundwater responses to Earth tides: Evaluation of analytical solutions using numerical simulation." Journal of Geophysical Research: Solid Earth 127.10 (2022): e2022JB024771.*

JMBE developed and designed the numerical models in RHEA, performed the simulations, made the figures and tables and wrote the first manuscript draft. GCR closely supervised JMBE and supported with technical advice. PB reviewed the manuscript and provided suggestions.

Chapter 4: *Bastias Espejo, J. M., Turnadge C., Crosbie R. S., Blum P. & Rau G. C. Technical note: Novel analytical solution for groundwater response to atmospheric tides. Manuscript submitted to Hydrology and Earth System Sciences (HESS), April 05 2023.*

JMBE derived the analytical solution, made the data analysis and signal processing of the field data, made the figures and wrote the first draft. Chris Turnadge (CT) and Russell S. Crosbie (RSC), performed the drilling, data acquisition and pumping test reinterpretation. PB reviewed the manuscript and provided suggestions.GCR closely supervised JMBE and supported with technical advice.

Chapter 5: JMBE wrote this chapter.

Eidesstattliche Versicherung

Eidesstattliche Versicherung gemäß § 13 Absatz 2 Satz 1 Ziffer 4 der Promotionsordnung des Karlsruher Instituts für Technologie (KIT) für die KIT-Fakultät für Bauingenieur-, Geo- und Umweltwissenschaften

1. Bei der eingereichten Dissertation zu dem Thema *Advancing hydro-geomechanical subsurface characterisation using the groundwater response to tidal forces* handelt es sich um meine eigenständig erbrachte Leistung.

2. Ich habe nur die angegebenen Quellen und Hilfsmittel benutzt und mich keiner unzulässigen Hilfe Dritter bedient. Insbesondere habe ich wörtlich oder sinngemäß aus anderen Werken übernommene Inhalte als solche kenntlich gemacht.

3. Die Arbeit oder Teile davon habe ich wie folgtbislang nicht an einer Hochschule des In- oder Auslands als Bestandteil einer Prüfungs- oder Qualifikationsleistung vorgelegt.

4. Die Richtigkeit der vorstehenden Erklärungen bestätige ich.

5. Die Bedeutung der eidesstattlichen Versicherung und die strafrechtlichen Folgen einer unrichtigen oder unvollständigen eidesstattlichen Versicherung sind mir bekannt.

Ich versichere an Eides statt, dass ich nach bestem Wissen die reine Wahrheit erklärt und nichts verschwiegen habe.

_____	_____
Place and date	Signed by José M. Bastías Espejo